A Parrot-inspired Tripedal Robot for Climbing Sparse Vertical Structures

by Clyde Webster

Thesis submitted in fulfilment of the requirements for
the degree of

Doctor of Philosophy

under the supervision of Prof. Robert Fitch, and Dr. Felix
Kong

University of Technology Sydney
Faculty of Engineering and Information Technology

December 2023

Certificate of Original Authorship

I, Clyde Webster declare that this thesis, is submitted in fulfilment of the requirements for the award of Doctor of Philosophy, in the School of Mechanical and Mechatronic Engineering at the University of Technology Sydney.

This thesis is wholly my own work unless otherwise referenced or acknowledged. In addition, I certify that all information sources and literature used are indicated in the thesis.

This document has not been submitted for qualifications at any other academic institution.

This research is supported by the Australian Government Research Training Program.

Clyde Webster

January 2024

A Parrot-inspired Tripedal Robot for Climbing Sparse Vertical Structures

by

Clyde Webster

A thesis submitted in fulfilment of the requirements for the
degree of Doctor of Philosophy

Abstract

Enabling robots to autonomously operate in sparse vertical structures will have a profound impact on the way we conduct inspection and maintenance of civil and space infrastructure. Whilst there has been substantial research on robots that climb vertical structures, few have focused specifically on the sparse vertical structures commonly found in infrastructure, which are characterised by a reticulated network of slender elements. In vertical climbing, these reticular structures are perhaps the most challenging. The thin, often non-symmetric, and non-uniform beams, highly constrain the available grasping locations, and add considerable uncertainty to the reliability of the contact points. To date, the literature is bereft of robots capable of traversing and performing useful work on reticular structures. This is likely due to a multitude of reasons, but the primary reason seems to be that the fundamental problem of locomotion on these structures is, as of yet, unsolved.

Most of the existing literature on such locomotion focuses on two- and four-limbed robotic concepts. In this work, we consider a novel three-limbed concept based on new inspiration; the morphology of parrots. Parrots are unique arboreal specialists, that are adept climbers and have a proven track record for in-structure manipulation. This combination of attributes makes parrots a prime candidate for study, as the behaviours they demonstrate day-to-day are analogous of the maintenance operations we aim to be capable of. Furthermore, the capabilities exhibited by parrots during foraging inspires us to question the traditional assumptions around the number of limbs that are necessary for a useful climbing robot. Having four limbs, whereby three are always in contact, is a common approach in the design of multi-limbed climbing robots. In contrast, the inchworm concept typically has a single point-of-contact during locomotion, and thoroughly disproves that four-limbs are necessary. The three-limbed climber we develop has redundant control of its body, which allows more options for control, more robust stability when compared to the inchworm robotic concept and saves on mass and cost with respect to the four-limbed robot, that may have excessive redundancy depending on the specific constraints of the contact.

In this thesis, we make progress in solving the problem of robotic locomotion in reticular structures by studying the morphology and behaviours of parrots. Through careful review of the biology, we identify several lessons that are useful in robotics development, as well as performing our own *in vivo* experiments on cockatiels (*Nymphicus hollandicus*). We then take a careful approach to the design of two tripedal robots of increasing complexity, culminating in a physically realisable tripedal climbing robot for locomotion on a simple subset of reticular structures: a vertical ladder. Through this exercise, we demonstrate that three-limbs are sufficient for the locomotion problem, making headway in progressing our understanding of the design of climbing robotic systems that may eventually allow us to realise our goal of autonomous civil and space infrastructure maintenance.

Acknowledgements

This thesis would not have been possible without the support of my supervisors, colleagues, friends, and family. First, I would like to acknowledge my primary supervisor, Prof. Robert Fitch. Thank you immensely for taking me on in the later stages of my PhD, and fostering an environment that was so welcoming, and so motivating. Your wisdom, and capacity to see the value in others is a marvel, and a skill that few master.

Next to my co-supervisor, Dr. Felix Kong., you are the absolute bedrock of my technical proficiency. Your support in learning control theory, and your patience as I relearned the basics of linear algebra, again and again, will never be forgotten.

To my housemates Ben Ellis and Tom Gollan, thank you for showing me that the outdoors is still there, and taking me on long, far-away trips that were genuine reprieves from the grind that is doing a PhD. The mental and physical catharsis did a lot to keep me healthy and (somewhat) sane.

To my partner Kate Leone, thank you for your patience and love during all the stressful moments. For thinking of me, and caring for me, especially when I had not the capacity to do so myself. Your request for an honorary PhD by proxy I'm sure is being taken very seriously, and will be processed in due course.

To Annette Leone, your support and copy-editing services are unparalleled in value. Thank you so much for the many hours you spent reviewing and improving my work.

Finally, thanks to my family, for their love, support, and patience.

Academic acknowledgements

Not all of the academic works presented in this thesis are entirely my own, and so two acknowledgments are made for technical contributions. For the model-based optimal trajectory work presented in Section 5.4.2.3, I would like to acknowledge Dr. Felix Kong, who devised and implemented this method in simulation. It is reported here for the sake of completeness, and I stake no claim to its ownership or development.

I would also like to acknowledge Prof. James Brown for his contributions to the multivariate mixed-effect modeling presented in Chapter 4. This work was a collaboration between Prof. Brown and myself, with Prof. Brown contributing the tools and understanding to formulate the model, and in interpreting its results scientifically.

Publications

This thesis is partially based on work described in the following publications:

- Clyde Webster, Ardian Jusufi, and Dikai Liu. “A comparative survey of climbing robots and arboreal animals in scaling complex environments”. In: *IFToMM International Symposium on Robotics and Mechatronics*. Springer. 2017, pp. 31–45
- Clyde Webster, Felix Kong, and Robert Fitch. “Bio-inspired 2D Vertical Climbing with a Novel Tripedal Robot”. In: *2022 IEEE/RSJ International Conference on Intelligent Robots and Systems (IROS)*. IEEE. 2022
- Melody W Young et al. “What does climbing mean exactly? Assessing spatiotemporal gait characteristics of inclined locomotion in parrots”. In: *Journal of Comparative Physiology A* (2023), pp. 1–15

Tangential work completed during candidature in the context of a graduate internship with NASA’s Jet Propulsion Laboratory:

- Clyde Webster and William Reid. “A Comparative Rover Mobility Evaluation for Traversing Permanently Shadowed Regions on the Moon”. In: *2022 IEEE Aerospace Conference (AERO)*. IEEE. 2022, pp. 1–15

Contents

List of Figures

List of Tables

Acronyms

2D 2-dimensional. xvi, xvii, 53, 65, 75–79, 81–83, 90, 101, 102

3D 3-dimensional. xviii, 51, 75, 76, 79–82, 90, 95, 109, 120

CoM centre-of-mass. 13, 42, 43, 48, 79, 82

CoT cost of transport. 104, 105, 126

DAE differential algebraic equation. 123

DoF degrees-of-freedom. xvii, 8, 11, 12, 14, 17–19, 21, 24, 27, 34, 77, 79–82, 95, 112–114, 136, 146, 149

EVA extra-vehicular activities. 150

FG Full-Goldman. xv, 32, 71, 149

FOV field of view. 145

IK inverse kinematics. 13, 114

LLS lateral leg spring. 71

MPC model predictive control. 149

OCP optimal control problem. xvii, 103–106, 109

ParCli Parrot Climbing. xvii, xviii, xxi, 10, 101, 109–112, 116, 117, 119, 125, 134, 136, 137, 140, 141, 143, 144, 148

PID proportional, integral, derivative. 99, 125, 146

ROS robotic operating system. 118

RSR reticular structure robot. 4, 6–8, 10, 16, 25, 37, 49, 52, 79, 139, 140, 149, 150

SHS square-hollow-section. 57

SLIP single leg inverted pendulum. 30, 71

SPART spacecraft robotics toolkit. 123

URDF universal robot descriptor format. xxi, 119, 121, 122

UTS University of Technology Sydney. 56

Chapter 1

Introduction

Amongst birds, parrots show a remarkable aptitude for climbing and manipulating objects [5, 6, 7, 1, 8, 9], especially in sparse, vertical structures such as trees. Robots on the other hand are not currently as capable, lacking the dexterity, strength, and intelligence that would facilitate their usefulness in these environments. The lack of robots deployed to sparse, vertical man-made structures (termed *reticular* structures in this work) for the myriad of maintenance tasks that are performed on them is notable. The man-made structures we refer to include power transmission towers, telecommunications towers, construction scaffolding, and many more. These structures are the analogue to the natural structures that parrots interact with in the wild. Mastery by robots of locomotion in these structures holds great potential to reduce cost, enhance worker safety, and increase the frequency of infrastructure maintenance, whilst further enhancing the locomotive capabilities of robots in general. Parrots demonstrate a unique and remarkable solution to the problem of working at heights that is currently under-explored in literature. Understanding of the way they use three limbs in a coordinated approach to climbing and manipulating objects at heights has the potential to inform new robotic designs that are stronger, lighter, and more capable of useful labour than ever before. This thesis presents preliminary studies into tripedal climbing in parrots, and a novel, bio-inspired robotic design based on their morphology, with the long-term goal of enabling robots to climb and work in reticular structures.

1.1 Climbing in Industrial Applications

This thesis is motivated by an industry-need for the capability to perform autonomous maintenance in power transmission towers. Power transmission towers, like all large steel infrastructure, require periodic maintenance to remove rust and old paint that no longer protects the steel, and to reapply a fresh coat to prevent further degradation. Maintenance operations are costly, laborious, and dangerous for the human workers, as it requires strenuous labour in awkward positions at considerable heights (Fig. 1.1). Failure of power infrastructure is also a significant problem as it can mean power loss to workplaces, hospitals, homes, and traffic control infrastructure. Whilst some regions have extensive resources devoted to the maintenance of large steel infrastructure, it is not ubiquitous, and the costs associated with energy infrastructure maintenance in sparsely populated areas can be a hindrance to maintenance activities. For example, the 2015 *Infrastructure Maintenance* Report by GHD Group Pty Ltd [10] stated that there is evidence of an infrastructure maintenance gap in the sparsely populated Northern Territory and Western Australia for the energy sector, as well as it being likely that infrastructure maintenance expenditure will increase as a result of ageing infrastructure. It is also likely that as more consumers go ‘off the grid’, and use local power generation technologies such as solar panels, the cost of electricity will become more expensive for those depending heavily on the network as a result of decreased revenue to the asset owners. Clearly, automated tools that can reduce infrastructure maintenance costs by complementing the existing labour force can have a significant impact on the utilisation and reliability of energy infrastructure, should we be capable of developing tools that are economical to deploy. There is also the possibility of reducing the use of consumables during blasting and painting, as well-planned robotic paths seek to minimise material usage when compared to the more human approach that is typically driven by discomfort and effort, which may further drive savings in the sector.

There is also a substantial and growing need in space for on-orbit robotic services, including assembly, maintenance, and upgrading of existing systems [12]. This task is best facilitated with the use of robots that can be used collaboratively with humans [13] or entirely autonomously. Of vital importance is that the robot can move safely on and around

Figure 1.1: Workers performing maintenance of a power transmission tower [11]

critical and delicate space assets. Climbing is a natural solution to this problem, as the risk of operating propulsive systems near the satellite or space vehicle is removed. Space structures often share the same reticulated style structures as we see on the ground. This is simply because it is the most material- and cost-efficient way to develop lightweight, stiff structures. Since our robots are designed for all manner of reticular structures, space infrastructure is a natural extension of the capability development we discuss in this thesis.

1.2 Climbing Robots

There are hundreds of examples of climbing robots in the literature, each having some combination of *locomotion type* and *adhesion principle* that facilitate contact with, and locomotion on some structure. Several detailed reviews of these principles have been conducted, including by Schmidt and Berns [14], and Silva and Machado [15]. Of the robots presented in these reviews, only a handful have been designed for use in reticular structures.[1] The sparsity, and non-uniformity of available contacts in reticular structures make development of robots for these structures a non-trivial challenge in all areas of robotic development. In designing robots for these structure, roboticists must choose

---

[1] Our name for tall, sparse, reticulated structures.

appropriate locomotion types and adhesion principles. Locomotion types for climbing robots include: arms and legs; wheels, chains and tracks; sliding frame mechanisms; and wires or rails. Mechanisms for adhesion include magnetic, pneumatic, mechanical, electrostatic, and chemical. In their review, Schmidt and Berns [14] identify the strengths and weaknesses of each locomotion type and adhesion principle, and give examples of the combinations used to date, as well as a guide for selecting these characteristics with respect to the type of structure being designed for.

1.2.1 Adhesion Principle and Locomotion Type for an RSR On a Power Transmission Tower

In line with their framework, and observing the approaches taken in literature thus far, we are able to reasonably discern what locomotion type and adhesion principle are suitable for a reticular structure robot (RSR). Given the sparse and discontinuous nature of reticular structures, legs and sliding-frame mechanisms that are capable of extending over free-space are the only practical approaches. Wheels have been used in end effectors to facilitate contact [16], but only in combination with some form of articulated appendage that is cable of moving the wheeled end effector through the space between elements of the structure.

As for for adhesion, mechanical adhesion (e.g., friction, hooking, or grasping) anecdotally appears to be the favoured approach; however, magnetic adhesion has also been used [17]. Magnetic adhesion is used widely where a lot of steel is present, for example in the hull of ships or in large storage tanks, but as a technology it is less proven in reticular structures, where steel use is minimised. The effect of variation on paint thickness, and loss of steel due to rust (Fig. 1.2) are underexplored, though using the formulas that describe adhesion in [14] it can reasonably be concluded that these variations in the substrate would have a negative effect. For the wheeled example in [16], and where rolling elements at the end effector are used, friction produced by a clamping force is generally used as the primary adhesion mechanism, which is suitable where the properties of the structure are known, and the contact is smooth and consistent enough to facilitate a good grip. This approach is suitable where long straight sections are present, with the caveat that frictional failure of the contact means loss of contact at that location, which can lead to the ultimate failure of a robot. The same is true for most adhesion types including magnetic adhesion, vacuum adhesion, electrostatics, and when utilising Van der Waals forces. For each of these adhesion types, the issue can be somewhat mitigated by having redundant contact points. However, where we want to minimise both number of limbs and contact locations as we do in a tripedal form, it is prudent to choose an adhesion method less prone to catastrophic failure (i.e. the robot falling) during a slip event. Considering this, an encompassing grasp is appropriate. An encompassing grasp, whereby a gripper fully or partially encompasses a structural member, can only fail completely where there is mechanical failure of the elements of the gripper itself. It is also the least prone to disruption from dirt and debris when compared to all other adhesion types. A slip condition can reduce the usable dimension of controllable forces at the contact point, but will not result in the complete detachment of the robot from the structure. Another advantage of an encompassing grasp is that it enables more options for approach angles when making contact, where magnetic adhesion (and other surface-based methods) requires the magnets and hence end effectors to be located normal to the surface. A summary of locomotion types and adhesion principles for the robots cited in this work is given in Table 1.1.

FIGURE 1.2: Rust that has degraded the surface of a structural element of a power transmission tower [18].

Whilst many robots are able to move in these structures, none have demonstrated the capacity to perform maintenance on them, and none have been deployed in our target application; power transmission tower maintenance. In this thesis, we present our argument for a new type of robot based on the tripedal climbing behaviours of parrots. We also take a look at a broad range of robotics technologies and approaches, some mature, and some

A **L**	Mechanical	Magnetic	Pneumatic
Legs	[21][22][23][16][24][25][26][27]	[17][28][29]	[30][31]
Sliding frame	[32][33]	[34]	
Wheels	[16]		

Table 1.1: Locomotion type (**L**) and adhesion principle (**A**) for robots cited in this work. Where a robot fits into more than one category (e.g., wheel-on-limb systems) it is included once for each category it belongs to.

in their early stages, that might in the future be utilised to enhance our designs, and make economically deployable RSRs a reality.

1.2.2 Drones for Physical Labor

Drones have seen an incredible rise in popularity over the last decade, with uses in agriculture, health, military, and in the inspection of civil infrastructure. By and large they are used in the collection of data, though use-cases involving tool-use are starting to arise in the literature [19, 20]. Early testing for specific applications, like drilling, show promise and require the development and addition of adhesion principles discussed above when performing labour. Whilst we believe there is a positive and productive future for this technology, we expect robots capable of climbing to play a strong role in the future due to the capability to be robust, produce high forces, and capacity to operate in sensitive areas.

1.3 Research Questions

The power transmission tower maintenance task, and more generally, preforming work in reticular structures, is a complex operation. There are open questions among many facets of robotics engineering that need to be addressed before a fully capable solution can be developed. These questions include, but are certainly not limited to:

1. What form of robot will best enable a robot to be utilised for exploration and maintenance of the tower structure?

2. What control algorithms are best suited to a robot in this environment? Are there multiple approaches for the different activities like climbing and performing maintenance work, or is one strategy sufficient?

3. What motion and foot-fall planning strategies are appropriate to enable the robot to climb and work?

With such a broad and substantial questions, it is reasonable to explore only a subset of this list as each could be its own body of work. In this thesis, we focus primarily on question 1, with special attention to the locomotion problem. We also include elements of question 2 and 3 as are necessary for the development of a robotic system. We make progress in advancing our knowledge of robotic forms by developing a novel, bio-inspired, tripedal[2] robotic concept and exploring its development with respect to kinematics, mechanical design, control, path planning, and trajectory planning.

The set of questions explored above can be greatly expanded when we consider additional streams of robotics research such as localisation, perception, sensing, global path planning, optimal trajectory planning, the list goes on and on. All of these are out of scope in this work, but we recognise they are all pertinent components of a complete robotic solution.

1.4 Climbing with Three Legs

The tripedal robotic concept we develop is inspired by parrots (*Psittaciformes*), who use their craniocervical system (neck and beak) as a third limb both in locomotion and manipulation tasks [1, 6, 9, 8]. Only recently has the first scientific basis for the treatment of the craniocervical system in parrots as a limb been published [5], though, it is common knowledge amongst ornithological and bird-enthusiast communities that parrots use the neck and beak in this manner.

Several tripedal robots have been been developed previously [35, 36, 37]; however, none have been designed as a RSR meant for climbing. When climbing, scansorial robots have have significantly different constraints on their end effectors when compared to cursorial

---

[2] Using three-limbs for locomotion.

robots. Whilst cursorial robots can only push into the ground, scansorial robots can rely on both push and pull, as well as being able to produce torques as constrained by the mechanics of the adhesion mechanism. Additional force producing capabilities at the end effectors allow for additional degrees of control, enabling a lower number of limbs than would be otherwise necessary. Inchworm robots, for example, have full control of their body with just a single point-of-contact, that can react forces in all dimensions. Unfortunately, several caveats in their design prevent them from being useful for maintenance tasks (see 2.1.1). With a third leg, we can make significant headway into overcoming these caveats, whilst still maintaining an approach that attempts to minimise the active DoF in the robot's design. Fortunately, this model is already used in nature in the tripedal behaviours of parrots, who often use their craniocervical system as a third limb during climbing, foraging, and social behaviours [1, 5, 6, 9]. Whilst four(or more)-limbed robots (section 2.1.2) are also common, we propose in this work that a three-limbed climbing robot makes better use of each limb resulting in a machine that is comparatively lighter, cheaper, and has a larger usable workspace for manipulation tasks than its four-limbed counterparts.

1.5 Principal Contributions

The main contribution of this thesis is to propose and demonstrate the feasibility and utility of using three legs in the design of a RSR. This is accomplished by taking a multidisciplinary approach to exploring tripediality. Firstly, by performing a biological study looking at the mechanics of tripediality in live parrots, and secondly, by approaching the model from an engineering design perspective and considering what additional functionality each leg of a robot enables based on an understanding of the contact physics. Expanding on this, our specific contributions can be separated into two lists; biology and engineering.
In biology:

1. We have proposed a never before explored model for climbing locomotion; tripediality, where three limbs are used in the legged propulsion of an climbing animal. The proposition that the craniocervical system operates as a limb has been hinted at

previously, we provide new evidence for this being the case in climbing behaviours and inspire a new stream of research into this concept.

2. Contributions to the definition of climbing; we propose that climbing behaviour be defined by a tangible quantitative change in the steady-state behaviour of the animal, which is further evidenced and supported by Granatosky et al. [7].

3. We develop a novel method for the study and comparison of animal kinematics through the use of a multivariate mixed-effect regression modelling, that allows us to determine how kinematic parameters vary with respect to confounding factors.

4. Identify that kinematic changes in parrots during climbing behaviours are not the hard boundaries that might otherwise be assumed. Parrots tend to gradually change climbing approaches based on still unknown factors.

In engineering:

1. Bridging the gap between biology and engineering, we propose several lessons, with examples from nature, that demonstrate tangible mechanical principles useful in the design of mobile climbing robots.

2. We perform a novel decomposition of reticular structures and describe a set of behaviours that should enable robots to master locomotion in this environment.

3. Provide evidence, through analysis of contact degrees-of-freedom, that support our claim that three-legs is a sufficient number for a climbing robot under certain conditions of the contact.

4. Produce two kinematic designs of a novel tripedal robot for climbing a simple ladder.

5. Complete the mechanical and mechatronic design of a novel tripedal robot.

6. Produce variations on the whole-body control of cursorial legged robot to make them suitable for implementation in climbing robots.

7. Present two novel tripedal gaits, the three- and four-step climbing gaits, derived from our *in vivo* experiments with cockatiels.

1.6 Thesis Outline

This thesis is organised as follows:

Chapter 2 explores relevant literature and state-of-the-art for climbing robots in terms of the morphology and capabilities. In this section, we cover important principles for climbing robots, including *locomotion type* and *adhesion principle*, and demonstrate that legs and mechanical grasping types have come to be the expected form for RSRs.

Chapter 3 presents the principles we rely on in the design of our robots. Beginning with an in-depth look at the biological literature, we distill several lessons that are relevant in robotic design, relying on a large range of climbing animals that demonstrate these principles. We then move on to designing for our environment; reticular structures. By breaking down this environment into its constituent parts, we present a set of behaviours that a RSR needs to master the sparse vertical environments that are our focus.

In **Chapter 4**, we present preliminary work on climbing in parrots and push towards understanding why parrots transition from bipedal to tripedal locomotion, and if they are truly using their craniocervical as a third limb. Data collected in this experiment goes on to inform footfall planning strategies in the proceeding chapter.

Chapter 5 details the design of two progressively more complex tripedal robots for climbing a simple ladder, culminating in a kinematic design that is suitable for the basis of a physical robot. We also detail several footfall planning strategies, trajectory planning strategies, and control methodologies that used for our tripedal designs.

In **Chapter 6**, we present the results of experiments conducted in simulation on our two kinematic design, validating the footfall planning, trajectory planning, and control algorithms developed in the preceding chapter. We also present the design of ParCli, the world's first tripedal climbing robot based on the kinematic design presented in **Chapter 5**. The robot actuator selection and configuration is assessed and validated in simulation, along with our modified control approach.

Chapter 7 provides concluding remarks, as well as detailing preliminary work in the hardware implementation of the ParCli robot.

Chapter 2

Related Work

Work related to this thesis falls into three categories. First, we discuss legged climbing robots, which are the most closely related in terms of current research. Most legged climbing robots can be placed into categories based on the number of legs they have, with two and four (or more) being the common categorisations. Since in this work there is a strong focus one developing a robot for power transmission towers, we next look at robots in application environments, presenting work that has been done to this end, and a successfully deployed robot in similar scenarios. Finally, we look into dynamic climbing robots that promise to pave the way for fast and efficient climbing.

2.1 Legged Climbing Robots

2.1.1 Inchworm-Inspired Climbing Robots

The inchworm-inspired robot is a two-limbed, minimal DoF robotic concept, whereby each end of a floating, serial-chain has a prehensile end effector; it has seen extensive development in the literature. Locomotion is typically achieved by extending a gripper and then pivoting off the forward gripper, or by inching forward, similar to a caterpillar or inchworm. Some noteworthy examples of this form of robot, shown in Figure 2.1, are the Shady3D robot [23], the inchworm climbing robot [28], the ROMA robot [21], and

Climbot [22]. The ROMA and inchworm climbing robot (Figure 2.1) have been designed specifically for civil infrastructure inspection. The primary advantage of this design is that it minimises the robots DoF in an effort to maximise mobility. Having more DoF requires more actuators and typically results in a heavier, more complex robot, which is used to justify the concept in these examples. The common, and unproven philosophy that accompanies this design, is that minimising the DoF will make for the most successful robot, as it will be both lightweight and dexterous enough to perform the desired functions. Whilst these robots have seen some impressive implementation in inspection tasks, they have yet to be widely adopted in the commercial sector or demonstrated that they are capable of significant autonomous maintenance operations. Even though inchworm robots are not often stipulated to have the capacity to perform maintenance, it is useful for us to discuss the reasons for this, as it helps us understand what attributes a robot might require to do so. Several caveats in the design may be preventing engineers from taking this step.

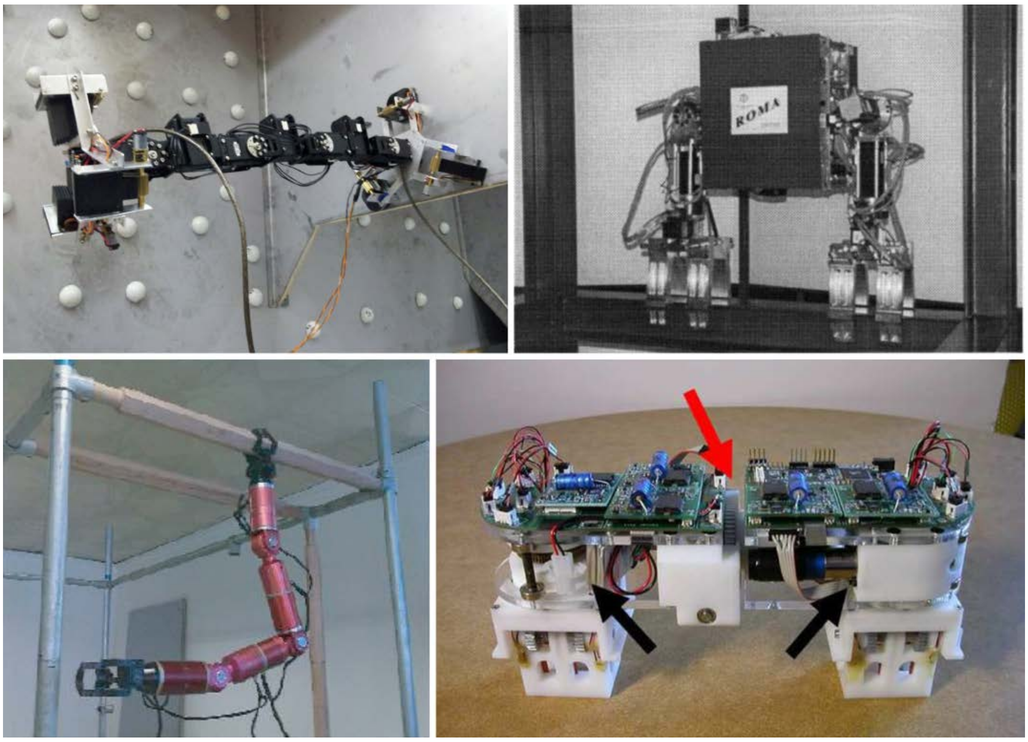

FIGURE 2.1: Top Left: Inchworm [28]; Top Right: ROMA [21]; Bottom Left: Climbot [22]; Bottom Right: Shady3D [23].

The first major caveat is the speed of the machine. These robots can take several minutes for each new pose and grip, making their locomotion around reticular structures slow. This slowness is often a function of the adhesion mechanism, which is necessarily slow and deliberate as contact failure can result in the destruction of the machine. Should the robot be able to operate completely autonomously, the speed of locomotion might not be considered such a significant hindrance to the robots operation. However, current technology is predominantly teleoperated, or operated under supervised automation, whereby an operator (or operators) has to watch the robot continuously.

We can easily reason why these robots should be slow; the cost of failure is high. With only a single point-of-contact with the structure during the swing phase, grip failure of the stance leg in a real scenario has the potential to mean the ultimate destruction of the robot. As the centre-of-mass (CoM) and opposing end effector are typically far from the substrate, large reactive moments must be produced at contacts, which can prove challenging in design and is why, where space is available, contacts are made sufficiently wide as in [38]. In reticular structures, due to the thin nature of the structural elements, the size of the contact is limited by the width of the structural members, imposing a limit on the capacity to design for torque loads. This limitation ensures that performing high-force maintenance operations like sand-blasting (Figure 1.1) will be difficult for inchworm-robots in these environments. With such critical constraints placed at the contact, inchworm robots are typically designed to climb very specific structures and are restricted in the tasks they can complete. With a long extended body, the end effector accuracy can also be an issue where traditional control approaches that rely on the inverse kinematics (IK) are used. Small joint errors and deformation of the contact compound over the robot's length to produce uncertainty in the end effector location. The same is true for all robots that use this strategy for locating end effectors and is a reason for robots to be relatively stiff, especially where there is a need for high-precision and repeatability. Though contact deformation may be maximised if all force is required reacted at a single contact point.

2.1.2 Four (Or More)-Legged Climbing Robots

Another common conceptual approach in the design of climbing robots is the use of four or more legs, with four-limbs (i.e. quadrupeds) being the most common variant. Robots that utilise four or more legs conceptually oppose the inchworm-inspired approach. Using four (or more) limbs seek to maximise the contact the robot has with the structure in order to achieve adequate stability in complex environments. Quadrupedal robots are often heavier due to more actuators, and they use more complex control algorithms when compared with inchworm robots, which is necessary to coordinate their multiple limbs. Compared to inchworm robots, the quadrupedal robots we have reviewed tend only to climb very simple structures, like ladders or smooth walls with obstacles. Transitions between planes or locomotion in more complex environments are non-typical and yet absolutely necessary if we are considering a robot for use in reticular structures.

Quadrupeds, theoretically at least, having a higher force production capacity should have a higher capacity for work. The multiple limbs ensure more contact with the structure, and therefore allow the robot to carry more higher payloads. Unfortunately, the author is unaware of any examples where a four-limbed robot is used to perform the type of work necessary for our application. We expect this is due to the challenges of designing a prehensile end effector that is also useful for maintenance works, or due to the locomotion challenges experienced by quadrupeds in climbing scenarios combined with the heavy mass and lack of efficient mobility that would otherwise enable battery powered operations. Quadrupeds are characteristically slow during motion and often have an unexplained tendency not to move the body during the swing phase of the leg, which likely has the effect of reducing the reach-ability of the swing leg but also reducing the dynamic forces experienced at the contact that are necessary to produce motion. This slowness is not necessarily a function of the morphology, but it is typical in the implementations we have encountered with a few exceptions. The first example of dynamic climbing in a quadrupedal robot is shown by Haynes et. al. in [25], which is discussed in more detail in section 2.1.2.9. A more versatile and higher DoF robot for climbing tank strictures has been published by Hong et. al. [29] that uses magnetic adhesion and is shown to climb on relatively flat continuous substrates with minimal substrate asperities (i.e. thick paint or advanced rust). Continuous locomotion in a climbing robot has also been demonstrated by Schultz et. al. [39], where the trajectories are generated from climbing lizards which display robust and continuous climbing behaviours.

In the remainder of this section we present a small history of a few notable examples of multi-limbed legged climbing robot and discuss the strengths, achievements and caveats with respect to their stated aims and our own.

2.1.2.1 Robug II

Robug II (Figure 2.2) was designed to be capable of remote deployment into environments that are dangerous to humans [30]. The ability of Robug II to perform floor-to-wall transfers meant that it could be deployed away from the target structure and could walk up to the structure and begin climbing without human assistance. Robug II is pneumatically powered, utilising pneumatic linear actuators for all four legs as well as the thoraxial joint located in the centre of the chassis that allows it to bend in the middle, as well as for the gripper which utilises a suction mechanism. Pneumatic actuators were chosen due to their high power-to-weight ratio and inherent compliance.

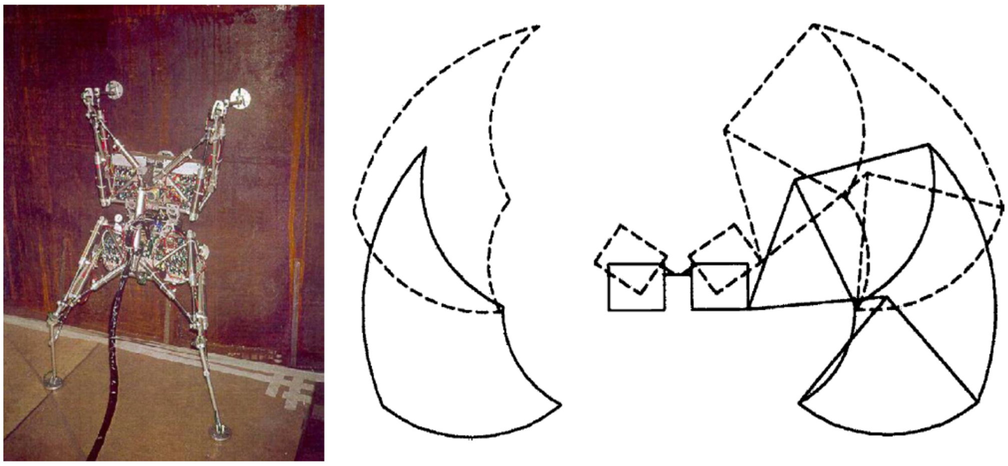

Figure 2.2: LEFT: Robug II midway through a transition from flat to vertical substrate. RIGHT: Motion range and kinematic envelope of Robug II's legs. Source: [40].

Perhaps something unique to Robug II is its ability to seek out potential holds by utilising pressure sensors and potentiometers in the feet and body to provide force and position feedback. Using these sensors, Robug II could feel for obstacles as well as the level of the surface. Due to the compliant nature of the pneumatic actuators it was able to perform this feeling operation without damaging the structure. A hold was verified by vacuum sensors that could sense for the presence of a vacuum in each one of the three suckers of Robug II's feet. To assist with ensuring a vacuum could be achieved, each foot was connected via a ball joint which allowed it to rotate to the precise pose needed.

Robug II was stipulated to be be capable of performing maintenance tasks or deployed in environments that required maintenance; however, it lacked the appropriate appendages to do so and seems only to have been used as a test platform to evaluate the locomotion system and control.

2.1.2.2 Robug III

Robug III (Figure 2.3) is a continuation of the design of Robug II. The design has been further developed to meet a specification determined by the nuclear industry. The specification stated that the robot needed to be able to drag loads of 100 kg horizontally, carry payloads of 25 kg, be capable of dragging 100 kg payloads when climbing vertically, make floor-to-wall and wall-to-floor transitions, and enter though small openings [31].

Based on a similar leg design, Robug III was upgraded to include eight legs, each with a dedicated controller. The increased number of legs gives the Robug III a higher payload capacity, which is capable of meeting the specification. The system relies on the same pneumatic drive mechanisms for locomotion and adhesion to the substrate.

This robot is designed to be teleoperated, but due to the required control framework, it can also be considered semi-autonomous. Instead of the operator controlling the movements of all limbs, they are able to give it commands for which direction they want it to travel, giving the robot tasks like performing a floor-to-wall transition or projects which are sequences or tasks. Once a command is given, the robot is responsible for coordinating the movements of the legs, finding foot holds, and carrying out the given commands. As all legs appear to only be for locomotion, it is unclear how the robot supports or manipulates payloads. This kind of semi-autonomy is a good example of the kind of remote operations we expect will be useful for RSRs in the coming years.

Figure 2.3: Robug III. Source: [31].

2.1.2.3 WAREC-I

WAREC-1 [26, 41] is a 28-DoF, 155kg, four-limb robot meant for hazardous environments. It is capable of both bipedal and quadrupedal locomotion, a capability that the authors claim make the robot more capable in moving around a diverse range of environments. It is unclear from the current published literature what level autonomy WAREC-1 is capable of; however, we expect these capabilities to be advanced and explored in their future work. WAREC-1 has been used to climb a simple ladder (Figure 2.4) using its hook-like end-effectors [41]. It moves in a slow, deliberate manner, much like the other quadrupeds we have encountered. Since no requirements on locomotion speed are discussed in their work, it is uncertain if the slow speed will be a problem for their target applications which includes search and rescue.

The long term goal of the WAREC-1 robot is to generate the capability to be both mobile and have "*high-manipulation ability*", though this current robot is only designed to address the locomotion problem, and so the dual purpose end effector that is necessary for this kind of work, without adding additional limb, is still elusive. Preliminary analysis of stability is considered in [41]; however, the planning seem only to consider quasi-static stability based on each time-step in the planned trajectory being in a statically stable state.

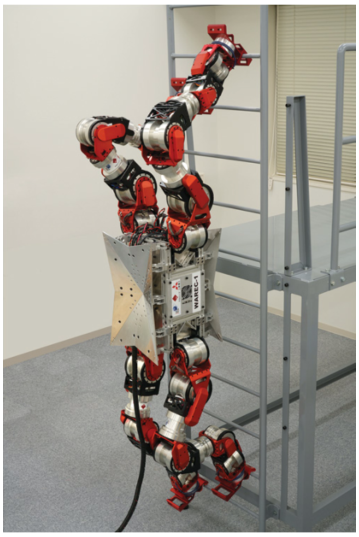

Figure 2.4: WAREC-1 is designed as a search and rescue robot and has the capability to climb as one of its locomotive styles [26, 41]

2.1.2.4 SCALER

SCALER is a four-limbed climbing robot that uses microspines to adhere to the substrate [27]. It has an innovative, lightweight 6-DoF limb design, that achieves a full system weight of only 6.3kg. The torso itself, instead of being rigid, is also actuated, which helps the robot boast an impressive payload capacity that can reach up to 233% of its body mass. It should be noted that power for the robot is provided externally. SCALER is not stipulated to be designed for maintenance work, and whilst the design is mechanically efficient, the intended use case is not explored.

Like other robots, during climbing, SCALER appears to only move one leg at a time rather than body and legs simultaneously. The reason stated is that the swing leg introduces significant dynamic effects, as the actuators that make up the wrist joint are at the end of the robot arm, adding significant inertia. During stance, this inertia is not an issue as the grasping end effector is connected to the structure and hence does not contribute significantly to the dynamics.

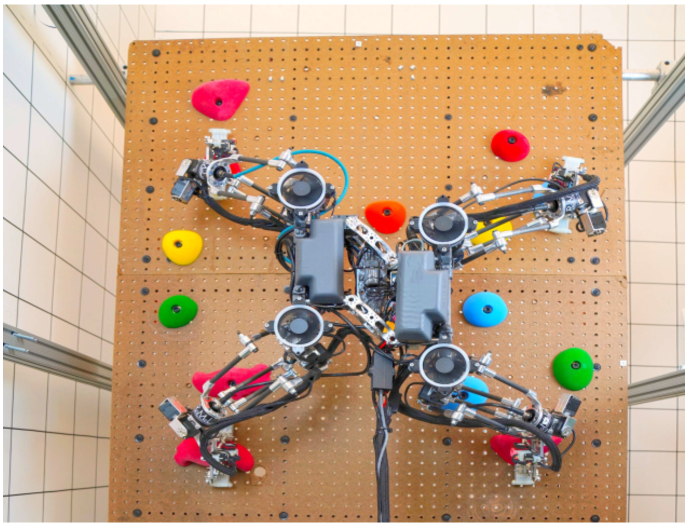

Figure 2.5: SCALER free-climbing on a bouldering wall. Source: [27]

2.1.2.5 Magneto

Magneto is a quadrupedal climbing robot for the inspection of confined spaces in large metallic structures like ship hulls and bridges. Each of its four limbs have three active DoF and a three-DoF passive wrist. Adhesion is facilitated through an electromagnet that can be switched on and off to perform attachment and detachment from the substrate. Magneto's form factor and high DoF allow it to reconfigure and squeeze into tight spaces. The control methodology is based primarily on kinematics with no active planning for contact forces. Force data from the contact is presented however, and validates the selection of the end effector magnets for the use case. Magneto, like other robots, tends to move a single limb at a time, which we expect is in an effort to reduce end effector transients. Magneto is stipulated for inspection tasks only.

2.1.2.6 LEMUR IIb

LEMUR IIb, shown in Figure 2.7, is a multi-use robot designed to be able to climb vertical structures using mechanical adhesion. It weighs 7 kg, and the body (referred to as the "pelvis") is 319 mm in diameter. Bretl et al. [42] outlined the need for robots that are capable of multiple functions including assembly, inspection, maintenance, and transport. For climbing, LEMUR IIb has been equipped with very simple grippers that utilise only

FIGURE 2.6: Magneto has magnetic feet and is designed for cluttered vertical environments [17].

the friction generated between the substrate, and the high-friction rubber the gripper peg is wrapped in. Each arm has 3-DoF and is capable of a maximum torque of 5.0 N.m and a maximum speed of 45 deg/s.

LEMUR IIb is designed to move with a slow, quasi-static gait. In this way, the task of ensuring that the robot maintains a stable equilibrium with the wall is ensured. The robot holds on with either three or four of its limbs at any given time. The control algorithm approaches the task of climbing up the inclined plane by breaking it into single steps (referred to as "one-step planning"). With this, the robot pieces together a path of holds, and it plots the joint torques and velocities to maintain quasi-static equilibrium during locomotion.

Whilst a successful endeavour into the notion of free climbing, LEMUR IIb is restricted to environments that are relatively flat (non-complex). This is largely demonstrated by the fact that, for control, it is assumed that the pelvis maintains a constant distance from the flat substrate. Whilst an interesting demonstration in planning based on contact constraints, it is unclear how the platform itself would be extended for its stated aims.

Figure 2.7: LEMUR IIb. Source: [42].

2.1.2.7 Claw Inspired Robot (CLIBO)

CLIBO (Figure 2.8) was designed as a proof-of-concept to be capable of climbing rough stucco walls for civilian and military uses. It has a mass of 2 kg and an overall length of 0.75 m. The maximum achieved climbing speed so far is 12 cm/min. Each one of CLIBO's grippers is comprised of 12 fish hooks that are capable of passive independent motion in the vertical direction. The entire gripper also has one passive DoF that allows it to rotate and self-align with gravity. A mass at the bottom of the gripper ensures that the gripper is re-orientated in the vertical direction regardless of the arm position. This setup enables the designers to make the assumption that grip is maintained during locomotion, although checks are performed after each motion to ensure that the robot is still in equilibrium. In practise this assumption held true only when they did not move the arms too fast. During experiments [43], the detachment speed of the leg was reduced from 1.0 m/s to 0.06 m/s to ensure stability.

Whilst the dynamics of the gripper were appropriately considered, the dynamics of the rest of the robot are neglected. With this in mind, the robot is only capable of very slow motions. One of the primary control assumptions is that this robot will maintain

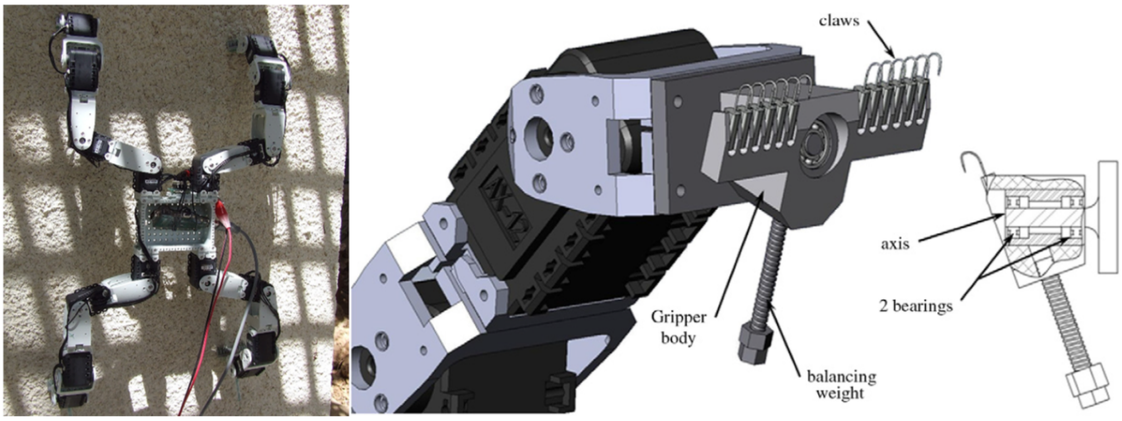

Figure 2.8: CLIBO. Source: [44].

its distance from the vertical substrate, which is an assumption that we will have to do without to be truly capable of climbing in complex 3D environments.

2.1.2.8 Robots in Scansorial Environments (RiSE)

RiSE (Figure 2.9) is a robot designed to be capable of performing horizontal and vertical locomotion on a diverse range of materials. It accomplishes this through clever implementation of gripper design and robotic morphology.

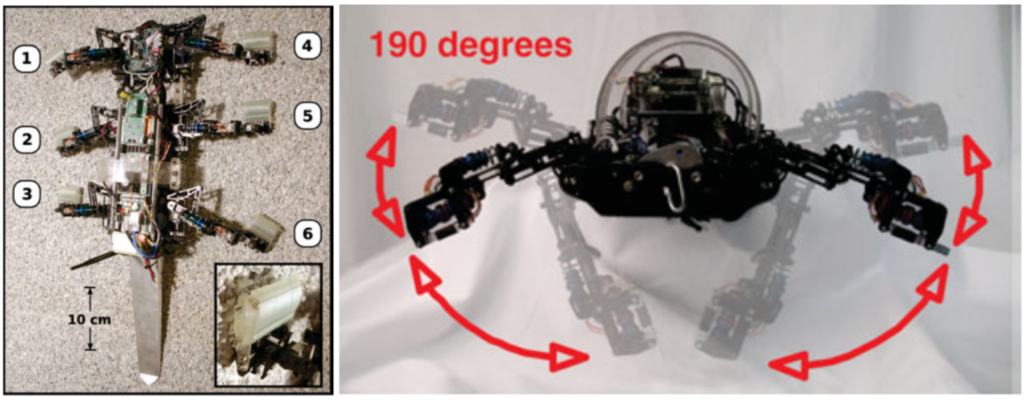

Figure 2.9: RiSE. Source: [24].

Recognising that animals often switch between an above-leg and sprawled gait when going from horizontal locomotion to vertical climbing, RiSE is designed to be capable of abducting/adducting its legs as shown in Figure 2.9. By having interchangeable feet, and with the reconfigurable leg position, the robot is able to walk as well as climb. Climbing is facilitated using micro-spines that hook onto asperities in the substrate. As asperities are usually in the order of tens of micrometers, so too are the radii of the spines on the feet. To ensure that grip is achieved, the legs are outfitted with an array or pressure and strain sensors, but more important is the effect of the legs compliance.

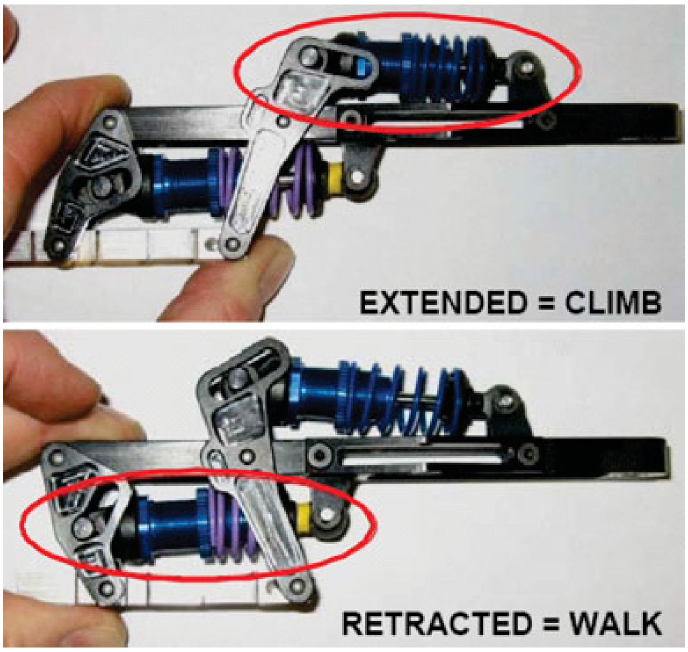

Figure 2.10: Leg of the RiSE robot. Red circles highlight the relative compression of each spring leg during walking and climbing. Source: [24].

Each shock absorber on the leg (Figure 2.10) has been tuned to ensure that the impulse reactions of the landing foot are sufficiently damped as to not affect the spine's ability to penetrate the substrate asperities.

Coupling the smart mechanical design with a distributed control framework and customised electronics, the robot is successful in climbing on brick, trees, locomoting over rough terrain, and even climbing on metals and glass (although only up to an incline of 65°). With this design, the 3.8 kg robot is able to take a payload of 1.5 kg.

The DARPA RiSE project also inspired the discovery of active tail use in biomechanics to reject perturbations in foot-substrate interactions during climbing [45]. It was found that geckos prevent falling by pushing into the substrate with their tails to compensate for ineffective footholds when debris on the substrate caused disturbances to footholds. Tailless animals were found to have a significantly reduced climbing performance and were subject to falling backwards.

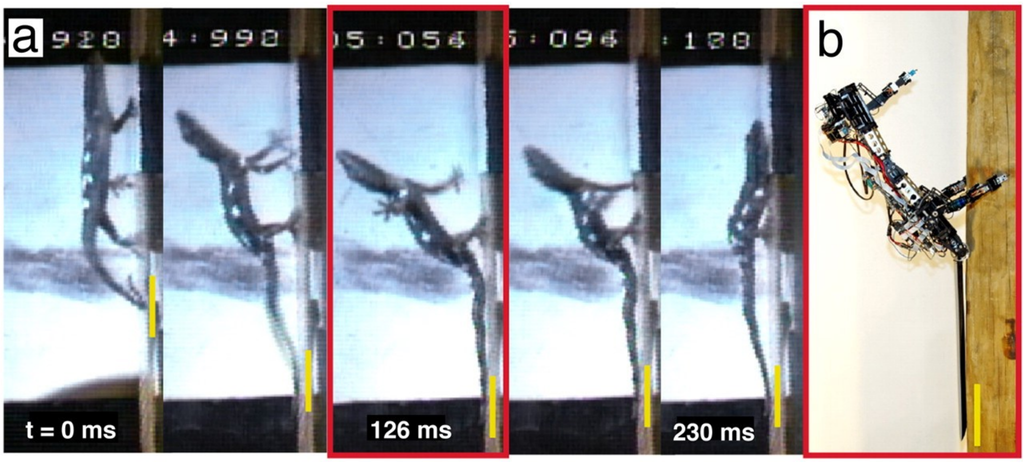

Figure 2.11: RiSE climbing with the 1-DOF tail. Source: [45].

One aspect that was found to have a substantial effect in increasing the climbing robustness of the quadrupedal RiSE platform was the addition of the tail. The robot utilised the tail to counter the over-turning (often called pitch-back) moment due to gravity, particularly when footholds were not secure. Even a passive tail was found to be useful for rejecting disturbances on both RiSE and later Stickybot [46]. The addition of an active tail with one DoF was found to enhance climbing robustness as it increased capabilities for rejecting perturbations and obstacles. Active tails also facilitated transitions from vertical wall to horizontal surfaces (e.g. roof). Moreover, to prevent loss of a robot, an active tail can also be utilised as an inertial appendage to reorient the main body attitude from upside-down to right-side up as realised in the RightingBot prototype based on Stickybot mass distribution [47].

Whilst this robot is very capable at wall-climbing it would not, however, be as capable in a complex 3D environments due to a lack of mobility in the limbs and chassis. Unless equipped with additional manipulators, it is unlikely that it would be capable of any significant maintenance.

2.1.2.9 RiSE III

RiSE III (Figure 2.12) has been designed with the goal of building on the characteristics that made the success RiSE II by enabling the robot to move faster with a more dynamic gait. It has a mass of 5.4 kg, a length of 70 cm with an additional 28cm tail. Building on the gaits developed in the RiSE II, the RiSE III has an order of magnitude high power output ability, being theoretically capable of an aerial phase. It has achieved the impressive feat of climbing up a pole (Figure 2.12) at a rate of 21 cm/s.

FIGURE 2.12: RiSE III. Source: [25].

The impressive speed is achieved by redesigning the mechanical linkages to be capable of variable ratio output force. This means, that whilst in contact with the substrate, the force produced can be high, and when recirculating the leg and not in contact with the substrate, forces can be low and speeds high. Similar to the RiSE II, the RiSE III is capable of abducting and adducting its limbs so that it is capable of gripping onto circular members of variable diameter. Compliance is built into this DoF (Figure 2.13) to control and limit the reaction forces in the chassis and other limbs generated from the large impulse action needed to penetrate the substrate for grip. The RiSE II utilises repurposed suture needles as claws that are pushed into the relatively soft substrate to achieve adhesion.

2.2 Robots in Application Environments

2.2.1 Power Transmission Tower Robots

Maintenance of power transmission towers is a prime example of the tasks we one day hope to see RSRs be capable of. Power transmission towers are a common example of a reticular structure that has periodic maintenance performed on it; specifically, and like most steel

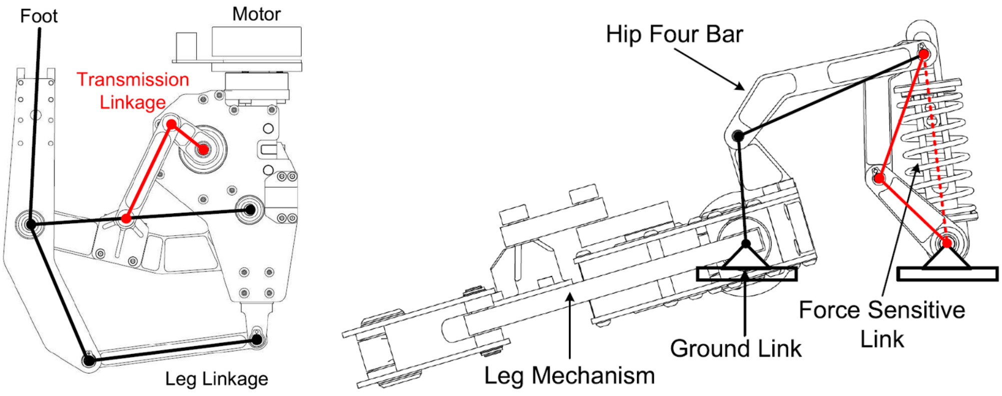

FIGURE 2.13: RiSE III Leg Mechanism. Source: [25].

infrastructure, power transmission towers require periodic cleaning of degraded protective coatings (e.g., paint, galvanic coatings, etc.) and rust, as well as a fresh application of paint to prevent further corrosion. The task of performing autonomous maintenance of a transmission tower with a robot was first attempted by [48] for Electricité de France. The aim of the study was to determine if then-current innovations in robotics could be used for remote controlled operations in the tower maintenance process. It was stipulated that the main benefits to be gained from roboticising the process was not to save costs on manual labour and training, but to minimise downtime of power because live line maintenance was not common practice at that stage. This increases the quality of power supplied in the overall network.

Their conclusion was that remote operation and robotics would not be implemented due to two key factors. The first factor was that only 30% of all transmission towers were accessible by road. The remaining towers must be accessed off-road in hilly or unstable terrain. It was likely that trucks would be used to transport a robotic system between towers, and this terrain would make the towers too inaccessible. The second factor was that only a very limited number of tasks could be completed using a their remotely operated robotic system. It should be noted that painting of towers was deemed infeasible very early in the study due to a lack of a satisfactory technical solution. This was the only study to be published, and no other group to the knowledge of the authors have published any investigation on the feasibility of using robots for the manual labour involved in transmission tower maintenance. Recently, an attempt to develop a maintenance robot

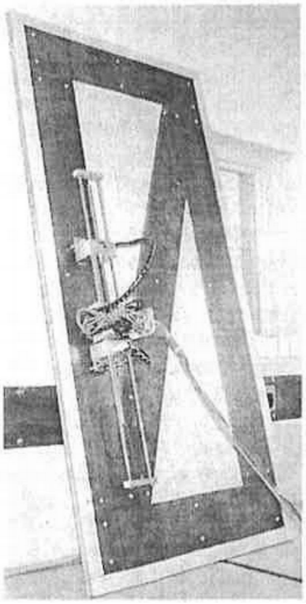

FIGURE 2.14: A tower climbing robot in lab conditions. Source: [34].

was conducted by the Tokyo Electric Power Company in collaboration with the Centre for Autonomous Systems [49]; however, no publications on the feasibility of the efficacy of this system have been made available.

Whilst a robotic solution to this problem may have been infeasible 20 years ago, robotic technology has grown and matured drastically since then. Robots have become a lot cheaper, are more effective, faster, more accurate, and are more flexible since the mid 1990s. With the costs of human labour increasing, more and more dull, dirty and dangerous tasks become strong candidates for robotic automation [50]. Though, the robots reviewed in the next few paragraphs indicate that there is still progress to be made yet.

A sliding frame, magnetic adhesion robot by [34] was proposed to be cable of inspection of power transmission towers (Figure 2.14). The robot produced for this work was a very basic representation of a particular element of a tower. In an attempt to reduce the DoF of the robot, it was only able to climb a flat wall, analogous of the transmission tower structures. For adhesion they used magnets, and its locomotion was akin to *inching* up a flat surface where one contact at a time is detached, moved, and then re-adhered to the structure in succession. The testing rig for the robot grossly simplified compared with a real tower, and did not encompass the set of features typical of the application environment. Although the robot was shown to work within lab environments, no work was ever published on further development, or deploying this robot to more complex tasks.

A similar robot (Figure 2.15) was developed in 2016 by Qing et. al. [32] based on the sliding frame locomotion type and mechanical grasping. This robot only had the capacity to traverse a beam in a single dimension. It was also unclear if the robot had the requisite clearance to get over obstacles should it encounter them. The robot gripper was designed to grasp a specific size angle-iron member from a specific orientation. Whilst this robot could grasp the 3D tower, it was capable of little more than the original work done in 2004 by [34].

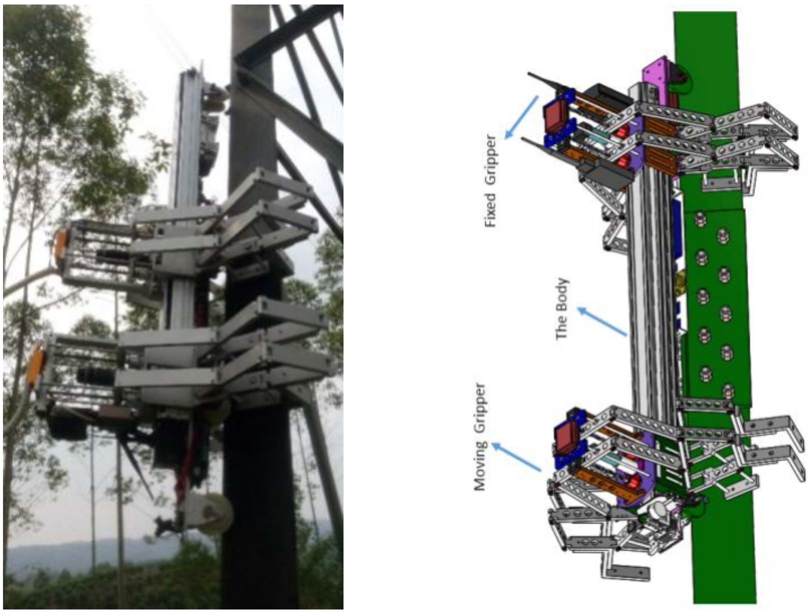

(A) (B)

Figure 2.15: The robot described in [32], with a sliding frame type design and mechanical grasping for adhesion. (a) Physical robot prototype on a transmission tower. (b) Annotated CAD rendering of the robotic prototype.

What form a robot should take to climb power transmission towers is still an active area of exploration, though by and large the concepts involve legged climbing robot using either mechanical of magnetic adhesion. Though not a very active area of development, work is ongoing to find the best form and size of robot for these structures [51].

2.2.2 Grit-Blasting Robot for Shipyards

Demonstrating that rust removal with a robotic agent in an application environment is possible, Faina et al. [33] developed a robot for grit blasting large and relatively flat steel surfaces in preparation for painting. The robot is based on a double sliding frame mechanism (Figure 2.16) which enabled it to translate and rotate on the relatively-flat steel surfaces. Ball joints in the ankle of the feet allow maximum adhesion on the slightly curved ship hulls.

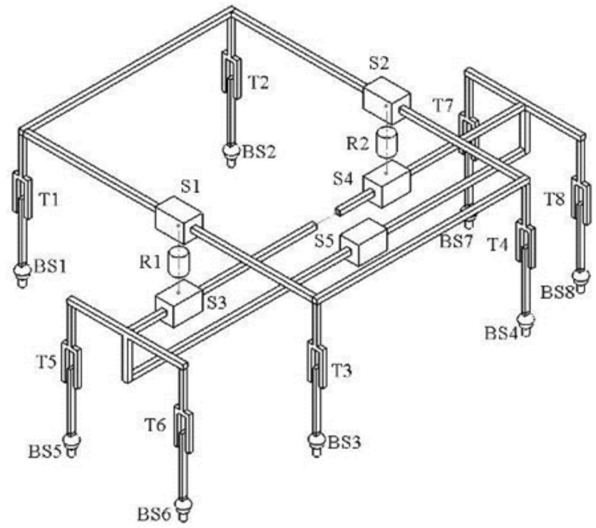

Figure 2.16: The grit blasting robot for shipyards. Source: [33].

The robot uses permanent electro magnets for adhesion on the steel surfaces. These magnets are capable of generating an electro-magnetic field that acts to suppress the permanent field generated by the neodymium magnet embedded in the device. Utilising this, the robot can detach individual feet from the structure for locomotion. The ability to generate a zero net magnetic field also enables the robot to be rid of the small ferromagnetic particles that are created from the grit-blasting process. This is important as particles stuck between the feet and the substrate greatly affect the ability of the magnet to provide normal force for adhesion. Combined with a well implemented controller and path planning algorithms this robot appears to be quite capable of its intended function.

Whilst suitable for its specific function, this robot would be hard-pressed to handle surfaces where a gap might be introduced between the magnetic feet and the substrate. Small gaps lead to large drops in the magnetic normal forces generated for friction, so on a steel surface that has a heavy coat of paint or some other occlusion to the bare steel, it would be possible for the robot to lose grip. It is also only appropriate to implement this device on a large, relatively flat surface. Any surface where the curvature is too great would not be reachable by the robot. The available DoF in this design do not allow for orthogonal plane transfers, so this design would not be appropriate for implementation in a complex 3D environment. We also question how capable this robot is of reaching the edges of a steel plate as the sand blasting head is only capable of reaching an area enclosed by the feet of the robot.

2.3 Dynamic Climbers

Several attempts to describe periodic dynamic climbing gaits have been attempted in the literature. These principles promises fast and efficient climbing by utilising a systems natural dynamics. Similarly to how the single leg inverted pendulum (SLIP) model helped to inform efficient motion of cursorial quadrupeds and bipeds, the hope is that a templated model might have a similar effect when it comes to designing and generating motion trajectories for climbing robots.

2.3.1 ROCR

ROCR is a pendular, two-link, serial-chain robot with a pivoting tail attached to the centre of its first link [52]. ROCR represents an important step forward in dynamic climbing abilities. It utilises the moments generated around the passive gripping mechanism (Dactyl Claw) by the pendular tail to rotate its body upwards. Using its tail, it is able to climb using both dynamic and quasi-static gaits. During its dynamic gait, ROCR was able to achieve a vertical speed of 15.7 cm/s. ROCR was able to achieve a climbing efficiency of greater than 20 percent, which is - as far as we know - the first benchmark for climbing robots, and something that would be appropriate to either match or exceed. Efficiency in this work is a measure of total energy expenditure divided by gain in gravitational potential energy.

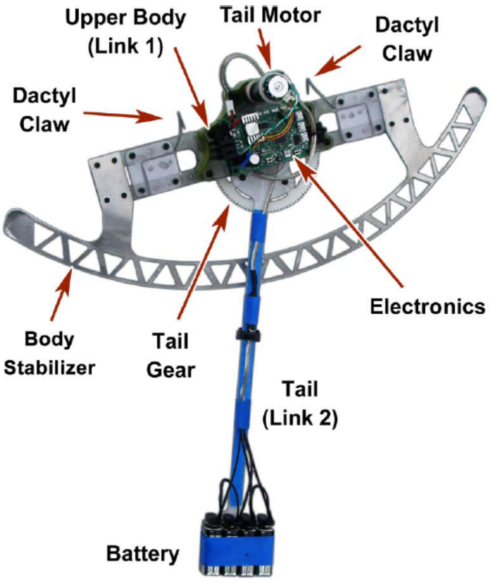

Figure 2.17: ROCR. Source: [52].

Whilst ROCR is designed only to move vertically on a 2D structure, the prototype displays how the dynamics of a climbing machine can be utilised to achieve high speeds and efficiencies in climbing.

2.3.2 Full-Goldman Climbers

Full-Goldman climbers are another example of a highly dynamic bio-inspired climbing robot that can run up walls [53], and even made feasible, aerial phases between consecutive strides of vertical climbing. The robot is designed around a template for climbing which was proposed by Goldman et al. [54], and shows promise in describing climbing behaviours in two remarkably dissimilar climbing animals; cockroaches and lizards. This template became known as the Full-Goldman template for climbing. Initial work to develop an anchor for this model as the basis for a robot were attempted by Clark et al. [55, 53], which was then furthered with the DynoClimber robot by Lynch et al. [56]. The DynoClimber robot boasted impressive speeds, climbing vertically at up to 0.66 m/s.

Whilst this is a very interesting model for dynamic climbing, it does not extend to the underexplored tripedal form. Whether parrots' locomotion can be represented by a variant of this, or any other similar model, is still an active area of development.

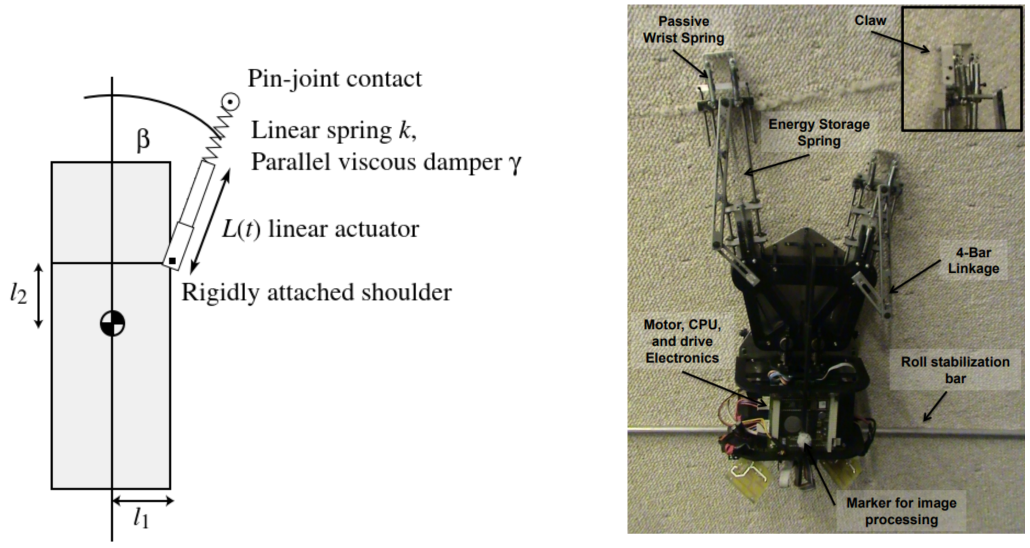

(A) The FG template for dynamic climbing.

(B) DynoClimber [56] bio-inspired climbing robot, based on the FG model for dynamic climbing.

FIGURE 2.18: The FG model for dynamic climbing and a robot designed based on this model.

2.4 Discussion

2.4.1 Current Gaps in Design of Climbing Robots for Reticular Structures

Through our review of existing literature, we have noticed several distinct gaps in our understanding and implementation of climbing robotic systems:

1. The contact constraints in climbing robots are often poorly understood (compared to cursorial robots) and often not used when considering the design of a robot, or in the control.[1]
2. Most systems are not tested or stipulated for structures that have the real features of our application environment, appear to be undertested, or very selectively tested on structures where success is ensured.
3. Multi-purpose prehensile end effectors that would enable robotic maintenance operations are underexplored.

---

[1] This is of course, not always true. There are examples of robots that utilise knowledge of the contact in their motion planning e.g., [42]

4. Most current implementations are characteristically slow moving, which is a barrier for having a robot perform useful work. In the authors experience, human workers can climb towers tens of meters high in mere minutes, where current robotic systems might take hours and require a human operator to supervise.

By identifying the deficiencies in the current approach, we tailor the development of our robot to address some of these gaps and develop a novel robotic concept. In the following section we will discuss how three limbs can reasonably be deduced as an appropriate number, and in the proceeding chapters discuss how we came to design the kinematics, and mechanics of a three-limbed climbing robot, as well as to begin exploration of appropriate footfall planning, trajectory planning, and control for this new form.

2.4.2 Three Points-Of-Contact

There is a persistent idea in legged-robot design that three points-of-contact are needed for stability, and therefore four legs are needed to account for the one in motion during any given step. This is of course true for cursorial, slow moving, quasi-static robots that use the well-known idea of a support polygon to ensure stability, and where the substrate being traversed is roughly normal to the gravity vector (i.e. on the ground); the latter condition being largely violated during climbing.

The inchworm concept counteracts this completely by demonstrating that even a single point-of-contact can be used to achieve full control of a system. It is easy to comprehend why. With the capacity to generate torques and forces in each of physical dimension (passively or actively), a robot is able to react any forces due to gravity, or through motion, that would cause system instability. That is, of course, as long as the forces generated do not violate the limitations of the adhesion mechanism, and herein lies the issue. We have in our research, found no evidence of consideration of contact constraints when selecting number of legs for legged robots. It seems reasonable where contact mechanisms like magnets, suction, and electrostatics are concerned that four or more legs should be used, due to their typical limited capacity for reacting contact torques. In general, engineers designing adhesion mechanisms must make smart use of geometry, that is to say, they need to be sufficiently wide to resist large contact torques typically resulting in bulky and heavy designs not well aligned with dynamic climbing principles [38]. Most climbing robots using position-based control strategies are also not cognisant of the forces they apply to the substrate during locomotion, and therefore cannot guarantee they will not encounter a contact-force limit violation. Designers can mitigate this risk by using a greater number of contact points, giving greater overall adhesion. This strategy is not as important where dynamic controllers (such as that implemented in section 5.5.2) are concerned, as contact-force limits for desired behaviours are programmable. Legged robots with small contact areas are also particularly susceptible to the “barn door” scenario during climbing, whereby they experience and uncontrollable motion around two contact points, which is easily mitigated with a third-point of contact.

Parrots on the other hand seem to regularly flaunt two or fewer points-of-contact during climbing and demonstrate that for a dynamic and well-controlled system the barn door scenario may be effectively mitigated with other, under-explored techniques, and even exploited where large end effector work spaces are desirable (see section 3.1.7). Dynamic legged robots like the MIT Cheetah 3 [57], or ANYmal [58], or any number of the cursorial bipedal robots have also shown that under-actuated robots, where the number of dimensions of force capable of being reacted through the end effectors is less than the DoF of the body, are able to dynamically stabilise, the caveat being active control is necessary at all times to maintain this stability. Whilst it is clear that climbing is possible with only three points-of-contact, several questions on how best to achieve this remain, including how to effectively mitigate the barn door effect? and how important are dynamic behaviours? Studying how parrots climb may hold answers to these questions and enable lighter, more mobile, and stronger designs for their mass.

The capacity to generate torques and forces at the contact point is a common feature of climbing robots. With evidence that inchworm robots are capable of climbing and being stable, controllable system with only a single point-of-contact, why then do most non-inchworm style robots choose four or more legs, especially considering that weight minimisation is still an important goal for a climbing robot? We do not have a definite answer to this question, but we believe it is simply due to the pervasive idea that three points-of-contact are necessary for stability.

2.4.3 Three Limbs

The three-point contact assumption is restrictive and superfluous in the climbing environment. Doing away with the assumption that three points-of-contact are necessary for stability, we now propose a three-legged climbing robot, with the goal of maintaining the weight minimisation features of the inchworm concept, but having the additional adhesion strength and lifting capacity of the other multi-limb systems. With a total of three legs, we are left with only two in contact, assuming we are attempting only quasi-static locomotion. We also make the observation that three-limbs for a climbing system capable of work, is not as uncommon as one might first imagine. It has recently been uncovered that the Parrot (*Order: Psittaciformes*) uses this precise form during climbing, foraging, and in social behaviours [1, 6, 7]. Whilst it is a common knowledge amongst bird keepers, watchers, and enthusiasts that parrots spend much of their time *clambering* about different structures, it has been largely ignored by the scientific community when studying the different forms of locomotion in animals. That is until this author suggested it was of interest for robotic development in [1], which was picked up by Dr. M. Granatosky and his team, a group of biologists at the New York Institute of Technology, who was inspired to study this model [5]. This paradigm shifting work is, to our knowledge, the first direct evidence of an animal having an odd number of primary limbs (i.e. used for propulsion) in locomotion, and the first quantitative description that measures the force profiles of an animal's craniocervical system and compares them to the legs to justify their classification as, or being used as, a limb.

With new inspiration from this unexplored form, and with a design philosophy inspired by nature and our knowledge of the gaps in the field, we explore the development of a parrot-inspired tripedal robot. First, in a simulated 2D environment, and then, in 3D with a simulation and a physical robot that at the time of writing, is undergoing initial testing for climbing trials in the lab. For these robots, we implement some rudimentary footfall planning techniques based on data we collect from live parrots, and explore different trajectory generation methods that are suitable for the task of climbing a simple ladder. This preliminary work lays the foundation for further exploration of tripedal climbing in the complex, reticular structures that make up a significant portion of the infrastructure in the energy, telecommunications, and space industries.

Chapter 3

Design Principles

Since there are no current robots that demonstrate the full suite of capabilities we desire, we thought it prudent to first develop a set of design principles that we could use as a guide in designing RSRs. In this chapter, we present those principles. We begin by looking to nature, where adept and capable animals have used their climbing prowess to master their environments. In our journey through biological literature, we uncover seven lessons that we distil into tangible principles for use in robotic development. Next, we look to our focus environment, reticular structures, and create a robot agnostic framework that details a set of necessary capabilities for the development of RSRs, on the observation that many robots that have been studied previously have had an incomplete set of climbing behaviours when compared to their biological counterparts.

3.1 Lessons From Nature

To gain some insight into the fundamentals of climbing for robots, it is wise to draw inspiration from a diverse range of sources, including where successful designs have flourished, and been tested and proven to work via the process of natural selection. Bioinspiration in robotics refers to studying animals to understand the principles of their success, with the goal of translating those key principles to robotic design. In the context of transmission tower maintenance, it is likely that the robot will have to be sufficiently large to reach between the sparse structural members and sufficiently powerful enough to manipulate tools and locomote in a timely and efficient manner. Furthermore it is very likely that the robot will utilise arms and legs for locomotion with an encompassing grasp to adhere to the structure. For this reason, a good group of animals to target initially are hominoids. As per Figure 3.1, the Hominoidea super family consists of humans, bonobos, chimpanzees, gorillas, orangutans, and gibbons, all of who are known to be good climbers. Of these, gibbons will receive significant focus as they are the most arboreal and have been stated to be the only ones capable of true brachiation [59]. Brachiation was defined by Hollihn [60], as "continuous bimanual suspensory locomotion that is neither interrupted by other positional behaviours nor given added support from the tail or hind limbs". Whilst it is unlikely that a brachiation gait will be implemented in an industrial robot in the near future, gaining an understanding of the behaviour and assessing how this behaviour affects the gibbon climbing style may give as valuable insight into the principles of their success. As stated by Laschi and Mazzolai [61],

> "The development of physical structures and behaviours that are more similar to those of living organisms can help robots to better negotiate real-world environments and accomplish real-world tasks".

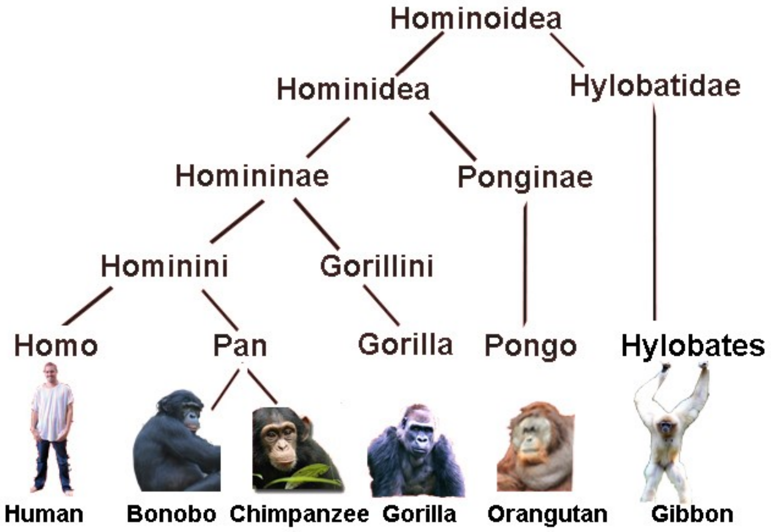

Figure 3.1: Hominoidea Family Tree. Source: [62].

3.1.1 Centralised Mass Distribution

It can be noted in all hominoids (and many other animals) that there is a proximal (close to body) to distal (away from body) distribution of muscle mass along each of limb. This can easily be observed in human arms and legs, with the bigger muscle groups being located nearer to the centre of mass than the smaller. Whilst it is observed in most animals, this distribution is exaggerated in the gibbon limb [63]. In gibbons, this is observed especially in the forearms, with the actuators for the fingers being located significantly further away from the wrist compared with other hominoids. The radial shafts in the gibbon forearm are also sagittally (toward the centre plane) thicker, which is a feature seen only in gibbons, even compared to other brachiating animals such as the spider monkey [59]. Figure 3.2 illustrates this point. This distribution is present in far more than just mammals, however. The limbs of arthropods, birds, and fish all seem to mimic this distribution. Take the hind limbs of a grass hopper as another example. The legs are characteristically thin compared with the body, and upon close inspection, the same distribution can be observed. Looking at the caudal fin of a fish, the tail tapers down before expanding out into the large lightweight fin meant for pushing water.

Figure 3.2: A gibbon. Source: [64].

Analysing this from a physics perspective, it can be observed that distributing the mass in the forearm to push it closer to the shoulder around which it pivots reduces the moment of inertia in the arm. During both climbing and brachiating, work is being done constantly in accelerating and decelerating the arms. To make this as energy efficient as possible, the moment of inertia of the arm should be reduced as much as is practicable. To take this further and into the realm of robotic development the first lesson can be summarised as thus:

The moment of inertia of any limb that experiences frequent angular acceleration should be as low as practicable.

3.1.2 Power-To-Weight Ratio

Whilst it is important to reduce the inertia of rotating components for the sake of efficiency, the mass of a vehicle and its ability to accelerate should also be properly considered. Typically, a high power-to-mass ratio correlates well with good dynamic abilities, and in general, mobile robots need greater power-to-weight ratios than their static industrial cousins. Reducing mass, whilst maintaining a robot's power and strength will only increase the mobility and endurance for that machine.

The major feature that animals have that allow them to be so light and strong are their muscles. Natural muscle has a very sophisticated design when compared with actuator technology used in modern robotics. They are light, strong, have adjustable compliance, built in sensory feedback, and are exceedingly scalable. The human body alone has approximately 650 skeletal muscles [65], and several million micro-muscles distributed on the skin and hair follicles. These muscles work synergistically to actuate the human skeleton in the 244 degrees-of-freedom present; although, biomechanists will often idealise this in simpler models when analysing internal forces or simulating movement [66]. This level of complexity in a robot is unheard of, primarily because the mechanical design, control complexity, and overall system would be overwhelmingly complex. Even if a mobile robot of this kind were attempted with our current actuator technology the robot would end up being so heavy it would be unlikely that it would be capable of substantial locomotion.

This principle of having a high power-to-weight ratio is even more important for scansorial robots as it is for cursorial robots. This is because the scansorial robot must be capable of accelerating its mass directly against gravity. This is reflected in nature by the rare occurrence of heavy arboreal animals. The largest animals that are capable of climbing we have encountered are the lowland gorillas, with the weight the largest found in our research being 211 kg [67]. Although these gorillas are capable climbers they do not do so without great need, are relatively slow at it, and can hardly be considered arboreal spending the majority of their time on the ground. More arboreal animals like the orangutan (*Pongo Pygmaeus Abelii*) are on average much lighter, with the average weight of the adult animal in one study being around 50 kg [68]. Highly arboreal animals such as the gibbon who live their whole lives in trees, and who depend on being capable climbers to reach food sources are much lighter. The average mass of the gibbons in one study was just 8.3 kg [63]. Whilst the discussion from an evolutionary perspective on why these animals are lighter than their cousins is out of scope in the engineering discipline, biologists have noted that "the lightweight gibbons climb more easily than the heavy great apes" [68]. This is something that we can take on board in our designs, and so the second lesson can be stated as:

A lightweight design will increase the chances of achieving a successful and capable climbing robot.

Jusufi et al. [47] describe this to be a requirement of all climbing robots, but the reason for it really lies in the scalability of robotic mechanisms which is discussed by Waldron and Hubert [69]. Summarised, an increasing proportion of power is needed to power larger and larger vehicles. For cursorial robots, ground impacts and reaction forces drive locomotion. As the robot gets larger so do the forces associated with locomotion. These forces scale proportionally to the mass. Inertia on the other hand increases at a faster rate than mass for a fixed density object, since mass scales to the third power of length, and inertia to the fifth. As such, larger machines and animals must be comparatively slender to maintain the same agility as a smaller machine or animal.

3.1.3 Pendulum-Like Motion

Pendulum physics and control methods for pendulum systems is a well-documented and researched field. In robotics, this research has often been applied in the design of walking machines and legged locomotion. Recently, work has been done to demonstrate the usefulness of pendulum dynamics in climbing robots [53, 52]. As stated earlier, animal locomotion is often facilitated by the periodic motion of the animal's limbs. Whilst before we discussed how from an energy perspective reducing the inertia of the limb relates to a proportional decrease in energy expenditure accelerating and decelerating the limb, here, we discuss how design of a system considering the natural frequency of the pendulum can further compliment the reduction in energy costs for locomotion.

Whilst this concept in relatively intuitive, further information can be extracted by observing this in nature. Perhaps the most pendular form of locomotion found in biology is brachiation. This behaviour is most notably found in the highly dynamic and arboreal gibbon. Many researches have attempted to model gibbon brachiation with a simple pendulum model, however more recent research has shown this to be inadequate in describing how gibbons locomote with such low energy costs [70]. Instead, researchers modelled in two distinct brachiation gaits, (1) continuous-contact brachiation and (2) ricochetal brachiation. The difference being that in continuous-contact brachiation the CoM makes a series concave arcs whilst in ricochetal brachiation the CoM path remain tangential and continuous during both contact and aerial phases. These models are still not accurate enough to accurately describe how gibbons utilise brachiating efficiency in such irregular environments, but according to the research, the locomotion should have close to negligible losses, indicating that gibbons have indeed maximised the utility of this locomotive style [59, 70]. In engineering, we know that this should only be possible if the gibbon's swing period is performed at frequencies close to or matching their natural frequencies. This is well stated by Waldron and Hubert [69] who wrote that, "Forcing a pendulum, such as a leg, to swing at frequencies far from its natural frequency is energetically expensive". Whilst the biologists continue to work on suitable models, engineers have already begun trying to mimic this behaviour in robotics [71, 72, 73, 74]. The principle derived in this section can be surmised as:

To ensure efficient locomotion, the required velocity of the robot should agree with the dynamics of those portions of the body that experiences regular acceleration and deceleration for locomotion.

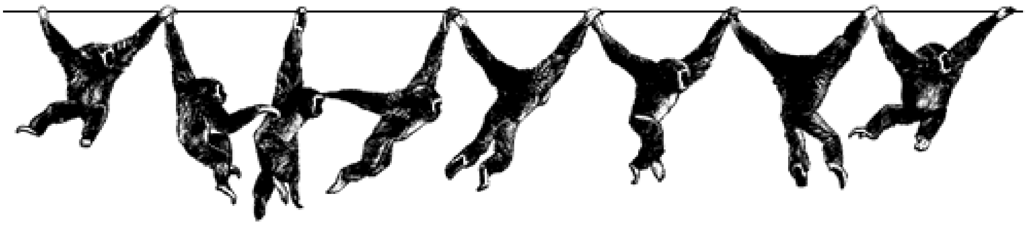

Figure 3.3: Brachiating Gibbon. Source: [75].

3.1.4 Gait Versatility

A feature that makes hominoids such versatile creatures is the adaptability of their locomotive gaits to irregular and complex terrains. They are also able to use the same morphology to implement different gaits depending on how fast they want to move and for what purpose. In robotics, this ability is often realised in reconfigurable machines [76], whereby the machine is able to change configuration in response to different functional demands. A good example of this for climbing is the ability of hominids to use either a flexed elbow or extended elbow climbing gait depending on the diameter of the substrate. As the name suggests, flexed elbow climbing is where the elbows are flexed (bent) during climbing. This style of climbing is used on thin substrates, where the animal has the ability to grasp the substrate with a single hand [68]. Extended elbow climbing is where the animal utilises its long arms to lean back away from the substrate, putting the arms in tension and moving the CoM away from the substrate, as described by Webster et. al. in [1]. Being able to hold the CoM away from the substrate increases the reaction forces at the contact points and allows the animal to utilise friction for locomotion. The high intermembral indices of the apes were inferred to be linked to this style of climbing, as the long arms allows the larger apes to climb greater diameter trees than smaller arboreal animals like the cercopithecoids (monkeys) [77].

It is also often seen in cursorial mammals (including humans) that the gait used for walking can be represented as an inverted pendulum system, and for running they switch

FIGURE 3.4: Gibbon using a bipedal gait. Source: [78].

to a spring-based energy exchange system [70]. Research has been done to mimic this in many robotic platforms, although mostly either one or the other gait is focussed on. Unfortunately, to date this has only been the case on surfaces with reliable and predictable contact points. In a complex 3D environment this is not the case, and robots and animals alike must adapt their locomotive behaviour in order to be successful. This ability has applications in cursorial robots as well where terrain is particularly rough, for example rough mountainous terrain where some level of climbing may be exhibited, and large degrees of variability in the terrain prevent a steady locomotive gait. Whilst animals are capable of implementing locomotive gaits at irregular frequencies and strides in order to accommodate the substrate, robots are typically less capable, though it is an active area of research [79]. In order gain some insight into this behaviour, we will review the literature on how it is characterised in gibbons. During brachiation, gibbons are far better adapted to changing stride length and frequency than compared to a running in a terrestrial animal [70].

During ricochetal brachiation, gibbons exhibit exceptionally smooth trajectories as they propel themselves from branch to branch. How they do this, seemingly effortlessly, in such a complex environment is still an underexplored area of research; however, some evidence for the remarkable adaptability is present in their approach to vertical climbing. Vertical climbing is also of greater interest in this thesis as a behaviour we are developing. During vertical climbing, it has been observed that gibbons exhibit an exceptionally uneven and irregular gait compared with all other hominoids [80]. Most animals will exhibit certain patterns during climbing, favouring a continuous diagonal (Rh, right hind; Lf, left front; Lh, left hind; Rf, right front) or lateral (RhRfLhLf) sequences. Instead, the gibbon will continuously vary between these patterns with occurrences of three legged strides in between. Whilst the exact cause of this gait variance was not identified, it has been stated that the gibbon's climbing style is heavily influenced by the adaptations that allow for such graceful brachiation [68]. Furthermore, gibbons are known to string together sequences of quadrupedal, triplet, bipedal, and bimanual gaits during locomotion in complex environments [81]. Whether their irregular climbing gait hold some implication that they are better adapted to irregular environments is not known. Though, certainly the ability to use a range of gaits in sequence provides more freedom to move as they chose, and this is the lesson we can take from them. From the evidence provided and the resources analysed the lesson we take from this is:

> *Multi-gait and configurable robots that are capable of quickly and fluidly adapting locomotion type to the task at hand, are more likely to be capable of performing in complex and irregular environments.*

3.1.5 Tail Utility

From the spider monkey to the kinkajou, many taxa of arboreal specialists have evolved prehensile tails that can support the entire body weight of the animal during climbing. This is also true for reptiles such as chameleons, that curl the tail to provide an additional anchor point. Moreover, research of highly dynamic vertical climbing at up to 30 steps per second also reveals that geckos can utilize rapid tail reflexes to compensate for foot-substrate perturbations imposed by challenging terrain [45]. Tails are known to be used for balance in primates [82] and cats. They are also used in leaping lemurs [83], assisting in aerial phases during such transient acrobatic manoeuvres carried out by prosimians following a running jump onto a tree trunk [84]. Caudal appendages also offer a location for a proprioceptive sensor to obtain spacial information while navigating a highly three-dimensional environment. The function of tails in mammals was well documented by [85], and includes mechanical, communicative, defence, and physiological functions. This has not gone unnoticed by the engineering community with much research being done to study and mimic the effect for robotic development [45, 47, 86, 87, 88, 89, 90, 91]. This research includes studies on, cheetahs, kangaroos, kangaroo rats, geckos, agma lizards, and spider monkeys.

For platforms that rely on dynamic stability to climb and overcome challenging terrain such as discontinuous supports, it is advantageous to consider capabilities for active redistribution of mass. This allows for modulation of the moment of inertia about chosen axes of rotation, allowing a robot to rapidly change from a stable mode to a manoeuvrable mode. For this purpose, the addition of a fifth appendage to a chassis was proposed which would facilitate rapid rotations about a chosen axis. Model predictions indicated that even a simple two-link system (i.e. body and tail, see [47]) with a two degree of freedom joint enables effective attitude control of the body without the need for external work. Such a system can maintain rotational control authority in the absence of an environment on which it can generate reactive forces. An airborne animal or robot could thus maintain control authority at zero airspeed or high angles of attack, where lift-based control mechanisms can generate little or no force. The utility of an inertial appendage extends beyond the aerial rotations however.

Undesired angular momentum injected by disturbances could be temporarily directed to the appendage, allowing the body to remain stable until substrate interactions allow dissipation of the perturbation energy. In this spirit, terrestrial or scansorial robots could use a tail as a control structure to generate transient torques to maintain body attitude in the face of unsteady or unpredictable surface forces [47]. Implementation of these biologically inspired principles has resulted in more robust platforms that can leap onto vertical substrates [92]. Beyond tail assisted pitch control in overcoming perturbations on level ground, novel platforms employ rigid and compliant legged leaping and demonstrate the utility of tails for simplified control of appendages for inertial reorientation [88, 92].

Challenging vertical substrata (e.g. tree bark and fences) were scaled by the RiSE robot [24] which incorporated bioinspired principles of locomotion. These included a tail that prevented pitch-back and compensated for substrate disturbances (e.g. debris). Pitch-back prevention was also noted by Norbeg in climbing treecreepers [93], representing another useful application for tails. From studying tails in animals the following principle is derived:

Incorporating a tail in the design of a climbing robot can give it added mobility, stability and increase its performance and function.

3.1.6 Multi-Function Limbs

Parrots, monkeys, apes, and in-fact most animals develop some capacity for manipulating the world around them, whether it be with their mouths or dedicated appendages. In the case of a birds, it is a little of both. Birds have developed enhanced capabilities with their craniocervical system, which has been said to operate as a "*surrogate forelimb*" [94], that takes the place of traditional forelimbs which lost that capacity when they specialised for flight [8]. The necks of parrots have developed especially for their role in tripedal locomotion [1, 5, 8, 6]. Further to this, parrots also use their neck and beaks for foraging, nurturing, fighting, playing, and solving puzzles [9]. Interestingly the multi-function capacity of limbs is not something as commonly observed in robotics. Challenges involving the design of grasping mechanisms, and in the intelligence to manipulate an object to one's benefit likely contribute to this. Without a doubt though, having limbs that can serve multifunctions is an effective way of reducing overall mass, complexity, and energy usage.

3.1.7 Additional Cases for Static Stability During Climbing

Arboreal animals give us some insight into how we might develop robots to operate in sparse vertical structures, especially where interaction with the structure is facilitated by an encompassing grasp. Vertical structures, especially sparse ones, allow us to observe some new cases of static stability when compared to cursorial animals. Due to the the differences in the forces producible at the substrate interface, a more diverse range of stable postures are available to us in vertical structures. These for example, include:

- Perching, which is analogous of standing, which usually considered an unstable state that must be dynamically compensated for, is perfectly stable where a torque can be developed at the contact.

- Cantilever/Clinging, especially where the contact points are aligned with gravity is statically stable as the two contact points can resist forces both in and out of the structure. When the feet are in line with gravity, this also allows for easy rotation around the axis through the contacts, as any producible torque at the wrist will result in motion.
- Hanging, is a another stable orientation. Where the feet are aligned and the hanging is pendulous, any small amount of torque that can be produced at the wrist will have the capacity to damp out osculations. Where the feet are not aligned, this stable condition can allow for significant force production as the stance becomes triangular (when drawing line between the two contact points and the CoM).

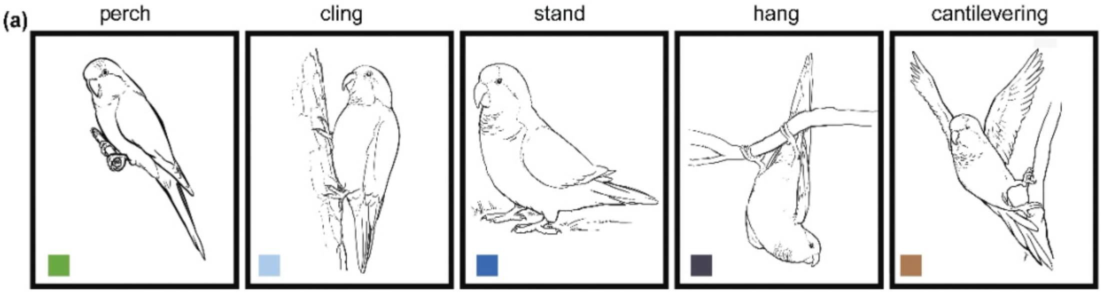

Figure 3.5: Postural behaviours of the monk parakeet [6]

Utilisation of these additional static stable orientations has strong implications for the development of legged robots, where producing a stable dynamic system is often one of the main points of contention. These statically stable position can be utilised to reduce control effort and improve force production capabilities for the purpose of maintenance works in reticular structures. It should be noted that with sufficient capacity to generate wrenches at the contact points, that any orientation could be stable as instability in the context of bipedal systems is usually due to their underactuation, which is due to the limitations of wrench production at the contact points. So in this context, when we are discussing stability, we mean to say that certain poses are favourable an minimise the forces necessary to produce at the contacts, where other poses may exceed the contact force limitations resulting in undesired or unstable motion.

3.2 Motion Primitives

In order for animals to specialise in reticular structures, it has been necessary for them to evolve many strategies to overcome the vast diversity of substrates they have to interact with. Roboticists on the other hand, take a comparatively narrow view when designing structures for their robots to climb on, that are often substantially different from application scenarios. In this section, we propose a new framework for breaking down reticular structures into their constituent parts, and suggest that if any entity can perform a basic set of motions over these constituents (motion primitives) than they should be capable of climbing any reticular structure as a sequence or combination of these primitives.

The constituent elements of reticular structures, and the motion primitive defined along them are outlined in Table 3.1, and discussed in the following paragraphs. The categorisation of reticular structure constituents here is preliminary work that is yet to be validated. Usefulness of this specific breakdown of primitives will be the subject of ongoing investigation, both in evaluating the motion strategies of animals and in the design of RSRs. The starting point for the breakdown of motion primitives is based on assumptions informed by changes in motion strategies of animals. This is a grey line; however, as even the definition for the term 'climbing' is still under debate in biology [7]. Each primitive described in Table 3.1, represent a set of cases. For example, motion primitive, M1, is likely to be significantly different for an entity to climb based on the direction the beam is pointing with respect to gravity. As it is hard to predict how or if an entity would need to change strategy based on the orientation of the substrate, then general category of substrate is defined, and it is assumed that for an entity to be successful for any particluar motion primitive, it could do so in any orientation.

Motion primitive, M1, is concerned with motions along a solitary beam, where all contact with the substrate is facilitated through the solitary beam. In navigating this beam, the primitives are broken down into two subcategories: a) along the beam vector normal to its cross section (Figure 3.6a); b) rotating around the beam vector (Figure 3.6b), for example transitioning from below a structure to above it. Whilst real motions might be a combination of these primitives depending on the orientation, the full primitive is fulfilled by showing the capability for each sub-primitive independently and in any orientation.

ID		Description	Figure
M1		Solitary beam	3.6
	a.	Parallel to beam vector	3.6a
	b.	Radial to beam vector	3.6b
M2		Transfers	3.7
	a.	Beam-to-plane transfer	3.7a
	b.	Beam-to-beam transfer	3.7b
	c.	Plane-to-plane transfer	3.7c
M3		Moving on a 2D plane	3.8
M4		Locomotion through a reticular structure	3.9a
		Complex locomotion through a plane	3.9b

Table 3.1: Motion primitives along the constituents of a reticular structure

This motion primitive is important especially for sparse structures where the likelihood for entities to periodically have a single beam for support is increased.

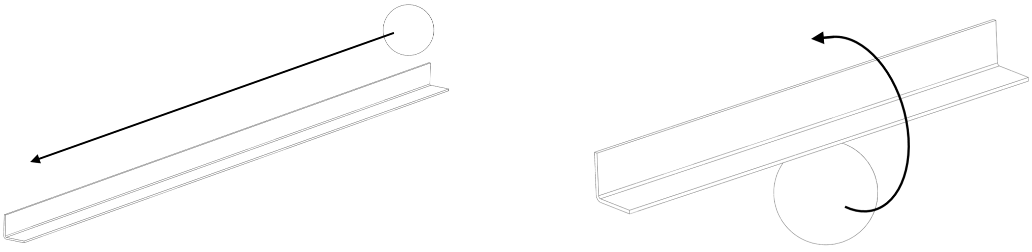
(a) (b)

Figure 3.6: Motion primitives M1(a) and M1(b)

M2 (Figure 3.7) describes various types of transfers, i.e. from plane to plane, from beam to beam, and beam to plane or vice versa. These primitives highlight how strategies change during the transition between substrates where a continuous gait might be feasible. Plane to plane transitions are rarely studied in climbing robots, though not unheard of [95, 96], with the literature focusing primarily on continuous motion up a continuous substrates. Most demonstrations start with the robot on the substrate and end when the robot has traversed the extent of it. Plane transitions can greatly increase the utility of a robot as it allows for less direct interventions from the user. To the author's knowledge, beam to plane transition of a robot capable of continuous locomotion of a beam elements and a sparse 2D plane is not found in the literature. Beam to beam transfers are common for the inchworm style robots discussed in section 2.1.1.

M3 describes simply moving along a sparse planar structure that has the majority of the surface removed. Little in the way of research has been conducted on these structures in robotics, with the closest analogue being locomotion over rough terrain [97]; however, these scenarios are often different in that the contact model is that of a cursorial robot relying on friction and reaction forces, rather than one of more of the many adhesion principles discussion in Section 1.2 for climbing robots. Where the gaps in the sparse 2D substrate are sufficiently small, an alternate strategy for contact has been explored in arthropods [98] that use hairs as one way hooks to catch edges. This strategy only works where the mesh is relatively fine and the gaps relatively small. For large sparse structures, we believe the best strategy is careful footfall placement. A simple example of traversing this kind of structure is climbing a simple ladder, which has been attempted in robotics on numerous occasions [26, 99, 100, 2]. Another example is traversing below the structure be means of brachiation which is a locomotive mode common to the gibbon as discussed in Section 3.1.3. An example we found no evidence of, is traversing across sparse horizontal structures from above the substrate.

M4 are climbing behaviours in any direction with respect to gravity that utilise any member of the reticular structure. This primitive is perhaps the hardest to categorise, as there is perhaps an infinite diversity of configurations the space could take. How an entity might address this primitive on the other hand, need not be infinite, as the condition this primitive imposes is that the structure is dense enough such that an entity could reach multiple diverging members. Were the members more sparse, the entity might need to default to M1 or M2. This motion primitive is what we would call a ‘true 3D climbing behaviour’, and in some sense can be thought of as a continuous M2 where by all actions are transfers between different planes, making regular gaits difficult to achieve.

3.3 Summary

This chapter drew on the biological literature to develop design principles that guide our design approach. These principles are based on tangible mechanical principles and are shown in animals to be utilised with strong effect. By making clear these principles, we define some guidelines for the design of climbing robots for reticular structures. When

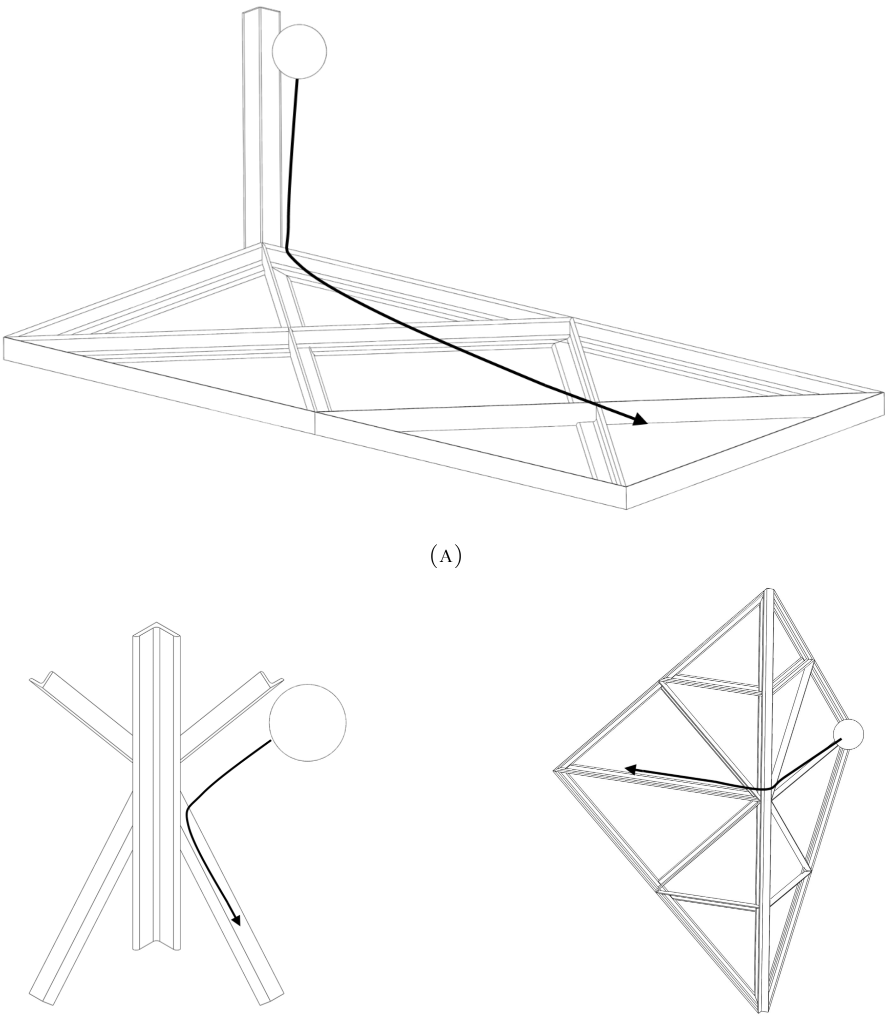

(A)

(B)

(C)

Figure 3.7: Motion Primitive: Transfers. Each different transfer could represent a distinct change in locomotion characteristics for a given entity.

considering the design of a RSR, the locomotive repertoire of the robot is constrained by the environment and should be carefully considered. For this reason, we break reticular structures down into basic elements and define motion primitives along these elements. In the next chapter, we will dive deeper in to the tripedal behaviours of cockatiels, a species of small parrot endemic to Australia, as they perform the planar climbing manoeuvre (M2) on a simple ladder.

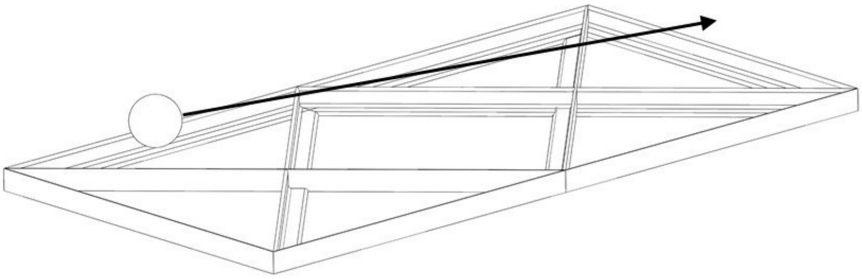

Figure 3.8: Motion along a sparse 2D plane.

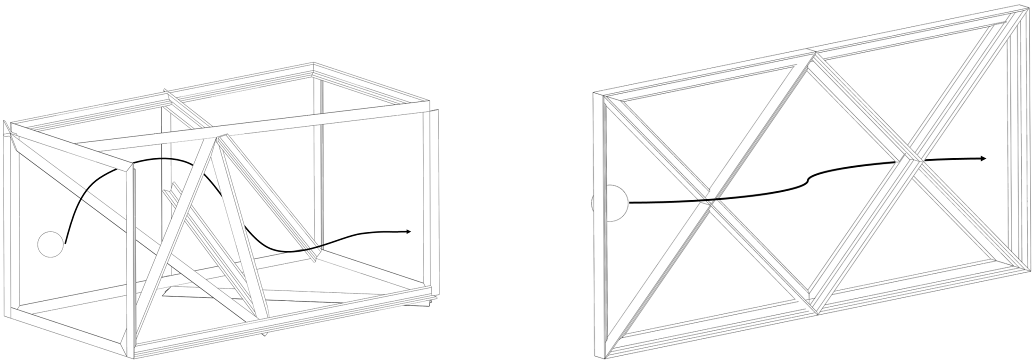

(A) (B)

Figure 3.9: True 3D motion in an irregular sparse structure.

Chapter 4

Bioinspired Tripedal Climbing

In the previous chapter, we have proposed many lessons that we can learn from nature. Unfortunately, tripedalism is an underexplored area of research, and so in this chapter we present our own *in vivo* experiments on cockatiels and gather more data to help us understand the intricacies of this intriguing form of locomotion. First, however, we will present a short background on tripedalism in the biological literature. Tripedal locomotion, whereby three limbs are used for continuous legged propulsion, is not commonly seen in the animal kingdom. Hunt et al. [101] documented tripedalism in primates whilst one limb is encumbered, and Isler [80] mentioned that gibbons occasionally display tripedal sequences during vertical climbing; however, in gibbons this appears to be a function of the highly variable hindlimb pattern as opposed to being deliberate continuous tripedalism. Vereecke et al. [102] documented tripedal sequences in the running and cursorial walking gaits of gibbons, though only as part of a larger quadrupedal gait. Dilger [103] acknowledged that parrots use their beak to assist in climbing, making special mention of a diagonally downward climbing behaviour, where the parrot grasps with its beak before swinging both hindlimbs downwards and sideways. Hartman [104] recognised that parrots have "fair-sized" legs and tend to make "good use" of them but does not specifically mention climbing as a behaviour. Marek et al. [94] noted the unparalleled versatility of the avian neck design, and suggested that the craniocervical system acts like a "*surrogate forelimb*", but does not specifically mention parrots, or climbing. The first study to look seriously at tripedalism in parrots was published by Young et al. in 2022 [6], which was inspired by observations from Webster et al. [1]. It is still, however, an open question in biology as to what capacity parrots use there craniocervical apparatus (neck and beak) during climbing behaviours. To shed some light on this, and to ensure our understanding of their behaviours are not misinterpreted, we endeavor to discover more about tripedalism in parrots by addressing two important questions: (1) When do parrots exhibit tripedalism?; (2) Is this behaviour fundamentally different with respect to quantifiable limb cycle characteristics?

4.1 Materials and Methods

4.1.1 Data Collection

The climbing structure (Fig. 4.1) was designed to simulate one of the most fundamental properties of a reticular structure, its discontinuity. To emulate this property, we chose a ladder. The regularity of this particular reticular element was chosen to reduce the variability we might see should the bird be climbing something more disordered. The ladder was capable of being set at any angle from 0 – 90° (vertical). For our study, 10° increments from 45° were chosen leading to angles of 45° , 55° , 65° , 75° , and 85°. The inclination of 45° was chosen as a starting point based on the standard definition for vertical climbing put forth bu Hunt et al. [101]. The 10° discretisation was chosen arbitrarily as a steady increase that would allow us to derive some relationship between behaviour and inclination. This research was approved by the University of Technology Sydney (UTS) Animal Ethics Committee (Approval no.: ETH17-1629). Eight birds climbed the ladder ten times for each inclination. One instance of a bird climbing the ladder is referred to as a 'run' for the purposes of this work. Birds are recorded with a PtGrey BlackFlyS USB3.0 camera, recording at 150 Hz with a resolution of 1440x1080. The code to run the cameras was written in C++ and developed in-house using the Spinnaker application programming interface (API) provided by PtGrey. The camera was placed behind the ladder to get a single view of the desired limbs and the intrinsic matrix was calibrated using a checkerboard and the camera calibration app in MATLAB. The camera pose with respect to the ladder was calibrated using MATLAB's `estimateWorldCameraPose` function based on the manual selection of known points on the ladder.

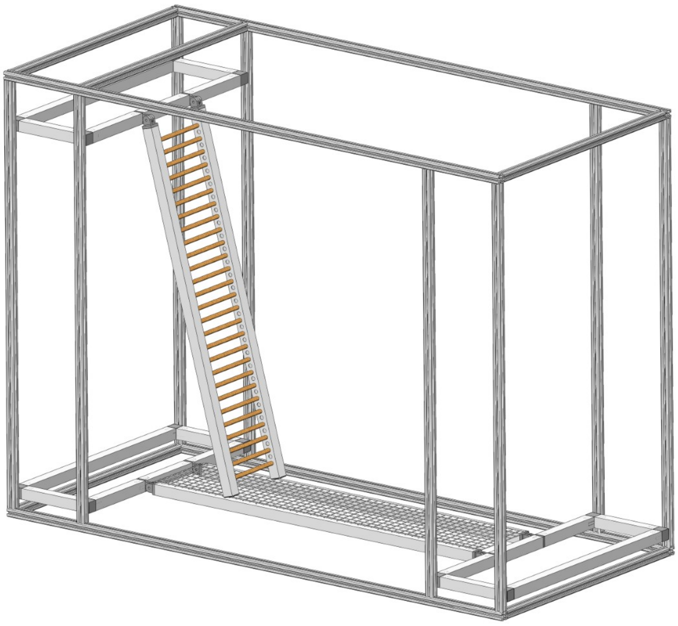

Figure 4.1: Render of the adjustable inclination climbing structure. The main frame is constructed from 20mm T-slot aluminum extrusion, with external dimensions 1390 x 640 x 1040 mm. The ladder and plate forms are made from 25.4mm aluminum SHS. Ladder rungs have a spacing of 30mm and are made from ⌀9.5mm Tasmanian oak rod. The ladder start and end platforms are fix with a wire mesh.

Little to no motivation was necessary to get the birds to climb the ladder as they seem to naturally desire to ascend. Birds were always kept in pairs, such that the other bird was often waiting near the top of the ladder, or such that the ladder was the most convenient path out of the enclosure. The birds had the ability to fly if they chose and were often observed to do so the first and second time they were placed in the enclosure. After this, the birds' temperament seemed to settle, and they opted for walking/climbing. The ladder measured 150 mm between the inner edges of the square-hollow-section (SHS) vertical members, and measured 780 mm between the first and last rung. Each rung was made from ⌀9.5 mm Tasmanian oak dowel rod and spaced 30 mm apart. Rung spacing was chosen arbitrarily, though it is noted that outstretched foot of the birds was not capable of passing through the 30mm gap without meeting some part of the structure, and that a single stride of the bird could encompass multiple rungs.

4.1.2 Data Processing

DeepLabCut [105, 106] was used to track the feet, beak and two body points on the birds (Fig. 4.2). The network was trained using twenty frames from each inclination recorded, for each bird, to give a reasonable representation of the dataset. Frames were selected using the k-means clustering function built into the DeepLabCut program designed to give a good spread of scenes representative of the data. Counting individual frames, approximately 0.17% of the dataset was marked manually for training the network. The results were filtered in MATLAB using a variety of techniques based on the noise observed in the data.

Temporal data for the limb contact sequences were marked manually with assistance from a custom MATLAB script. Frames corresponding to instances when limbs would touch-down or lift-off from the ladder rungs were labelled for analysis. The temporal data was segmented into bipedal sequences (referred to as cycles) for the measurements of cycle duration, duty factor, and stride length. Due to large variability in sequential cycle-durations we marked the cycles twice. Initially, treating the touchdown of the left foot as the gait start, and secondly treating the right foot touchdown similarly. This was done as measurements of the duty factor are inconsistent for the trailing foot when the cycle duration varies from stride to stride. Cycles were rejected if the bird slipped, stopped, or otherwise behaved inconsistently with steady locomotion. The cycle was marked by the touchdown of the lead foot (either left or right) and ended at the touchdown of the same foot proceeding the completion of the trailing foots swing phase. In approximately 5.4% of the beak-supported cycles, the lead foot would have a second swing phase before the trailing foot completed its swing phase. These ‘double step’ sequences are excluded from our analysis of the cycle metrics. For the purposes of this work, the tripedal cycle is defined as any cycle where any support from the neck and beak is oberserved. As there was often some overlap for transition between bipedal and tripedal cycles, a cycle was considered tripedal if it had support for more than ten frames (66.7 ms) for any given cycle.

FIGURE 4.2: Points tracked using DeepLabCut. Beak: Dark blue, Torso top: Yellow, Torso bottom: Red, Left foot: Green, Right foot: Blue

4.2 Simplified Kinematic Model

In order to interpret the limb function during bipedal and tripedal climbing, a simple 2D kinematic model (Fig. 4.3) is used to represent an idealisation of the birds in their coronal plane. Templates for locomotion have been derived for hexapods and quadrupeds [107] and have resulted in simplified models that have informed the design of legged robots. The model we present here is not intended to be a template for locomotion in parrots, but is intended to be a stepping stone to test hypotheses until further analysis reveals an informed template. In this model, we wish primarily to represent two things: 1. the orientation and motion of the body, 2. the orientation and extension of each limb with respect to the body. The model is designed around an idealisation of the bird's skeleton, with the body being represented as a fixed length rigid link, the two hindlimbs extending from the base of the torso (approximately the hips) and the neck extending from the top of the torso. A fixed length torso is appropriate as birds are unique among vertebrates for having a fused thoracic vertebra and synsacrum, resulting in little to no articulation along the vertebrae between the fore and hind limbs. This fusion is thought to be an adaptation for flying [108]; however, it is also remarkably convenient for our robotic models, and is in stark contrast to the locomotion of quadrupedal vertebrates where articulation along the vertebrae between the fore and hindlimbs has significant functional implications [109, 110, 111, 112]. Whilst Raibert [113, 114] used symmetry in quadrupeds to reduce the template to the minimalistic spring-loaded inverted pendulum (SLIP) configuration, and Schmitt and Holmes [115, 116] developed the analogous lateral leg spring (LLS) template studying insects, the same templates might not be appropriate to represent the climbing parrot. We suspect this due to the apparent asymmetry we have observed in the hindlimbs during tripedal climbing behaviours. In Section 4.3 we investigate the presence of this asymmetry with respect to our model. As an approach, we believe it to be prudent not to assume symmetry is present as it is in most polypeds, until motivated by the data to do so. It is also unclear how the craniocervical system in the parrot ought to be modelled. Hindlimbs have been modelled as a spring-mass system in most legged animals [117]; however, the neck of the parrot may not share the same properties given its fundamentally different morphology to vertebrate hindlimbs. Investigation into whether the neck can be modelled using a SLIP, LLS, or other analogous model is not in the scope of this work, though some initial models are being explored [118].

4.3 Results

4.3.1 Transfer From Bipedal to Tripedal Climbing

As previously stated, tripedalism is defined as beak-assisted bipedalism for the purposes of this study. That is, each cycle is defined by the bipedal sequence of the hindlimbs. Figure 4.4 shows the transition from bipedalism to tripedalism with respect to the ladder inclination for each bird with a logistic regression mapping the mean transition for all birds. For each inclination the percentage of observed cycles that were tripedal are recorded from the total valid cycles observed. All birds show a marked increase in beak utilisation as the inclination increases. There is noticeable intraspecific variation across the specimens used; however, we are unable to comment on the relative magnitude of variation due to a lack of prior studies. Unfortunately, data on the birds age and gender were not available, and no factors we are aware of readily explain the variation. Data was taken in highly dynamic environment, as the cage and climbing structures were somewhat open to the elements,

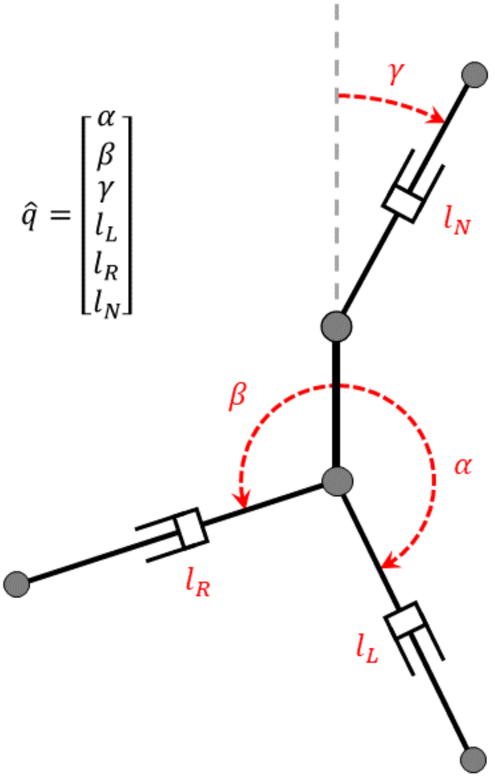

FIGURE 4.3: Simplified 2D bird kinematic model. Limbs are represented as prismatic joints (l_L,l_N,l_R) with revolute joints (α,γ, $beta$) at their base. The body is treated as a link of fixed length.

being covered only by a tarp during rainy days. Future work could contain birds to a more controlled environment to understand if some of the variability could be explained by the environmental conditions.

The finding that tripedalism increases with the substrate inclination is expected. It is unexpected how gradual this transition would be. Birds often seemed to at random lean down and contact the structure with their beak with no clear marker or indication that it should be necessary. What we can say with confidence is that as the substrate inclination increases, parrots' tendency to employ their beak for additional support increases until locomotion is consistently tripedal. Only one bird continued to show instances of bipedalism at the steepest inclination tested (85°). We consider this to be an aberration, yet evidence of the bird's remarkable ability to climb and balance dynamically on only two limbs during steep inclinations. This may be evidence of the principle discussed in Section 2.4.3, whereby the additional degrees of control enacted by torque production about

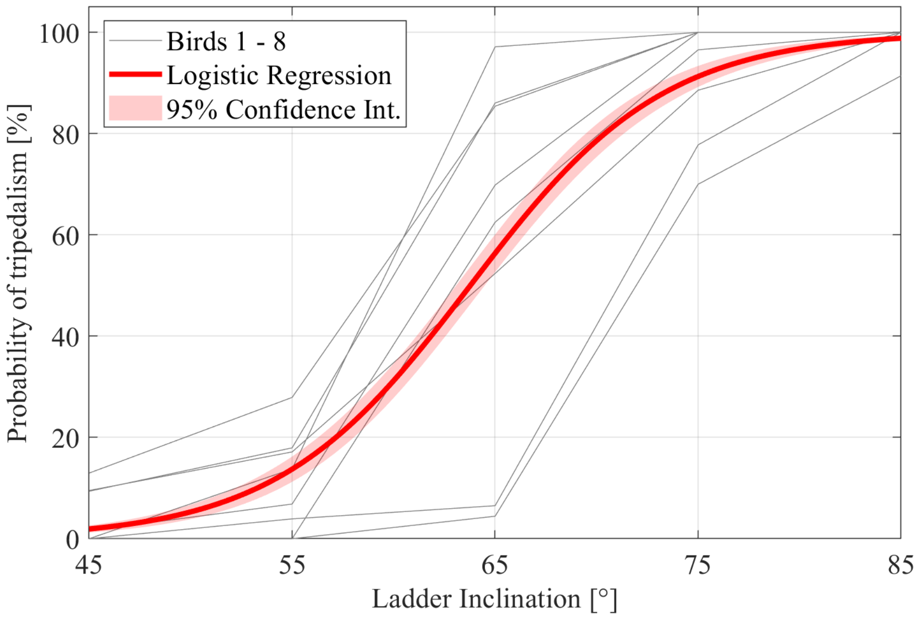

Figure 4.4: Percentage of cycles that were classified as tripedal across all cycles per bird with respect to inclination. A logistic regression model is fitted to the data showing the mean probability for the group to perform a tripedal cycle with respect to the rising inclination. The confidence interval of the mean is shown. According to the regression, on average the birds are equally likely to use either mode at 63.8 ± 0.7°

the contact area play a key role in stabilising the system. Another hypothesis (for this particular climbing behaviour) is that the birds were sufficiently capable of using their tail as an additional support, which reduced the need to utilise its third limb. We noted significant adduction of the tail into the climbing structure (Figure 4.5) in what could be a similar pitch-back prevention mechanism that has been observed in climbing geckos [45], or that which has been documented in woodpeckers [119, 120]. Evidence of parrots using their tail for pitch-back prevention has been suggested in other work, for example the small green pygmy parrot (Micropsitta finsrhii tristrami) has been described to have developed spines at the base of the tail which is can use to brace itself [121]. The contribution and capabilities of tails with regard to parrots' climbing has yet to be explored quantitatively.

4.3.2 Differences in Cycle Metrics

To understand if there are tangible differences in the hindlimb cycle parameters between bipedal and tripedal behaviours, we performed multiple 3-way ANOVAs considering the individual bird, the inclination, and the locomotion mode (bipedal or tripedal, referred

Figure 4.5: A cockatiel appearing to actively adduct its tail for pitch-back control

to as 'mode' for this work) as the driving factors. The parameters being measured are cycle-duration, duty factor, and stride-length which are common metrics to parameterise gaits [122]. As we used inclination to drive tripedalism, we attempt here to separate the confounding influence the variables have on each other. Tables 4.1 to 4.3 show the results of these operations. All results are significant, and it can be seen that after controlling for runs, the mode variable has significant impact on all parameters.

Source	Sum Sq.	Mean Sq.	F	ProbF	
bird	7.19	7	1.026	44.01	0.001
inclination	6.48	4	1.620	69.46	0.001
mode	0.44	1	0.438	18.77	0.001
Error	77.49	3322	0.023		
Total	104.31	3334			

Table 4.1: 3-way ANOVA on Cycle Duration

Source	Sum Sq.	Mean Sq.	F	ProbF	
bird	13638	7	1948	40.04	0.001
inclination	3815	4	953.9	19.60	0.001
mode	442.2	1	442.2	9.09	0.001
Error	161649	3322	48.66		
Total	197672	3334			

Table 4.2: 3-way ANOVA on Duty Factor

Source	Sum Sq.	Mean Sq.	F	ProbF	
bird	80828	7	11547	20.74	0.001
inclination	62423	4	15606	28.02	0.001
mode	12755	1	12755	22.91	0.001
Error	1615983	2902	556.9		
Total	2030554	2914			

Table 4.3: 3-way ANOVA on Stride Length

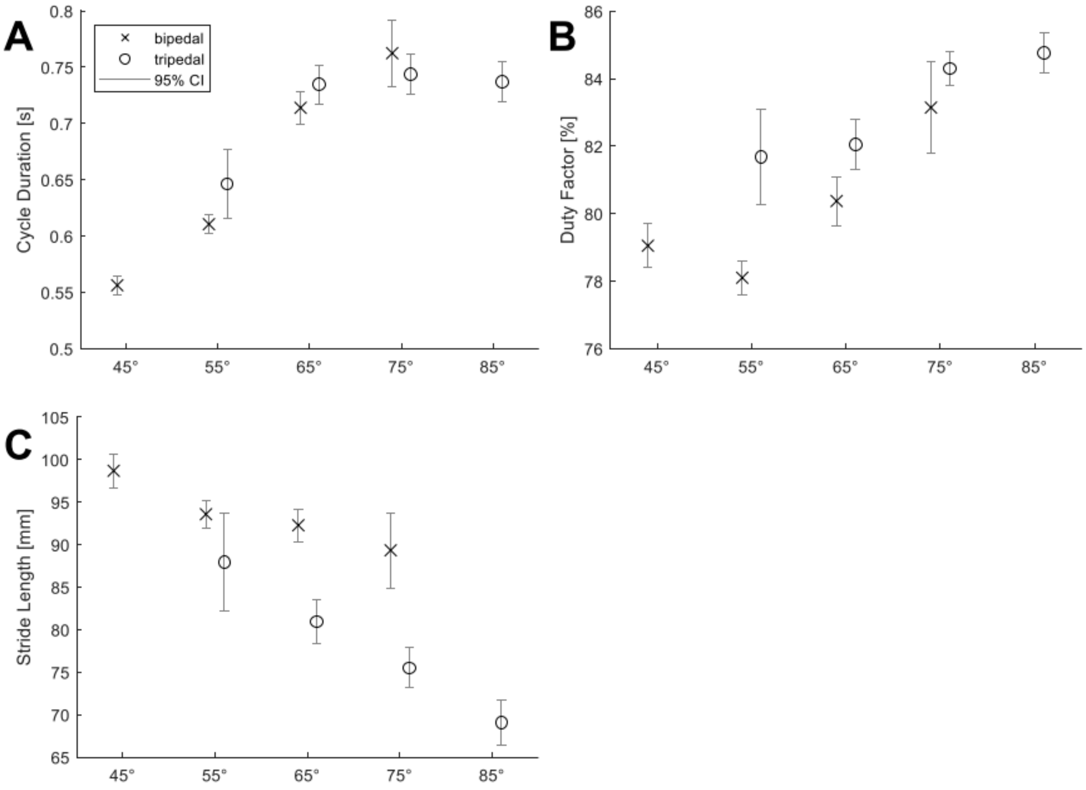

Figure 4.6: Mean values of cycle parameters with respect to support mode and ladder inclinations. The 95% confidence interval is shown for each mean. A: Cycle Duration, B: Duty Factor, C: Stride Length

In each test, accounting for the effect of inclination, the mode has a significant difference on the measured parameters, implying that bipedal and tripedal behaviours indeed occupy different areas of the parameter space. Whilst it is difficult to completely unconfound the effect of inclination and locomotive mode on these parameters, we are confident that each in isolation has an effect. Increasing the inclination changes the loading on the birds significantly due to the change in the direction of the gravity vector. We make a similar conclusion regarding tripedalism and infer from this that the craniocervical system is acting in a similar role to that of a limb. The premise being that the hindlimb parameters would need not change should the neck be acting as a kind of tether rather than a propulsive limb. Whilst this is not definitive proof, it lends support to our current inference on the limb-like role the craniocervical system is playing during tripedal locomotion. To demonstrate the effect of the mode, the mean is plotted for each parameter in Figure 4.6. Interestingly, the inclination and mode seem to have a similar effect on how the parameters change, with the tripedal cycles apparently leading the bipedal cycles in their effect that quantifies a change in behaviour.

4.3.3 Analysis of Hindlimb Kinematics

The motion of the hindlimbs (in 2D) are presented with respect to the model presented in Fig. 4.3. Each limb has 2-DoF parameterised by the length and rotation of the joint with respect to the body. For any single cycle, we can plot the spatiotemporal progression of either parameter and understand on average if there is some change with respect to a confounded driving factors inclination and mode. Whilst this idealistic representation of the bird cannot give us an in-depth look at the birds' configuration or control, it does allow a simplistic look at the leg motions being employed; enough to understand if they differ with respect to each other and our driving factors, and to warrant further investigation if differences are found.

For the purposes of this study, we are particularly interested in describing the differences in kinematics between locomotive modes and between the left and right legs. When reviewing the data, we began to suspect limb function tended to be asymmetric during tripedal operations, which should be evident in the kinematics. To explore this, a multivariate mixed-effect regression model [123] is used to determine how the side and mode variables interact with the polynomials describing the spatiotemporal progression of hindlimb kinematics through time. The mixed-effect portion of the model allows us to understand the variances in the data with respect to cycle and bird. Initially, we also considered the variance per run (each sequence of cycle up the ladder); however, the computed variance was insignificant and removed from the model. The covariance between the limb parameters is also present in our model. A quartic model is used to approximate the leg kinematics for both length and angle with respect to time with a high coefficient of determination

($R_l^2 = 0.89 \pm 0.084$, $R_\theta^2 = 0.93 \pm 0.06$). Both quadratic and cubic polynomials appear to underfit the data, with quadratics failing to explain the skew, and cubics failing to match the convex nature of the curve. In the model below l is the length response (l_L or l_R depending on the side interaction state), θ is the angle response (α or β depending on the support mode interaction state), x_t is the locomotive mode interaction variable (0 for bipedal, 1 for tripedal), and x_s is the side interaction variable (0 for left, 1 for right). Regression models are computed on each inclination individually with two models described below.

Model 1: Data for the 45° bipedal cycles and 85° tripedal cycles are computed without the mode interaction variable as there is insufficient data to reliably compute the coefficient for this interaction (for tripedal 45° and bipedal 85° there is only 11 and 2 cycles respectively). With respect to the model below, all coefficients with an x_t component were not computed, and only coefficient $\beta_1 - \beta_{14}$ are presented.

Model 2: Each inclination from 55° to 75° is computed separately to forgo the complexity of adding inclination in as an interaction term. This model enables us to view the mean change in parameter progression as inclination increases for the left and right leg individually, and as mode changes.

Details and formulation of the model can be found in Appendix A.

4.3.3.1 Results of Regression Modelling

The results of Model 1 (Figure 4.7) show a clear distinction between the bipedal and tripedal progressions for both hindlimbs. The results here are confounded with the inclination, but as suggested by our results in Section 4.3.2, both are likely to have a significant effect on the measured parameters. Interestingly, a significant difference appears to exist between the shapes of the curves between the left and right legs for the tripedal climbing, more so than the during bipedal locomotion. This could be evidence of the asymmetry we observed whilst taking and reviewing the footage. It does not suggest if this difference is due to the inclination or the change in mode. More data is necessary to truly uncover if an asymmetry exists. An asymmetry would not be surprising considering handedness documented in parrots [124, 125, 126, 127], as well as the cerebral asymmetries present in parrots and other birds [128, 129, 130, 131]. This style of locomotion, that is unique to parrots does not seem to be accounted for in current literature. Interestingly, asymmetries can emerge even in bipeds under the right conditions [132].

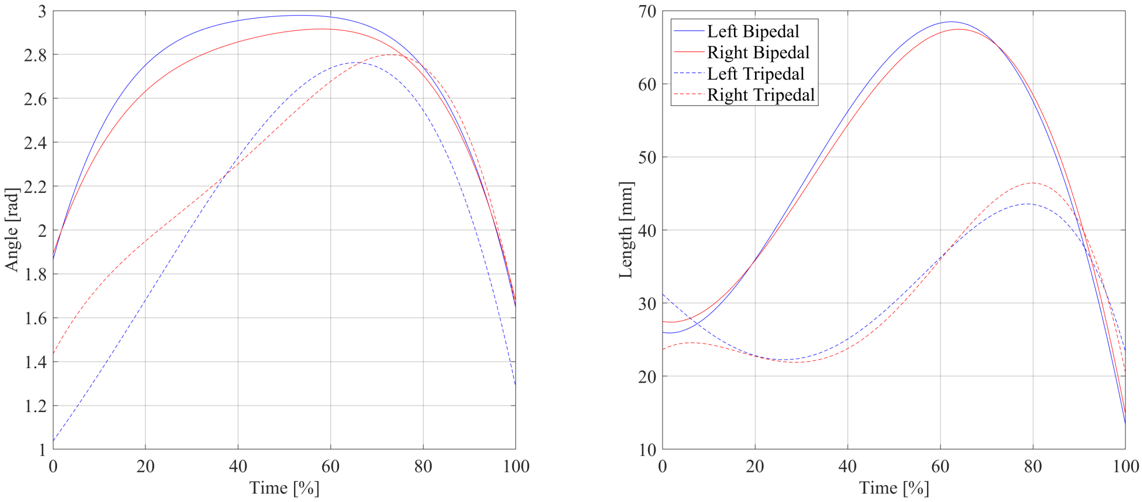

FIGURE 4.7: Model 1: Results of a multivariate regression on the length and angle of birds' hindlimbs during cycle progression separated into side (left and right), and gait (bipedal, tripedal). All bipedal data in this model is taken at the lowest inclination (45°) and all tripedal data is taken at the steepest inclination (85°). All cycles are normalised such that time progression is measured as a percentage of the cycle duration.

For Model 1, we see considerable difference in the shape of the curves between 45° bipedal and 85° tripedal. The peak length clearly decreases, which is in line with the results presented in Figure 4.6 which shows a similar pattern for the stride length. It should be noted that the stride length is measured with respect to the ladder, whilst the limb length is measured with respect to the body which accounts for the differences in values.

The results of Model 2 with Model 1 superimposed (Figure 4.8) show the gradual transition in both bipedal and tripedal progressions as inclination increases. In this figure, the effect of both support mode and inclination is clearer, as we can see the differences between the bipedal and tripedal polynomials for each inclination. Interestingly, the change in inclination and change in mode have similar effects on the responses, with the tripedal response leading the effect of the inclination increase. We can relate the changes in kinematic progression to the changes in the cycle parameters presented in Figure 4.6. We note that for both duty factor and stride length we see a relative shift between bipedal and

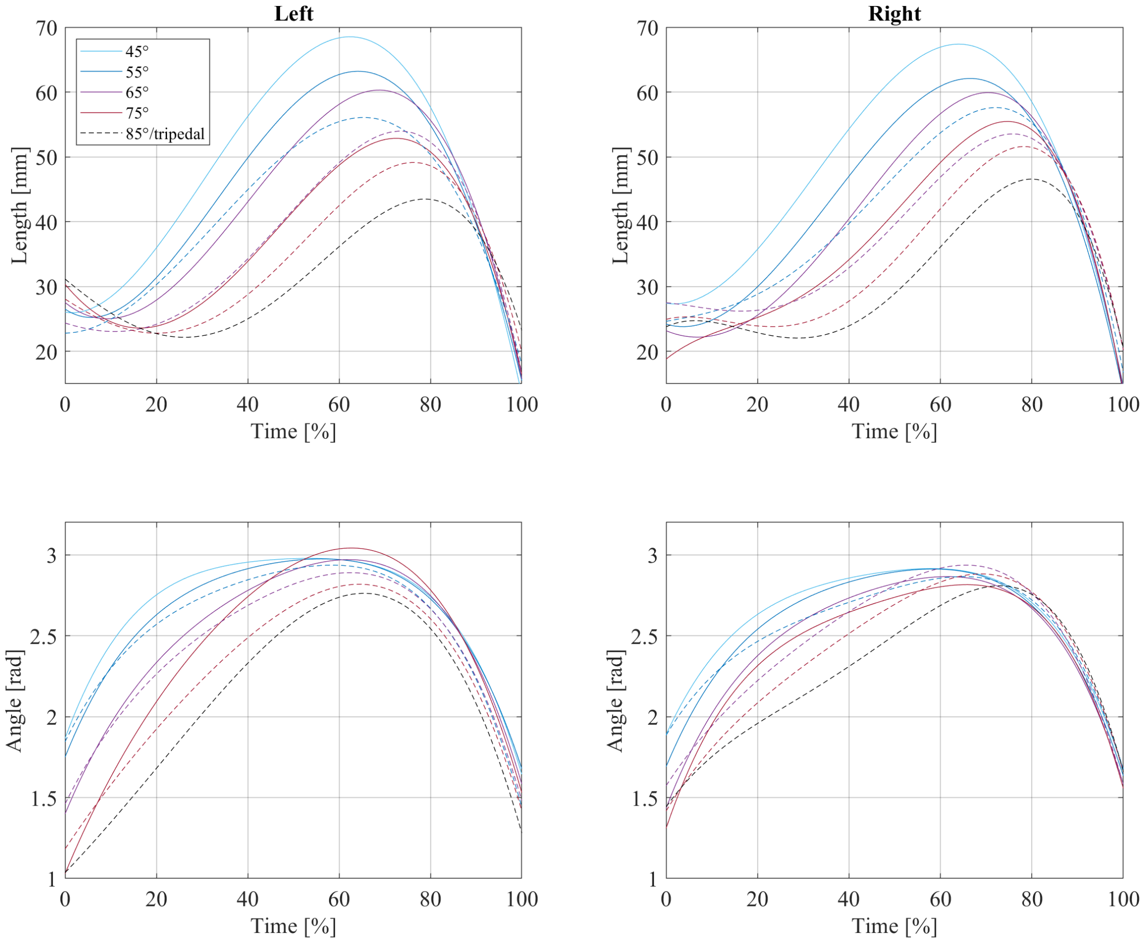

FIGURE 4.8: Model 1 & 2: data for each inclination is shown as a different colour. Solid lines are bipedal cycles, dashed lines are tripedal. Model 1 (light blue solid, and black dashed lines) has been included to show the relevant differences as inclination increases.

tripedal behaviours for each inclination, with the effect occurring in the same way as the change is predicted by the inclination for each parameter. In our kinematic responses, and length especially, it seems as though the steeper gradient end to the curve is being forced into a smaller percentage of the cycle as inclination increases and as the tripedal mode is utilised. Considering we measure cycle start at the foot touchdown, and considering the duty factor tends to increase, we can view the steep gradient at the end of the curve as the swing phase of the leg, which we would expect to have swifter motion compared to the stance phase. As the duty factor increases, we can expect this portion of the response to behave as we have observed in our data and be pushed towards the later portion of our cycle. A similar observation is made for the stride length. As inclination increases and as tripedalism is favoured, the stride length tends to decrease. We therefore expect to see a relative shortening in the peak extension of the leg as we do in our length data.

Whilst differences in the polynomials are seen, these represent the mean paths of the fit through the data and are only significant if the standard error (SE) is relatively small. The coefficients and their significance are detailed in Appendix B and should be referred to when viewing the plots. The spread of the data is also significant as noted by the large cycle variance in Table 4.4 and 4.5 which is too large to make a reasonable prediction on the progression of the of a step parameters with much accuracy.

Variance in the model coefficients can be understood at multiple levels; however, it should be noted that it is only computed on the intercept coefficients ($\beta^{(l)}$, $\beta^{(\theta)}$) in our model. As such, the variances do not allow us to make conclusions about the relative shape of the curve. Each run of a bird up the ladder is split up into multiple cycles (typically 6 - 9 cycles occur in a run). The mixed-effect portion of our model allow us to compute the variance with respect to what we might expect to influence the data, such as the bird and individual cycles. The effect of each run was analysed to attempt to understand if the runs themselves injected any variance into our measurements. The run variance was found to be insignificant and has be disregarded from our model. This result suggests the birds took the same approach to climbing each time and did not change approach as runs were completed. The rest of the variances computed for Model 1 and 2 are presented in Table 4.4 and 4.5 respectively.

At the bird level, significant variance is observed. We speculate this is due to the morphological differences between the birds. We cannot prove this with our data, however, as specific measurements of limb segments were not collected.

45°	Bird	Cylce	Response
$\boldsymbol{\sigma_l^2}$	14.53 (5.916)	77.70 (4.57)	95.89 (0.622)
$\boldsymbol{\sigma_{l\theta}}$	0.197 (0.11)	0.837 (0.059)	0.752 (0.011)
$\boldsymbol{\sigma_\theta^2}$	0.008 (0.003)	0.016 (0.001)	0.058 (0)
85°			
$\boldsymbol{\sigma_l^2}$	5.709 (2.436)	31.47 (2.267)	78.32 (0.489)
$\boldsymbol{\sigma_{l\theta}}$	0.207 (0.128)	0.965 (0.092)	-0.264 (0.014)
$\boldsymbol{\sigma_\theta^2}$	0.025 (0.01)	0.076 (0.005)	0.135 (0.001)

Table 4.4: Model 1 multi-level covariance structures

55°	Bird	Cylce	Response
$\boldsymbol{\sigma_l^2}$	4.475 (1.873)	35.82 (1.91)	70.48 (0.397)
$\boldsymbol{\sigma_{l\theta}}$	0.142 (0.071)	0.512 (0.035)	0.754 (0.009)
$\boldsymbol{\sigma_\theta^2}$	0.01 (0.004)	0.016 (0.001)	0.057 (0)
65°	Bird	Cylce	Response
$\boldsymbol{\sigma_l^2}$	5.674 (2.263)	28.06 (1.583)	59.52 (0.32)
$\boldsymbol{\sigma_{l\theta}}$	0.232 (0.118)	0.538 (0.041)	0.436 (0.009)
$\boldsymbol{\sigma_\theta^2}$	0.024 (0.009)	0.026 (0.002)	0.087 (0)
75°			
$\boldsymbol{\sigma_l^2}$	4.982 (2.176)	32.24 (2.03)	60.07 (0.354)
$\boldsymbol{\sigma_{l\theta}}$	0.173 (0.098)	0.689 (0.066)	0.245 (0.011)
$\boldsymbol{\sigma_\theta^2}$	0.016 (0.007)	0.054 (0.004)	0.117 (0.001)

Table 4.5: Model 2 multi-level covariance structures

4.4 Discussion

4.4.1 Transition to Tripedalism

With regard to our first query, we find that the ladder inclination is a strong driver of tripedalism, and on our particular structure, we observe a strong preference for bipedalism at 45° to an almost unanimous preference for tripedalism at 85°. In our data we observe a 50:50 split in mode at approximately midway through the test inclinations at $63.8 \pm 0.7°$. The reason and for inclination having this effect are still unknown, but it is likely that considerably more factors exist than we have tested, and that might influence the birds' behaviour. We speculate that the increase in inclination is disruptive enough for bipedal walking to no longer be the most appropriate approach. The same might be said of most bipedal mammals. It is intuition for us (homo sapiens) to reach for an extra support when climbing steep or unsteady structures; however, a mathematical proof is thus far elusive, and it is possible this effect may be the result of some intuitive safety factor rather than some energetic optimality. The exploration of this might be assisted with robotic models, where we have an enhanced ability to control experimental parameters; or in a full dynamics model of the birds' form that would enable insight into the kinetics during either mode of locomotion. For the latter case, it is likely that an explicit solution is unachievable considering the notorious effect working with animals has on data collection. The robotic approach might provide us an explanation that consider the mechanics alone.

4.4.2 Limb-Like Functions

In terms of behaviours, our data suggests that bipedal and tripedal modes are markedly different, with a considerable step in all measured parameters present as a result of the transition. We find it likely that the neck is being used in an active limb-like role in tripedal locomotion considering the change in hindlimb parameters, under the premise that the hindlimbs would need not change should the neck be used as a passive, tether-like system. Whilst we find this likely, the full role of the craniocervical system in locomotion is still under-explored and much more work needs to be done before we can complete our understanding of its mechanics and role during locomotion and foraging. From a robotics perspective, the neck's dual role as a limb and manipulator make it desirable to emulate. However, to achieve a fully capable system, we should understand further what is significant about the kinematics and kinetics of the design that fosters the parrots' desirable abilities.

4.4.3 Towards a Template

In terms of modelling the neck for robotic emulation, it is clear that we ought not to make too many simplifying assumptions before further analysis is conducted. The legs appear to operate similarly to that of other legged vertebrates and might be modelled similarly with the SLIP and lateral leg spring (LLS) models; however, the neck is entirely different in its form and more work needs to be done to understand it fully. Furthermore, the presence and effect of asymmetry in the tripedal behaviour need more rigorous testing to understand if a tripedal model can be simplified as it has been done for quadrupedal and bipedal legged models. The Full-Goldman (FG) model [54] is another interesting model that might be considered. However, since the FG model was based on cockroaches and lizards, both that have a symmetric number of laterally sprawled limbs, further testing is needed to determine the appropriateness of this model, or if elements of it exist in the parrot approach to climbing.

4.4.4 Definition of Vertical Climbing

The slow transition from bipedal walking to tripedal climbing makes us question relevance of the current definition for ‘vertical climbing’. The use of the 45° inclination being the mark where we define a behaviour as vertical climbing seems too arbitrary to have significant meaning. It might be better to suggest that vertical climbing be a function of some significant change in behaviour or gait for a given animal or machine, as recently suggested by Granatosky et. al. in [7]. Climbing has also been used in robotics to describe ascent up relatively small inclines that do not mandate a significant change in the conditions of gait or substrate contact [133], and so it is clear in an academic context, especially in robotics locomotion, climbing ought to be better defined. In the context of the remainder of this work, all behaviours developed are defined as climbing, as we do not venture into developing machines capable of cursorial to scansorial transitions.

4.4.5 A Note On Tripedal Gaits

In this work we were not able to identify or characterise tripedal gaits that might usually have been used in such an analysis. The reasons for this are: 1. There is no prior work identifying tripedal patterns; 2. Discontinuous structures injects noise into the footfall sequences that does not exist in the continuous case; 3. Lack of prior understanding on the parrot coordination system, which is an important input into gait analysis as described by Abourachid in [122]. Should these items be addressed, work into identifying and characterising true tripedal gaits might be better facilitated.

4.4.6 Tail Utilisation

Tail utilisation for pitch back prevention was observed in both bipedal and tripedal behaviours. This was seen in what seemed to be the active adduction of the tail, and in the deflection of the tail against the ladder. Though it is unclear how much assistance the tail might be giving, this strategy has also been observed in lizards [45], treecreepers [93], woodpeckers [119, 120], other parrots [121], and used in robotics [134, 92, 24]. In robotics, it is shown to drastically increase stability and the inclination climbable. We suspect the cockatiels in our study are utilising their tails with similar effect, and that it could play a part giving feedback to the bird with regard to when to use its beak. Tail length in different species of parrots vary enormously, yet all seem to share in their unique tripedal abilities. Whether different species would transfer to tripediality sooner or later depending on this length and utility of their tails is an open question.

4.5 Summary

True unencumbered tripediality is rarely seen in nature. In this chapter we have shown one condition that effects the cockatiels' decision to utilise their craniocervical system in a form of tripedal locomotion. Whilst many driving factors for tripedalism are still to be tested, we can say with certainty that parrots favour using a tripedal mode of locomotion on steeper structures. Further exploration of the drivers of beak usage may be explored with additional modelling techniques, but would require more insight with a reasonable dynamic description of the parrots' form. From our study, we consider bipedal and tripedal locomotive modes quantifiably different behaviours, and consider the craniocervical system to possess limb-like capabilities in locomotion. We discovered some evidence for asymmetry that should be explored further in future work, and lay a foundation for future work into the classification of tripedal gaits; questions that might be explored by developing a full neuromusculoskeletal model for the birds during locomotion. With additional support from Young et al. [5], we are now confident that parrots are indeed using their craniocervical system as a third limb, and inspired by this, we begin development of the world's first parrot inspired climbing robots.

Chapter 5

Kinematic Design and Control

In this chapter, equipped with the knowledge gained from our review of biological literature, our knowledge of the application environment, and our study on climbing cockatiels, we explore the design of a tripedal climbing robot. We begin by discussing the general form of our inspiration, parrots, and what aspects of their design are useful as inspiration in robotic development. Then, we develop two kinematic designs of increasingly complexity before moving into simple footfall and trajectory planning strategies. Finally, we describe several types of control approaches that are suitable for our robots of varying complexity.

The kinematic design of a parrot-inspired tripedal climbing robot has never been attempted. The use of three limbs has the potential to simplify the design of climbing robots, whilst enhancing their mobility and capabilities to perform work, especially where one of the limbs is designed to be capable of multiple functions including locomotion, and manipulation. The approach in this thesis is to begin with a simple, feasible design, in a basic scenario: planar vertical climbing on a ladder. We select a ladder as it is a simple, common, and regular structure, and motion along this structure is an example of an M3 motion primitive (Section 3.2; Table 3.1), the same primitive performed by cockatiels in the previous chapter. In this chapter, two robots are designed in quick succession, the first, in true 2D with the body and contact points fixed to a 2D vertical surface; and secondly, a more complex 3D design that is physically realisable. By exploring the mechanics and kinematics of the parrot form, we come up with a basic design that is progressed in complexity as necessary when moving from 2D to 3D.

5.1 Parrot-Inspired Design

The experiments in Chapter 4 gave us an interesting insight in the tripedal behaviours of cockatiels. Given the opportunity to observe them closely, additional features of their design that are of interest to us in robotics are observed, including: 1. A strong, hyper-redundant, dual-purpose, craniocervical apparatus (head and neck), used for climbing and manipulating objects; 2. A body which can be reasonably modelled by a single rigid block; 3. Hindlimbs that have mobility compared to the shoulder joints of most hominids; 4. Zygodactyl claws that are thought to be an adaptation for perching [127], or rather, producing an encompassing grasp on thin structures as animals often do in climbing; 5. A deceptively simple beak that is used with impressive dexterity. Whilst we do not yet take inspiration in our design from all these aspects, we do start with the one that is conceptually the most simple, the rigid block body.

The body of the parrot, and other birds, is comparatively simple to model when compared with a quadruped. Quadrupeds have a long, redundantly articulated spine joining the shoulders and pelvis, which is still being given consideration today in an attempt to make quadrupeds faster and more agile [112, 111, 110, 109]. Parrots on the other hand, do not require this, as they perform all the functions we draw inspiration from with a stiff, fused spine that can be modelled as a single rigid body. This characteristic exists is an adaptation for flying [135]. The spine connecting the fore and hind limbs (the thoracic spine) is entirely fused, which gives the birds the necessary stiffness for maintaining continuous flight. Whilst we are not interested in flight in this work, this characteristic gives us confidence that we are not missing any fundamental contributions towards climbing by needing a spine as we would were we studying hominids. The block body therefore features in both simple (2D), and more complex (3D) kinematic designs.

5.2 2D Kinematic Design

The kinematic model of the 2D robot is shown in Figure 5.1. Since the function of this robot is only to perform climbing on a 2D plane, unnecessary DoF are minimised with the exception of the centre limb, that has one more than strictly necessary to maintain robot symmetry. The resulting robot has a rigid block body, with three limbs extending out from it; two on the side and one in the middle. Each of the two hindlimbs has two DoF, with rotation axes ($\theta_{1,3}$ and $\theta_{2,4}$) aligned with the normal vector to the climbing plane. The centre limb extends from the top of the body and has three DoF. The third DoF allows the the arm to extend out of plane, which enables the limb to remain symmetric. Symmetry is not an absolute requirement of this design for the function of 2D climbing; however, we felt a lopsided design would be undesirable when turning to more complex models for more varied work. Having a symmetric centre limb also ensures the workspace of the robot either side of it is symmetric when considering body collisions.

The body of the robot is a “floating base” that has one rotational DoF and two translation DoF, all constrained to the climbing plane. Each of the three contact points are able to rotate and translate freely in plane but are constrained to stay on the climbing plane. The end effectors are allowed to rotate passively when making contact with the structure for climbing.

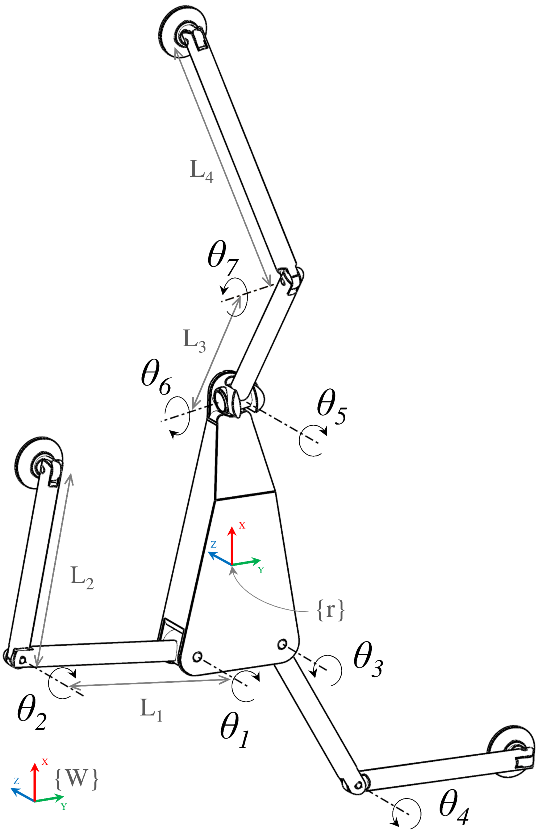

FIGURE 5.1: Kinematic description of the 2D vertical climbing, tripedal robot. The robot has seven actuated degrees of freedom and is free floating in 2D on the climbing plane. The axes of the hind limbs, composed of joints 1 through 4, are constrained normal to the climbing plane. The manipulator limb (joint 5 through 7), extend out of plane, however; the end effector is constrained to the vertical climbing plane. Shown are two frames, the world frame, $\{W\}$, and the frame coincident with the robot CoM at $\{r\}$. The end effector model is for display only; it is meant to represent adhesion to the 2D climbing plane. No mechanism for grasping is implied in this design

This robot is implemented in simulation in Section 6.1 with the strategies presented in the later part of this chapter.

5.3 3D Kinematic Design

The next step in exploring the climbing capabilities of our tripedal robot is to translate the ideas generated in the 2D robot into the real world in order to validate the underlying principles and claims. In order to have the robot climb a real ladder, significant changes are made to the kinematic design, the control strategy, and the trajectory planning, and the system is designed, fabricated, and integrated.

One of the more significant modifications we have made moving from a 2D simulation to a real 3D system, is the assumptions made about the contact points, which for this work are still highly idealised when compared with the application environment. In the 2D environment, the assumption was made at each contact point, translation in the climbing plane is locked, but rotation around the point is allowed passively. This condition is very similar to that modelled in most cursorial quadrupedal robots, where there are no considerations of the torques that can be generated about the contact, and the assumptions is that the limb is free to rotate. In a reticular structure, where adhesion is facilitated with an encompassing grasp, this condition is no longer valid, as torques can now be generated. Perhaps more significantly, force can be reacted in both push and pull, whereas in cursorial robots it is generally assumed that the robot is unable to pull itself toward the ground. The effects of the change in contact condition are essential to considering the form of a reticular structure robot (RSR). Taking an n-DoF robot with c legs, with the contact assumption of most cursorial robots, we get up to $3c$ degrees of control when all limbs are in contact with the ground. In order to control the body in 3D euclidean space at least two legs must be in contact with the ground to achieve control of the body. This is marred by the fact that there are additional constraints on the contact points, so even when two legs are in contact, constraint violations can cause the loss of static control. In fact, achieving control of a system such as a biped, where single and even no points of contact remain during the swing phase of the legs, is largely the challenge of the field of *Underactuated Robotics.* The anecdote that is born of these contact assumptions is that a robot needs to maintain the CoM within the support polygon to be statically stable, and to do this generally requires four or more legs such that there is a minimum of three points of contact at any given time. When considering RSRs, where we can assume six degrees of control at the contact point (three translational, three rotational), we can fully control the body with just a single point of contact, which is generally the operating assumption of the inchworm style robot described in Section 2.1.1. With two points of contact, there are 12 degrees of control over the 3D body. Assuming that the capacity to generate significant torque at the contact point is a constraint that is easily violated, we are still left with a fully actuated system, that is more stable than its cursorial counterpart simply as the remaining constraints are not as easily violated due to the encompassing grasp. In reality, since the torques at the contact point are likely always to be able to make some contribution towards the control goal when a system has two points of contact, it seems likely that in this configuration a robot should always have a redundant capacity for control when performing locomotion or manipulation.

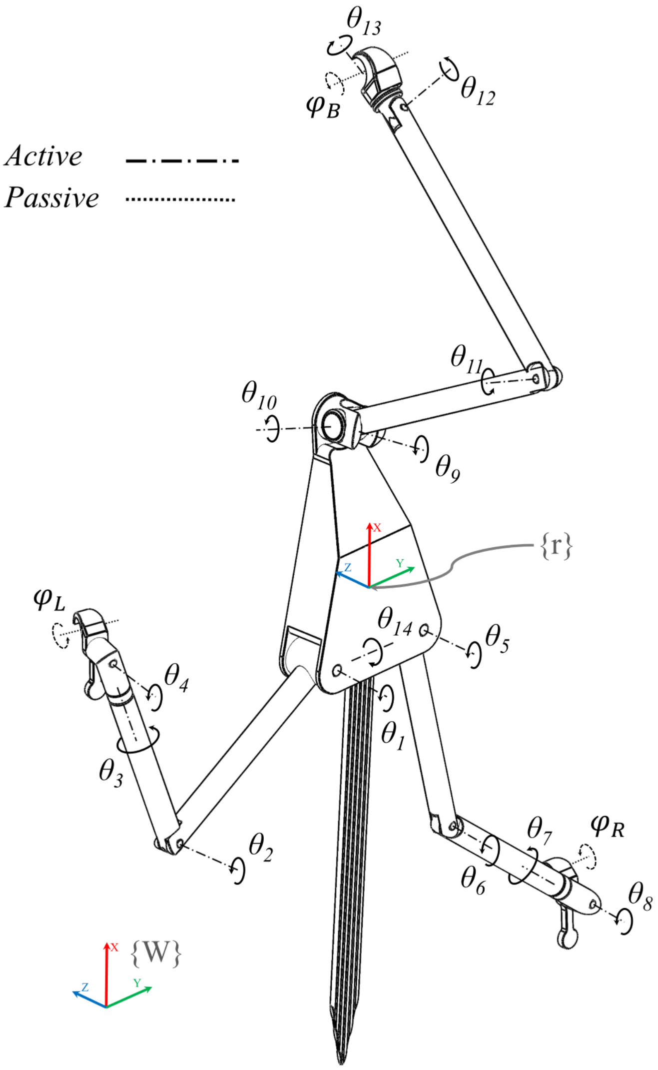

FIGURE 5.2: Kinematic design of a 3D robot for tripedal climbing. This design has a total of 14 DoF, four in each hindlimb, five in the centre limb, and a one DoF tail. Each of the prehensile end effectors are able to rotate passively about the contact axis φ_i for $i \in \{L, R, B\}$.

In the design of our 3D robot, we exploit the redundancy of the contact to reduce the DoF of the robot by allowing free rotation about a single axis at the contact (axes φ_i in Fig. 5.2). This is in line with the general principle for mass and inertia minimisation (Sections 3.1.1 and 3.1.2) and helps to simplify the robot design and construction by allowing us to develop a simple hook like end effector (further described in Section 6.2.2.5) that requires no actuation. Being designed to climb on a simple ladder with cylindrical rungs, each of the contacts is idealised as a simple hook, where each end effector can rotate axially about the rung. The hook design means that the robot can only apply forces in the direction towards from the hook opening, similar to the constraint that is placed on cursorial robots, where they cannot apply forces pulling themselves into the ground. This is appropriate for this design as we are only performing vertical climbing, and the robot will remain relatively vertical with respect to gravity. The orientation of the hooks will therefore always be such that the opening is on the underside which does not need to react forcefully as the robot weight will always keep force downwards. The hook design does allow force production in both the positive and negative Z-direction shown in Figure 5.2, as well as in positive and negative Y-direction; although, this is limited by the friction that can be developed between the end effector and the substrate. The alternative of not embracing this free rotation axis is that we would have to add this joint in as part of the kinematic design. This is due to the robot needing a 3-DoF wrist to enable out of plane body motions for the hindlimb swing phases. In addition, we would also need to design a grasping mechanism that prevents rotation about the rung axis, which due to the cylindrical nature of the rung, is a significantly harder design problem than producing torques in the other two rotation axes.

Now that we have developed the end effector contact kinematics, we can add additional degrees of freedom to our 2D design as needed to facilitate locomotion in 3D. The first additional DoF we analyse is in the hindlimbs, which enables rotation of the hindlimb end effectors in one of the two dimensions orthogonal to the end effector free axis. This joint is typically aligned with the world z-axis and makes up joints 4 and 8 in Figure 5.2. This joint replaces the passive joint we have in the end effectors of 2D design. Thought was given to the idea of making this contact passive, weighting it such that it always aligned with gravity, similar to [44]. However, we would like the robot to be able to attach to rungs that are not horizontal in future work, and for this, active control of this joint is required.

Active control also allows us to apply some level of torque; however, in line with the lesson described in Section 3.1, this motor ought to be kept small as it is distally located. Along with this joint, a small offset is given that pushes the robot off the structure, allowing for clearance between the robot and the structure.

Next, in order to be able to move end effectors over the rungs, we need the capacity to move the end effectors out of plane. In order to achieve this without fundamentally changing the design of the legs, we add the capacity to rotate at the wrist; joints 3 and 7 in Figure 5.2. When one of the hindlimb end effectors is detached, this allows the robot body to rotate such that the end effector can lift out of plane, hence enabling the robot to reach up over the next rung on the ladder. This is the final modification we need to add to the hindlimb, and gives each in total four active DoF and one passive DoF. The distal DoFs facilitate approximately a ball and socket type joint at the end effector, enabling free rotation of the body in all dimensions when only one hindlimb is in contact. In a parrot, this motion is facilitated by the ball and socket type joint of the hip, giving the legs a resting position below the body. This, however, pushes the body much further out from the substrate, which is less optimal for climbing a vertical ladder as the additional distance of the CoM from the substrate increases the contact forces that must be resisted.

The base of the centre limb is kept identical to the 2D robot. Since the body must move in 3D to facilitate motion of the legs over the contact points, and some constraint on motion of the body is achieved with the 5-DoF hindlimb design, the centre limb must connect to the ladder with 6-DoF, as any less would cause the kinematics to lockup, as the constrained motion of the legs would combat and constraints placed on the centre limb. Since there is a single passive DoF in the centre limb end effector due to the hook design, two additional active joints (joints 12 and 13) are added to complete the 6-DoF the arm needs.

As the legs are only 5-DoF, they lack the ability to actively apply forces in and out of the climbing plane, which are necessary to prevent pitch-back when the centre-limb is detached, or to produce body roll when a hindlimb is detached. For this function we add a single DoF tail (joints 14) that assists in both these functions. The tail also acts to reduce the contact forces, but does so without needing to add an entire limb, a limb being defined as an appendage that contributes actively to propulsion, which is unmet as the tail contact force causes a drag against the body motion.

With the kinematics of both robots now fully defined, we turn our attention to footfall and trajectory planning algorithms.

5.4 Footfall and Trajectory Planning

Here, we explore several footfall and trajectory planning used across the 2D and 3D implementations of our robot. Three footfall planners are used for comparison: two bioinspired footfall planners that are inspired by the data we collected from climbing cockatiels (Chapter 4) and a sampling-based footfall planner. Two trajectory planners are also considered, a simple minimum-jerk trajectory planner and a trajectory optimisation approach that attempts to minimise the reaction forces as the robot traverses between waypoints.

5.4.1 Footfall Planners

Footfall planning is concerned with where the feet should make contact with the substrate and where the body should be positioned and oriented for the selected foot placements to facilitate locomotion. In this section, we investigate three different footfall planning methods; two are inspired by observations of cockatiels climbing ladders and the other a sampling-based method. The two bioinspired footfall planners utilise different footfall patterns, a three-step cyclic pattern and a four-step cyclic pattern. All planners in this work are completed in 2D only, which is appropriate for our 2D climbing robot presented in Section 5.2.

For the planning methods developed here, the robot state is modelled in 2D such that the state vector is express as

$$\mathbf{x} = \begin{bmatrix} x & y & \phi & \dot{x} & \dot{y} & \dot{\phi} \end{bmatrix}^\top . \tag{5.1}$$

Given a 2D substrate that defines feasible footfall locations, the goal of the footfall planner is to produce a discrete set of footfall positions $\{\mathbf{p}_j\}$ and body states $\{\mathbf{x}_j\}$, for $j \in \{1, \ldots, n_f\}$, where n_f is the number of footsteps.

A simplified method for finding valid robot poses underpins each planner and is based on an approximation of the robot's kinematics. If each limb is in its most extended configuration and three circles are drawn with the centre at each of the end effector locations and passing through the body centre, $\mathbf{b}(p)$, then for any given set of end effector positions, the body centre position $\mathbf{b}(p)$ should lie in the overlapping region of these circles (Figure 5.3). This approximation is sensitive to body orientation, and as such, an empirical multiplier is used on each limb to reduce the radius of the circle such that the robot foot positions are not chosen that might violate the robot's kinematics. For this work, multipliers of 0.7 are chosen for the legs, and 0.85 for the manipulator limb. This approximation is necessary as full workspace analysis of a robot for a given pose has not yet been completed, and a fast method was needed to facilitate sampling-based planning.

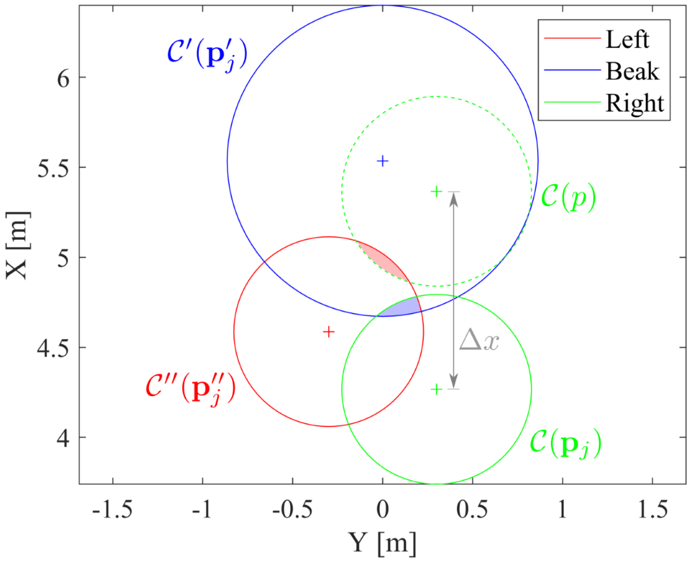

FIGURE 5.3: Circles $\mathcal{C}(p), \mathcal{C}(\mathbf{p}_j), \mathcal{C}'(\mathbf{p}'_j)$, and $\mathcal{C}''(\mathbf{p}''_j)$. Initial and candidate final foot positions are marked +. Initially, valid body positions $\mathbf{b}(p)$ are constrained by the shaded-blue region. After finding valid step $\mathcal{C}(p)$, the new region for valid $\mathbf{b}(p)$ is shown by the shaded-red region. The final $\mathbf{b}(p)$ for the step is chosen as the centroid of the shaded-red region

5.4.1.1 Bioinspired three- and four-step footfall cycles

The three-step footfall strategy was the approach we most commonly observed during climbing locomotion in cockatiels. The strategy favours one leg to be positioned near the beak contact point and another to land roughly mid-torso and is repeated cyclically. A single cycle is depicted in Figure 5.4, and is characterised by moving the beak, the right leg, and then the left in that order ($\{B, R, L\}$). Different birds seemed to favour different legs to be placed next to the beak during climbing, changing the order from $\{B, R, L\}$ to $\{B, L, R\}$, which may be indicative of the previously documented handedness in parrots [125]. We refer to the limb being brought up to the beak as the forward leg. In our observations, six of the ten birds seemed to favour the right leg as the forward leg, three of ten the left, and one bird seemed to favour neither and often switched the forward leg each cycle in a flurry of smaller steps.

The four-step footfall strategy utilises a $\{B, L, B, R\}$ footfall sequence. This strategy was observed in our data rarely but seems to be quite effective when utilised.

Figure 5.4: An example of a cockatiel's (*Nymphicus hollandicus*) three-step {B,R,L} footfall strategy seen in our observation of live birds. Starting with motion of the beak, followed by its right leg up to around the centre of its body, and then followed with its left (forward) leg up to approximately the beak contact point

5.4.1.2 Maximal reach footfall planner

A myopic footfall planner was used to find contact locations for both the three- and four-step strategies using a simple maximum-reach heuristic. Consider the swing leg of the

j-th footstep; let the initial swing foot location be $\mathbf{p}_j \in \mathbb{R}^2$. Let the foot locations of the two limbs that remain in contact be $\mathbf{p}'_j, \mathbf{p}''_j$. Also, for some candidate swing foot touchdown placement $p \in \mathbb{R}^2$, let $\mathcal{C}(p), \mathcal{C}'(\mathbf{p}'_j), \mathcal{C}''(\mathbf{p}''_j)$ be the circles centered at $p, \mathbf{p}'_j, \mathbf{p}''_j$ with radii equal to their respective maximum leg lengths (see Figure 5.3). We set the body position $\mathbf{b}(p)$ to be the centroid of $\mathcal{C}(p) \cap \mathcal{C}'(\mathbf{p}'_j) \cap \mathcal{C}''(\mathbf{p}''_j)$. Then, given $\mathbf{b}(p), p, \mathbf{p}'_j, \mathbf{p}''_j$, we can check kinematic feasibility by solving the whole-body IK problem to yield $q \in \mathbb{C}^7$, where the imaginary component of q, $\mathfrak{Im}(q) = 0$ when the configuration is kinematically feasible. When checking kinematic feasibility, we solve the IK problem for a fine grid of body orientations ϕ in $[-90°, 90°]$ and set $\phi^\star$ be the closest such ϕ to zero, if one exists.

Then, we write $p = \mathbf{p}_j + [\Delta_x; 0]$, and solve

$$\Delta x^\star = \underset{\Delta x \in \mathbb{R}}{\arg\max} \quad p \tag{5.2}$$

$$\text{subject to } \mathfrak{Im}(q) = 0. \tag{5.3}$$

Finally, let $p^\star = p - [\varepsilon; 0]$; then the desired body waypoint is set to $\mathbf{x}_{j+1} = [\mathbf{b}(p^\star); \phi^\star; 0; 0; 0]$, and the footfall location $\mathbf{p}_{j+1} = p^\star$ (the small $\varepsilon > 0$ is subtracted to avoid singular configurations). For the case of the "ladder" substrate, the point on the rung below closest to $p^\star$ is used instead.

5.4.1.3 Sampling-based footfall planner

In contrast to the myopic planner that only considers the next step, we have also implemented a non-myopic planner that considers all n_f footsteps in the experiment. Pseudocode is listed in Algorithm 5.1.

For each leg, a region for sampling candidate foot placement p is empirically defined. For example, in our experiments, $\mathcal{B}_L, \mathcal{B}_R$ are the sectors of radius 1.05 m from 0° (directly upward) sweeping an angle of 60° to the left/right, and $\mathcal{B}_B$ is the sector of radius 1.73m between ±30°. These values were defined as twice the maximum reach computed for each leg, as it was thought that accounting for body motion, a new contact point could not approach this limit. Line 7 uniformly at random chooses a leg (L, R, or B) that was not the previous swing leg. Once a leg is chosen as the swing leg, p are uniformly at random sampled from the region $\mathcal{B}_i, i \in \{L, R, B\}$ until a feasible one is found. IsFeasible() checks (1.) that the configuration q (computed via IK as in Sec. 5.4.1.2) is purely real, (2.) that the body pose is not identical to the one of the previous footstep, and (3.) that the "shoulder" joint (axis 5) is below the beak contact. When this is completed for all remaining footsteps, the "rollout" is scored: we use the vertical distance of the body as Score(). This way, the effect of later possible footsteps is accounted for even when taking the first step.

In the "ladder" substrate case, let the contactable area of the rungs of the ladder be $\mathcal{R}$; instead of sampling within B, we instead sample uniformly on the set $B \cap \mathcal{R}$.

Algorithm 5.1 Monte-Carlo footfall planner

```
best_score $\leftarrow -\infty$
best_rollout $\leftarrow$ [ ]
for $j = 1 : n_f$ do
    for 1:max_iter do
        rollout $\leftarrow$ [ ]
        for $j : n_f$ do
            $i \leftarrow$ Random($\{B, L, R\}$) //choose leg
            $p \leftarrow \emptyset$
            while !IsFeasible($q(p, \mathbf{p}'_j, \mathbf{p}''_j)$) do
                $p \leftarrow$ Random($\mathcal{B}_i$) //choose pt
            end while
            rollout.append($p_l$)
        end for
        S $\leftarrow$ Score(rollout)
        if S $>$ best_score then
            best_rollout $\leftarrow$rollout
            best_score $\leftarrow$ S
        end if
    end for
end for
return best_rollout,best_score
```

5.4.2 Reference Trajectory Generation

In this section we explore two methods of producing a desirable trajectory $\mathbf{x}^{\star}(t)$ between any two consecutive body states given by the footfall planner $\mathbf{x}_j$ and $\mathbf{x}_{j+1}$.

5.4.2.1 Minimum-jerk body and swing leg trajectories

A standard method in the trajectory generation of robotic manipulators is the minimum jerk trajectory (e.g., [136]), which is a simple way to generate smooth trajectories between waypoints. Minimum jerk trajectories are defined by piecewise quintic polynomials. Given the time T to complete the maneuver, the minimum-jerk straight-line trajectory segment between the $\mathbf{x}_j$ and $\mathbf{x}_{j+1}$ is given by

$$\mathbf{x}^\star(s(t)) = (1 - s(t))\mathbf{x}_j + s(t)\mathbf{x}_{j+1}, \tag{5.4}$$

where the time-scaling parameter $s(t)$ is

$$s(t) = \frac{6}{T^5}t^5 - \frac{15}{T^4}t^4 + \frac{10}{T^3}t^3 \in [0, 1], \tag{5.5}$$

for $t \in [0, T]$. Trajectory segments defined this way have the property that the endpoint accelerations are zero, i.e., $\ddot{s}(0) = \ddot{s}(T) = 0$, allowing smooth transitions from one trajectory segment to the next.

An analogous approach was used for swing leg end effector trajectory generation. The end effector position trajectory $\mathbf{p}^\star(t) \in \mathbb{R}^2, t \in [0, T]$ between swing leg liftoff position $\mathbf{p}_i$ and swing leg touchdown position $\mathbf{p}_{i+1}$ is given by

$$\mathbf{p}^\star(t) = (1 - s(t))\mathbf{p}_i(t) + s(t)\mathbf{p}_{i+1}(t). \tag{5.6}$$

This was used for all body trajectory planning approaches, including the optimisation-based body trajectory planner in the following subsections.

5.4.2.2 Simplified body dynamic model

In preparation for the optimisation-based trajectory generation method, we consider the dynamics of the 2D rigid body. Let m be the mass of the rigid body, and I its rotational inertia in the plane, and the ground reaction forces at the feet be

$$\mathbf{f} = \begin{bmatrix} f_L & f_R & f_B \end{bmatrix}^\top, \tag{5.7}$$

where $f_L, f_R, f_B \in \mathbb{R}^2$ are the 2D reaction forces from the substrate at the left, right, and beak end effectors, respectively. We can then write the continuous-time dynamics

$$\dot{\mathbf{x}} = \begin{bmatrix} \mathbf{0} & \mathbf{I_3} \\ \mathbf{0} & \mathbf{0} \end{bmatrix} \mathbf{x} + \begin{bmatrix} \mathbf{0_{3\times 6}} \\ \mathbf{M}^{-1} \begin{bmatrix} \mathbf{I_2} & \mathbf{I_2} & \mathbf{I_2} \\ (\mathbf{N}r_L)^\top & (\mathbf{N}r_R)^\top & (\mathbf{N}r_B)^\top \end{bmatrix} \end{bmatrix} \mathbf{f} + \mathbf{g}, \tag{5.8}$$

where $\mathbf{M} = \text{blkdiag}(m, m, I) \in \mathbb{R}^{3\times 3}$ is the inertia matrix, $\mathbf{0}, \mathbf{I}$ are the appropriately sized zero and identity matrices, $\mathbf{g} = [0, 0, 0, -9.81, 0, 0]^\top$, and r_L, r_R, and $r_B \in \mathbb{R}^2$ are the position vectors of the end effectors (left, right, and beak, respectively) in the robot frame, and $\mathbf{N} = \begin{bmatrix} 0 & 1 \\ -1 & 0 \end{bmatrix}$. We have omitted the time-dependence on $\dot{\mathbf{x}}, \mathbf{x}, \mathbf{f}$ for notational simplicity.

The position vectors r_L, r_R, and r_B are functions of the robot's state $\mathbf{x}$ and the foot contact locations $\mathbf{c}_L, \mathbf{c}_R, \mathbf{c}_B \in \mathbb{R}^2$, i.e., the places where the stance legs have grasped the structure. The foot contact locations are constant during one trajectory segment, or "footstep". In this paper, we consider only the cases where there are two or three contact points. With this, we rewrite (5.8) in a more compact way as

$$\dot{\mathbf{x}} = \mathbf{A}_{cts}\mathbf{x} + \mathbf{B}_{cts}(\mathbf{x}, \mathbf{c}_p)\mathbf{f} + \mathbf{g}, \tag{5.9}$$

where $\mathbf{c} = [\mathbf{c}_L; \mathbf{c}_R; \mathbf{c}_B]$ is constant during a single footstep.

The simplified dynamics (5.9) are then discretized using an explicit 4th order Runge-Kutta formulation. Letting N be the number of timesteps between 0 and T, and $k \in \{1, \dots, N\}$ be the timestep number, we write the discrete-time dynamics compactly in the following form:

$$\mathbf{x}_{k+1} = \mathfrak{f}(\mathbf{x}_k, \mathbf{f}_k, \mathbf{c}_p). \tag{5.10}$$

5.4.2.3 Model-based optimisation of body trajectory

Using the dynamics (5.10), we can generate the trajectory between $\mathbf{x}_i$ and $\mathbf{x}_{i+1}$ by solving an optimal control problem. We consider a problem of the form:

$$\begin{aligned}
\mathbf{x}^\star = \underset{\mathbf{x},\mathbf{f}}{\arg\min} \quad & \sum_{k=1}^{N} \|\mathbf{x}_k\|^2_{\mathbf{H}} + \|\mathbf{f}_k\|^2_{\mathbf{G}}, && (5.11)\\
\text{subject to}\; & \mathbf{x}_{k+1} = \mathfrak{f}(\mathbf{x}_k, \mathbf{f}_k, \mathbf{c}_p) && \\
& \mathbf{x}_0 = \mathbf{x}_i && (5.12)\\
& \mathbf{x}_N = \mathbf{x}_{i+1} && (5.13)\\
& \underline{\mathbf{f}} \le \mathbf{f}_k \le \overline{\mathbf{f}}, \quad \forall k \in \{1, \ldots, N\} && (5.14)\\
& \mathbf{E}\mathbf{f}_k = \mathbf{0}, \quad \forall k \in \{1, \ldots, N\}, && (5.15)
\end{aligned}$$

where $\underline{\mathbf{f}}, \overline{\mathbf{f}} \in \mathbb{R}^6$ are substrate reaction force limits, $\mathbf{H}, \mathbf{G}$ are positive semidefinite weighting matrices, and $\mathbf{E} \in \mathbb{R}^{2\times 6}$ selects the elements of $\mathbf{f}_k$ corresponding to the swing leg, which are to have zero reaction force. The notation $\|a\|^2_H$ is used to mean the weighted norm $a^\top H a$.

In our trajectory optimisation formulation, we have set $\mathbf{H} = \text{blkdiag}(0, 0, 0, h_{\dot{x}}, h_{\dot{y}}, h_{\dot{\phi}})$, so as to have no penalty on any pose but still regularise with respect to velocity.

5.5 Control

Now that the trajectory $\mathbf{x}^\star$ between any two consecutive pose waypoints can be computed, we turn our attention to designing a controller to track $\mathbf{x}^\star$. In this work, two separate controllers are developed, a lumped mass controller for the 2D system, and a whole-body controller for the 3D. It was originally assumed that the lumped mass controller was appropriate as we assumed the limbs would make up approximately 10% of the body mass, which in line with the assumptions made in other work [137, 138]. Whilst this controller performs well for the 2D system where this assumption can be implemented in simulation, the design of our 3D robot could not meet this specification. Instead, the limbs of our physical 3D robot (described in Section 6.2) make up approximately 30% of the mass, and their dynamics and distribution do effect the robot performance. For this reason we use a whole-body controller instead, that considers the full dynamics of the floating base system.

5.5.1 Lumped Mass Control

Control of the robot body is achieved through feedback control of the 2D body state $\mathbf{x}$, to track $\mathbf{x}^\star$. For the purpose of trajectory tracking, we consider a slightly different dynamical system than (5.9) with the same state but under a different forcing term $\mathbf{u} \in \mathbb{R}^3$, the 2D wrench acting on the simplified rigid body:

$$\dot{\mathbf{x}} = \begin{bmatrix} \mathbf{0} & \mathbf{I_3} \\ \mathbf{0} & \mathbf{0} \end{bmatrix} \mathbf{x} + \begin{bmatrix} \mathbf{0_{3\times 3}} \\ \mathbf{M}^{-1} \end{bmatrix} \mathbf{u}. \tag{5.16}$$

Our controller is an infinite horizon linear quadratic regulator (LQR) with cost function

$$\mathbf{J}(x, u) = \int_0^\infty \mathbf{x}^\top Q \mathbf{x} + \mathbf{u}^\top R \mathbf{u} \, dt, \tag{5.17}$$

where Q, R are symmetric, positive definite matrices of the appropriate dimension. The LQR is chosen as it is optimal for linear time invariant (LTI) systems. The solution to the algebraic Riccati equation associated with (5.16) and (5.17) yields an optimal gain matrix K, and the desired 2D body wrench is given by

$$\mathbf{u}(t) = K(\mathbf{x}^\star(t) - \mathbf{x}(t)) + u_g. \tag{5.18}$$

From the desired body wrench, we compute the reaction force at each of the contacting limbs. The mapping between the reaction forces at each limb end effector $F_i \in \mathbb{R}^3, i \in \{L, R, B\}$ and the body wrench is

$$\mathbf{C} \underbrace{\begin{bmatrix} [r_L]_\times & [r_R]_\times & [r_B]_\times \\ \mathfrak{s}(t)\mathbf{I_3} & \mathfrak{s}(t)\mathbf{I_3} & \mathfrak{s}(t)\mathbf{I_3} \end{bmatrix}}_{\mathbf{D}} \underbrace{\begin{bmatrix} F_L \\ F_R \\ F_B \end{bmatrix}}_{\mathbf{F}} = \hat{\mathbf{u}}, \tag{5.19}$$

where $\hat{\mathbf{u}} = \begin{bmatrix} 0 & 0 & u_3 & u_1 & u_2 & 0 \end{bmatrix} \in \mathbb{R}^6$ is the 3D version of the 2D body wrench $\mathbf{u}$; $[r_L]_\times$, $[r_R]_\times$, and $[r_B]_\times \in so(3)$ are the skew-symmetric matrices that implement the cross product, i.e. $[r]_\times f = r \times f$; $\mathfrak{s}(t)$ provides smooth contact transitions by taking the form

$$\mathfrak{s}(t) = \begin{cases} \frac{1}{2}[1 + \tanh\Big(\pi + \frac{2\pi}{T_s}(t_c - t)\Big)] & \text{(making contact)} \\ \frac{1}{2}[1 - \tanh\Big(\pi + \frac{2\pi}{T_s}(t_c - t)\Big)] & \text{(releasing contact);} \end{cases} \tag{5.20}$$

and $\mathbf{C}$ is the selector matrix,

$$\mathbf{C} = \text{blkdiag}(\begin{bmatrix} c_L\mathbf{I_3} & c_R\mathbf{I_3} & c_B\mathbf{I_3} \end{bmatrix}), \tag{5.21}$$

where $c_i, i \in \{L, R, B\}$ is

$$c_i = \begin{cases} 1 & \text{if limb } i \text{ is in contact,} \\ 0 & \text{otherwise.} \end{cases} \tag{5.22}$$

With $\mathbf{F}$ being underconstrained, a simple way to choose F_L, F_R, F_B is to use the minimum 2-norm solution for $\mathbf{F}$, which can be found via the psuedoinverse. The desired reaction forces can then be written as

$$\mathbf{F} = (\mathbf{CD})^\dagger \hat{\mathbf{u}}. \tag{5.23}$$

The in-contact limbs are tasked with applying end effector wrenches to produce the desired reactions $\mathbf{F}$. Since the limbs of the robot are lightweight and moving relatively slowly, we ignore the limb dynamics and apply the “static” torque relation

$$\tau_i = -J_i(\theta_i)^\top F_i, \tag{5.24}$$

where τ_i, θ_i are torques and joint angles for the limbs i that are in contact with the structure, and $J_i(\theta_i)$ their corresponding Jacobians.

5.5.1.1 Swing Leg Control

The swing leg controller aims to track (5.6) via PD and feedforward control on the end effector position $\mathbf{p}$. The controller computes a force $\mathbf{u_s} \in \mathbb{R}^3$ at the end effector tip

$$\mathbf{u}_s = K_p(\mathbf{p}^\star - \mathbf{p}) + K_d(\dot{\mathbf{p}}^\star - \dot{\mathbf{p}}) + [m_i g; 0; 0], \tag{5.25}$$

where $m_i, i \in \{L, R, B\}$ is the mass for the current swing leg. Joint torques to realize $\mathbf{u}_s$ are then computed via (5.24).

5.5.2 Whole-Body Controller

The whole-body controller is based on a constrained representation of the whole-body dynamics. The following approach builds on top of the ‘floating base’ control described in [139], with novel modifications used for scansorial locomotion.

The unconstrained dynamics of a floating base system can be written in its canonical form as

$$\mathbf{M}(\mathbf{q})\ddot{\mathbf{q}} + \mathbf{h}(\mathbf{q}, \dot{\mathbf{q}}) = \mathbf{S}\tau + \mathbf{J}(\mathbf{q})_\phi^\top \lambda, \tag{5.26}$$

where $\mathbf{M}(\mathbf{q}) \in \mathbb{R}^{n \times n}$ is the mass mass matrix, $\mathbf{h}(\mathbf{q}, \dot{\mathbf{q}}) \in \mathbb{R}^n$ is the combined Coriolis and gravity vector, $\mathbf{S} \in \mathbb{R}^{n \times n}$ is the actuator selector matrix, $\mathbf{J}(\mathbf{q})_\phi \in \mathbb{R}^{6n_c \times n}$ are the stacked set of Jacobians to each end-effector, $\lambda \in \mathbb{R}^{6n_c}$ is a vector of reaction forces at the contacts, and $\tau \in \mathbb{R}^n$ is a vector of joint torques. The arguments of each function are dropped in the remainder of this section for the reader’s convenience.

In order to ensure contact points do not move during the stance phase for each leg, we impose a constraint on the acceleration of the end effector. A common way of stating the point should not move, is to define a holonomic constraint at the end effector, constraining the velocity to be zero. If the forward kinematics can be expressed as $\phi(\mathbf{q})$, then the holonomic constraint can be written as

$$\frac{d}{dt}\phi(\mathbf{q}) = \mathbf{J}_\phi \dot{\mathbf{q}} = 0. \tag{5.27}$$

Taking the time derivative of (5.27) we get the Pfaffian constraint

$$\frac{d^2}{dt^2}\phi(\mathbf{q}) = \mathbf{J}_\phi\ddot{\mathbf{q}} + \dot{\mathbf{J}}_\phi\dot{\mathbf{q}} = 0, \tag{5.28}$$

which is the necessary form to include in our dynamic system. This can be rearranged into the form

$$\mathbf{J}_\phi\ddot{\mathbf{q}} = \underbrace{-\dot{\mathbf{J}}_\phi\dot{\mathbf{q}}}_{\mathbf{b}}. \tag{5.29}$$

Whilst this works well during the stance phase, an additional term can be added in order to achieve some desired end effector acceleration, $\ddot{\phi}$, during a limb's swing phase. This can be expressed as

$$\mathbf{J}_\phi\ddot{\mathbf{q}} = \mathbf{b} + \ddot{\phi}. \tag{5.30}$$

With the end effector acceleration constraints now determined, we can write the constrained dynamics of a general legged system as

$$\begin{aligned} &\mathbf{M}(\mathbf{q})\ddot{\mathbf{q}} + \mathbf{h}(\mathbf{q},\dot{\mathbf{q}}) = \mathbf{S}\tau + \mathbf{J}_\phi^\top\lambda \\ &\mathbf{J}_\phi\ddot{\mathbf{q}} = \mathbf{b} + \ddot{\phi}, \end{aligned} \tag{5.31}$$

which can be expressed in matrix form as

$$\begin{bmatrix} \mathbf{M} & -\mathbf{S} & -\mathbf{J}_\phi^\top \\ \mathbf{J}_\phi & & \end{bmatrix} \begin{bmatrix} \ddot{\mathbf{q}} \\ \tau \\ \lambda \end{bmatrix} = \begin{bmatrix} -\mathbf{h} \\ \mathbf{b} + \ddot{\phi} \end{bmatrix}. \tag{5.32}$$

5.5.2.1 Additional constraints for climbing

The constraints expressed in (5.32) are valid for all instances of legged robots where the contact points are non-moving during stance. In this work, however, it is necessary to define axes where free motion at the end effector is possible. The prehensile end effectors of our 3D robot utilise free motion about the contact as a strategy to reduce DoF in the limb (as described in section 5.3). To enable this in the control, we have made two modifications to (5.32), in order to: 1. constrain force production about free axes to zero; 2. relax the Pfaffian constraint such that accelerations and velocities around the free axis can be developed.

5.5.2.2 Wrench production constraint

In order to prevent forces or torques being developed in dimensions where this force cannot be reacted, we add an additional constraint that exploits the redundancy of the system. This constraint takes the form

$$\mathbf{P}\lambda = 0, \tag{5.33}$$

where $\mathbf{P} \in \mathbb{R}^{(3n_c+5)\times 6n_c}$ is a projection matrix that acts to constrain a projection of the reaction wrench, $\lambda \in \mathbb{R}^{6n_c}$, to be zero. $\mathbf{P}$ is constructed as the block diagonal matrix of the individual projection matrices that operate at each contact point, and takes the form

$$\mathbf{P} = \begin{bmatrix} \begin{bmatrix} P_L & \mathbf{0_3} \end{bmatrix} & & & \\ & \begin{bmatrix} P_R & \mathbf{0_3} \end{bmatrix} & & \\ & & \begin{bmatrix} P_B & \mathbf{0_3} \end{bmatrix} & \\ & & & P_T \end{bmatrix}, \tag{5.34}$$

where each projection matrix, $P_i \in \mathbb{R}^{3\times 3}$ for $i \in \{L, R, B\}$ is constructed from the unit vector, $u_i \in \mathbb{R}^3$, which points along the free axis of rotation of each end effector;

$$P_i = \frac{u_i u_i^\top}{u_i^\top u_i}. \tag{5.35}$$

In this formulation, we exploit the fact that we only wish to constrain torques about a particular axis, u_i; however, were it necessary to provide additional constraints, each block element in **P** can be extended up to $P_i \in \mathbb{R}^{6\times6}$. As an example, a common constraint that is present in this work is for the ladder rung to be aligned with the y-axis (i.e. $u_i = [0 \quad 1 \quad 0]^\top$) in the world frame, which results in

$$P_i = \begin{bmatrix} 0 & 0 & 0 \\ 0 & 1 & 0 \\ 0 & 0 & 0 \end{bmatrix}. \tag{5.36}$$

The constraint on the tail $P_T \in \mathbb{R}^{5\times6}$ is defined differently to the others, as unlike the other it is not designed to grasp the structure, but provide pitch-back support. As a simplification, the tail is considered only to apply forces in the direction normal to the climbing plane, which for the experiments in Section 6.3 make up the X-Y plane. To achieve this, all elements of λ associated with the tail contact are set to zero with

$$P_T = \begin{bmatrix} 1 & 0 & 0 & 0 & 0 & 0 \\ 0 & 1 & 0 & 0 & 0 & 0 \\ 0 & 0 & 1 & 0 & 0 & 0 \\ 0 & 0 & 0 & 1 & 0 & 0 \\ 0 & 0 & 0 & 0 & 1 & 0 \end{bmatrix}. \tag{5.37}$$

The projection matrix **P** is combined with (5.32) to produce

$$\underbrace{\begin{bmatrix} \mathbf{M} & -\mathbf{S} & -\mathbf{J}_\phi^\top \\ \mathbf{J}_\phi & & \\ & & \mathbf{P} \end{bmatrix}}_{\mathbf{B}} \begin{bmatrix} \ddot{\mathbf{q}} \\ \tau \\ \lambda \end{bmatrix} = \begin{bmatrix} -\mathbf{h} \\ \mathbf{b} + \ddot{\phi} \\ \mathbf{0} \end{bmatrix}. \tag{5.38}$$

5.5.2.3 Relaxing the Pfaffian constraint

Whilst torque production about the free axes of the end effectors are quashed, accelerations and velocities around these free axes must be permitted. We achieve this by projecting the Pfaffian constraint into the nullspace of the free axis vector, u_i for $i \in \{L, R, B\}$ with

$$\mathbf{U_i} = \text{null}(u_i),$$

$$\mathbf{U} = \begin{bmatrix} \mathbf{U}_L & & & \\ & \mathbf{U}_R & & \\ & & \mathbf{U}_B & \\ & & & \mathbf{U}_T \end{bmatrix}, \tag{5.39}$$

$$\mathbf{U}(\mathbf{J}_\phi \ddot{\mathbf{q}} + \dot{\mathbf{J}}_\phi \dot{\mathbf{q}}) = 0, \tag{5.40}$$

$$\underbrace{\mathbf{U}\mathbf{J}_\phi}_{J^*_\phi} \ddot{\mathbf{q}} = \underbrace{-\mathbf{U}\dot{\mathbf{J}}_\phi \dot{\mathbf{q}}}_{\mathbf{b}^*}. \tag{5.41}$$

This projection is only valid during the stance phase of a limb. During the swing phase the constraint is removed and $\mathbf{U_i}$ is reverted to the identity.

Just as it is for defining force production of the tail, the tail is also treated specially due to the unique constraints defined by its modelling. For the purposes of this work, the tail is modelled as a point contact that is constrained to the climbing plane. In the sense that acceleration and velocities need to be constrained, the tail therefore is only constrained to produce zero acceleration in the Z-direction, hence

$$\mathbf{U}_T = \begin{bmatrix} 0 & 0 & 0 & 0 & 0 & 1 \end{bmatrix}^\top. \tag{5.42}$$

5.5.2.4 Joint torque optimisation

Now that we have adequately modelled our constrained dynamical system, we formulate our motion control problem as a quadratic program with linear constraints, which can be solved in real time for online motion control. Taking (5.38) and rearranging using the pseudoinverse, we get

$$\begin{bmatrix} \ddot{\mathbf{q}} \\ \boldsymbol{\tau} \\ \boldsymbol{\lambda} \end{bmatrix} = \underbrace{\mathbf{B}^{\dagger} \begin{bmatrix} -\boldsymbol{h} \\ \boldsymbol{b} + \ddot{\phi} \\ 0 \end{bmatrix}}_{\boldsymbol{v}} + \mathbf{V}_{\perp}\beta. \tag{5.43}$$

Using this definition (5.43) allows us to describe the space of feasible dynamic quantities as

$$\begin{bmatrix} \ddot{\mathbf{q}} \\ \boldsymbol{\tau} \\ \boldsymbol{\lambda} \end{bmatrix} = \boldsymbol{v} + \mathbf{V}_{\perp}\beta = \begin{bmatrix} \boldsymbol{v}^{\ddot{\mathrm{q}}} \\ \boldsymbol{v}^{\tau} \\ \boldsymbol{v}^{\lambda} \end{bmatrix} + \begin{bmatrix} \boldsymbol{V}_{\perp}^{\ddot{\mathrm{q}}} \\ \boldsymbol{V}_{\perp}^{\boldsymbol{\tau}} \\ \boldsymbol{V}_{\perp}^{\lambda} \end{bmatrix} \beta, \tag{5.44}$$

for which we can extract rows to use in constructing our optimisation problem. In our optimisation problem, we seek to minimise torques whilst producing some desired body acceleration, $\ddot{\mathbf{q}}_0^*$. In early versions of the optimisation, we considered only joint torques and set the desired body acceleration, $\ddot{\mathbf{q}}_0^*$, as an equality constraint. This approach worked well when $\ddot{\mathbf{q}}_0^*$ was in the space of feasible solutions as defined by (5.44); however, when it was not, and the optimiser failed to solve, we are left only with the pseudo-inverse solution, $\boldsymbol{v}$, which does not produce torques that can be considered useful for the control objective.

Instead of including $\ddot{\mathbf{q}}_0^*$ as an equality constraint, we try to minimise the error between the desired acceleration and the commanded acceleration. By extracting rows from (5.44) we define the following equation for use in our optimisation

$$\ddot{\mathbf{q}} = \boldsymbol{v}_{\ddot{\mathrm{q}}} + \boldsymbol{V}_{\ddot{\mathrm{q}}}^{\perp}\beta - \ddot{\mathbf{q}}_0^* \tag{5.45}$$

$$\boldsymbol{\tau} = \boldsymbol{v}_{\boldsymbol{\tau}} + \boldsymbol{V}_{\boldsymbol{\tau}}^{\perp}\beta. \tag{5.46}$$

Letting $\boldsymbol{a} = \begin{bmatrix} \ddot{\mathbf{q}} \\ \boldsymbol{\tau} \end{bmatrix}$, the motion control problem can be expressed as the following quadratic problem:

$$\begin{aligned} \min_{\beta} \quad & \boldsymbol{a}^{\top}\boldsymbol{W}\boldsymbol{a} \\ \text{s.t.} \quad & \underline{\boldsymbol{\tau}} \leq \boldsymbol{\tau} \leq \overline{\boldsymbol{\tau}} \\ & \underline{\boldsymbol{\lambda}} \leq \boldsymbol{\lambda} \leq \overline{\boldsymbol{\lambda}} \end{aligned} \tag{5.47}$$

where $\boldsymbol{W}$ is the block diagonal weighing matrix,

$$\boldsymbol{W} = \begin{bmatrix} \boldsymbol{W}_{\ddot{\mathbf{q}}} & 0 \\ 0 & \boldsymbol{W}_{\boldsymbol{\tau}} \end{bmatrix},$$

and the solution is bounded by the joint torque limits $\underline{\boldsymbol{\tau}}$ and $\overline{\boldsymbol{\tau}}$, and reaction force limits, $\underline{\boldsymbol{\lambda}}$ and $\overline{\boldsymbol{\lambda}}$.

5.5.2.5 Acceleration-based Trajectory Tracking

In order to track trajectories, the following feedback controller is implemented. The control law defined is a combination of proportional, integral, derivative (PID) feeback and acceleration feedforward. Since we can command accelerations of the arm directly, the feedback is intended to modify the feedforward term as errors accumulate in position and velocity. Set points can also be used with this approach; however, instead of modifying the trajectory acceleration, the PID controller will generate the appropriate acceleration to push the end effector or body towards the set point. In this case the feedforward term simply remains equal to zero. The desired acceleration, $\ddot{\mathbf{q}}_0^*$, passed into the quadratic program (5.47) is defined as

$$\ddot{\mathbf{q}}_0^* = K_P^{\mathbf{q}}(\mathbf{q}_0 - \mathbf{q}) + K_I^{\mathbf{q}} \int (\mathbf{q}_0 - \mathbf{q})\, dt + K_D^{\dot{\mathbf{q}}}(\dot{\mathbf{q}}_0 - \dot{\mathbf{q}}) + \ddot{\mathbf{q}}_0, \tag{5.48}$$

where $\mathbf{q}_0$ and $\dot{\mathbf{q}}_0$ are the trajectory or set point position and velocity, and $\mathbf{q}$ and $\dot{\mathbf{q}}$ are the feedback real time values for position and velocity for the frame being tracked. An identical strategy is used to determine the desired acceleration, $\ddot{\phi}_i$ for any given leg ($i \in \{L, B, R\}$) in its swing phase.

5.6 Summary

In this chapter, we have presented the kinematic designs of two tripedal robots of increasing complexity. The first robot (Section 5.1) is for exploration of simple concepts in control, path planning, and trajectory planning, methods that we have also described in this chapter. The second robot (Section 5.2) has been designed to work in 3D and to be the basis of a physical robot design. Extending concepts we explore in our initial control descriptions, we have made novel modifications to whole-body control algorithms for application to this 3D robot. In the next chapter, we perform experiments with each of our robot designs in simulation. We also present the mechanical design of the worlds first tripedal climbing robot and validate the design and whole-body control algorithms also in simulation.

Chapter 6

Experiments

Two sets of simulations and the hardware design of a 3D climbing robot are presented in this chapter. First, experiments with the robot defined in Section 5.2 are performed in simulation, and a comparison is made between the different climbing scenarios and planning approaches defined in Section 5.4. Next, the hardware design of the ParCli robot based on the kinematics defined in Section 5.3 is presented. The ParCli robot is implemented in simulation with the goal of validating the hardware design, control strategies, and understanding their limitations. By the end of this chapter we are in a good position to begin migrating our whole-body control algorithms over to the physical robot.

6.1 Simulated 2D Climbing

The 2D robotic design, presented in Section 5.2, is our first attempt at creating a simple tripedal climbing robot. The robot is designed, tested here as a preliminary evaluation on the validity of the tripedal concept, and also acts as a stepping stone for the development of path planning, trajectory planning, and simplified control algorithms.

Table 6.1: Simple robot data and control parameters

m	10 kg	K_P	diag([100 50 0])
I_{zz}	0.1 kgm^2	K_D	diag([15 10 0])
$-g_x$	9.81 m/s^2	Q	diag([1e+6 1e+6 100 0 0 0])
Body Length	0.4 m	R	diag([0.25 0.25 4])
Body Width	0.15 m	$\mathbf{H}$	diag([0,0,0,1e1,1e2,1e1])
L1	0.3 m	$\mathbf{G}$	1e-2$\mathbf{I}_6$
L2	0.3 m	T_s	0.2s
L3	0.35 m	T	1s
L4	0.4 m	N	100

6.1.1 Simulation Setup

A simulation model of the 2D robot (Figure 6.1) has been created in MATLAB 2021b using the Simscape Multibody package in Simulink. For the lumped mass controller (see section 5.5.1) to perform adequately, we make the assumption that the total mass of all limbs is less than 10% of the total mass of the robot (as is achieved in similar research [57]), and assign equal masses to the each link of each limb accordingly. The motion between the end effectors and the world frame are modelled as planar joints. Pitch-back moments (about the Y-axis) are resisted by these contact joints passively. Table 6.1 gives inertial, kinematic, and control parameters used for the simulation.

Adhesion to the vertical climbing surface is achieved using the Simscape Multibody Contact Forces Library [140]. Specifically, the Sphere to Plane Force Enabled block is used. The Enabled blocks in the Contact Forces Library allow switching of the contacts to simulate swing and stance phases of each limb. Adhesion with this block is applied as a frictional force, where the coefficient of static friction is set artificially high ($\mu = 1000$) to ensure no slipping at the contact point. Attached to a planar joint, the contact is embedded a small fraction (1mm) into the climbing plane, which is resisted passively by the planar joint and does not interact with the robot dynamics or control.

The footfall planner, trajectory optimisation, and LQR control gains are computed offline. The trajectory optimisation problem between each consecutive pair of waypoints (5.11) was solved using `acados` [141]. After about four seconds of compiling, `acados` solved the optimisation problem for ten footsteps in about 98ms on a desktop PC with a 3.8GHz AMD Ryzen 7 processor. The maximum reach footfall planner planned 10 footsteps in

782ms, and the Monte Carlo footfall planner with `max_iter` = 1000 took 1535 seconds on the same machine.

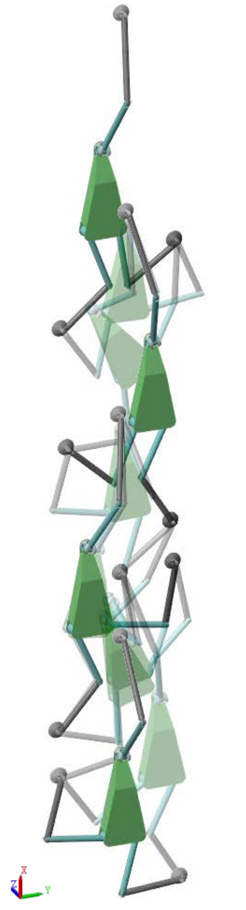

FIGURE 6.1: Simulink model of climbing tripedal robot using the three-step footfall strategy. Each frame depicted represents the end of a single foot step. Some frames have been made translucent for visual clarity. A video of this experiment and others is available at `https://youtu.be/vRVGraIyQgQ`

6.1.2 Climbing On Ladders and Walls

Vertical climbing experiments on a continuous substrate and a reticular structure were performed. For the continuous substrate ('wall') case, the foot placements were allowed to be anywhere on the plane. For the reticular structure ('ladder') case, foot placements were enforced in the footfall planner to be on the rungs of the ladder. For each of the two substrate types ('ladder' or 'wall'), and each of the two trajectory generation methods (minimum-jerk or OCP-based trajectory optimisation), three footfall strategies were considered: the Monte Carlo sampling method, and the three- and four-step maximum reach methods. A video of a few of these climbing experiments is available at `https://youtu.be/vRVGraIyQgQ`. Figure 6.2 shows the path of the body over the twelve simulated experiments.

6.1.3 Characterisation of Climbing Efficiency

Climbing efficiency is often measured with respect to cost of transport (CoT), a useful metric for comparing the energy efficiency of real systems. Whilst our system is simulated only, CoT is still a useful metric to compare between the different combination of factors present in this study. Cost of transport is defined as

$$\mathrm{CoT} = \frac{E}{mg\Delta x}, \tag{6.1}$$

where $E = \int_0^{T_f} |\dot{\theta}(t)|^\top |\tau(t)| dt$, where T_f is the total time duration of the ten footsteps.

6.1.4 Results

Figure 6.4 shows the CoT versus height climbed for each combination of footfall planner, trajectory generator, and substrate evaluated over a ten-step trial. In every case, the OCP -based trajectory yields a better CoT result over the minimum-jerk trajectory. This is a result of the fact that the minimum jerk trajectory (5.4) is constrained to be a straight line, while OCP-based trajectories are allowed to deviate (notice the relative straightness of the blue lines versus the red curves in Figure 6.2). The Monte Carlo footfall planner yielded the highest CoT in our experiments, though the Score() function in Line 14 of Algorithm 5.1 considers only of the height climbed. If Score() were to have considered energy expenditure as well, it is likely the CoT would decrease for Monte Carlo footfall plans. On the wall substrate, all footfall strategies show very similar results for CoT; however, the four-step footfall scheme covered the most ‘ground’ in the 10 steps the simulation was run over. Interestingly, the lowest CoT was displayed by the three-step footfall scheme on the ladder structure. The three-step scheme was the footfall strategy most often used by the cockatiels in our observations, this may be mere coincidence, or it could indicate

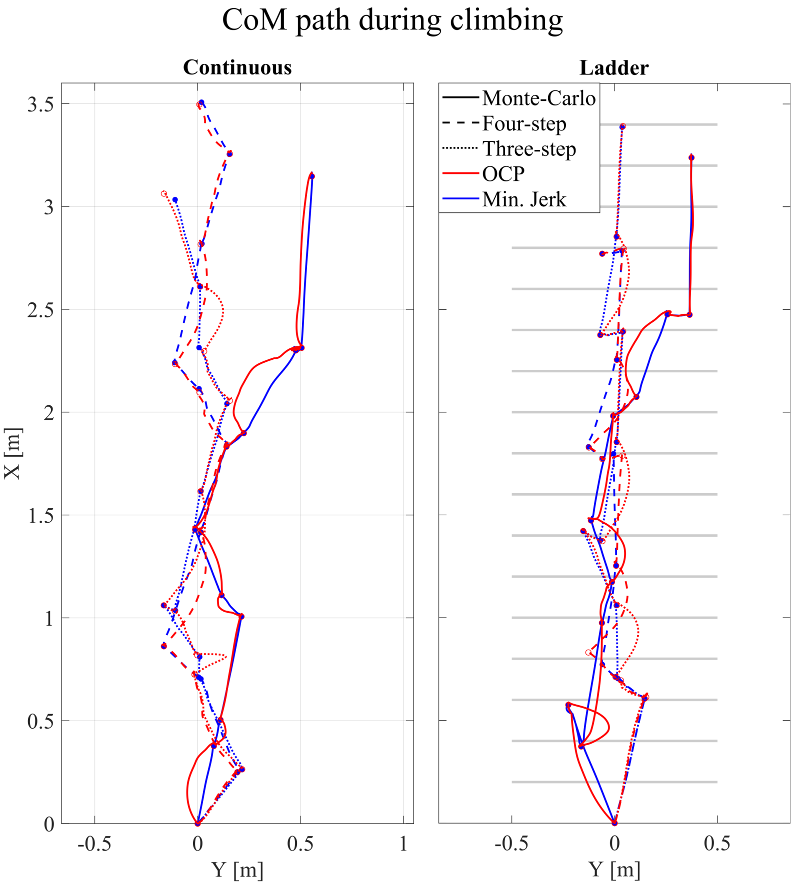

Figure 6.2: Body center of mass (CoM) path $(x(t), y(t))$ taken during different simulations. The circles show stationary points of the body, where all feet are in contact as weight is transferred off the next leg to be moved

the strategy of the birds was a deliberate attempt to reduce CoT. Further experiments, analysis, and modelling would be required in order to establish any more substantive claim.

An example of the torque profiles during climbing can be seen in Figure 6.3. This figure shows the torque used by each actuator and compares the torque between the OCP and minimum jerk trajectories for the case of ladder climbing with the cyclic three-step footfall plan. Typically, tracking the OCP trajectory requires similar or lower torque than tracking the minimum jerk trajectory (see right limb torque plot from 5.5 to 6.5s), resulting in small energy savings, driving down the CoT in Figure 6.4. A full tables of results for each run is shown in Table 6.2.

Idealised power and velocity performance for our robot fall in line with the reported figures in literature. The WAREC-1 for example, draws about 1500W for its 155kg [26] giving

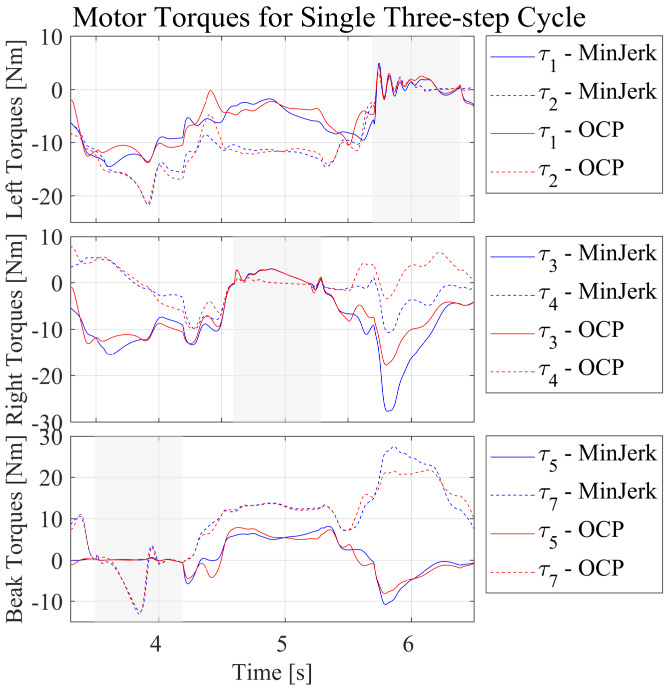

FIGURE 6.3: Comparison of motor torques between the OCP and minimum-jerk strategies for trajectory generation when climbing the ladder and with the footfall plan generated by the three-step scheme. Grey bands correspond to times where the limb is in the swing phase and not providing propulsive force for climbing. Note that actuator 6 is not shown due to the motor torque being 0. This occurs as the reaction force vector is constrained to the climbing plane which also is coincident with the axis of joint 6

it a rough power to mass ratio of 9.67 W/kg and achieving a vertical speed of 2.5 cm/s. The dynamically excited ROCR robot achieves a stunning 0.12 W/kg when climbing at a rate of 14 cm/s [142]. Our robot, in simulation, uses a mean of 6.6 W/kg when climbing 36 cm/s. We expect this power figure to climb and velocity figure to drop considerably if implemented in a physical prototype; however, the performance in simulation is within the range suggested by robotic hardware experiments.

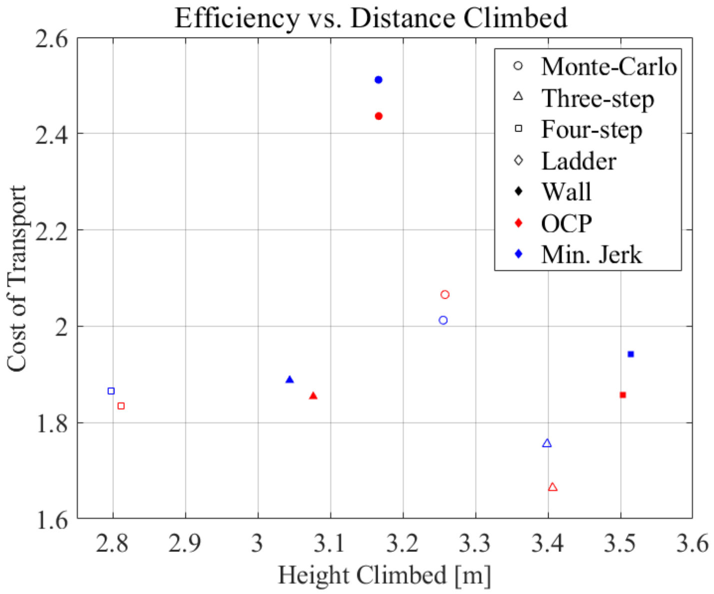

FIGURE 6.4: Graph show the relation ship between climbed vertical distance and cost of transport for each combination of factors

Table 6.2: Performance metrics during climbing

Substrate	Footfall	Traj.	Mean Power [W]	Peak Power [W]	Mean Vertical Velocity [m/s]	Mean Velocity [body lengths/s]
Continuous	Sampling	Min. jerk	58.1	337	0.32	0.81
Continuous	Four-step	Min. jerk	68.3	259	0.39	0.97
Continuous	Three-step	Min. jerk	60.9	255	0.36	0.90
Continuous	Sampling	Acados	56.2	233	0.31	0.78
Continuous	Four-step	Acados	62.9	225	0.35	0.88
Continuous	Three-step	Acados	57.0	230	0.32	0.80
Ladder	Sampling	Min. jerk	62.5	197	0.32	0.79
Ladder	Four-step	Min. jerk	62.3	199	0.39	0.98
Ladder	Three-step	Min. jerk	64.6	198	0.42	1.05
Ladder	Sampling	Acados	61.6	208	0.30	0.75
Ladder	Four-step	Acados	56.5	180	0.35	0.86
Ladder	Three-step	Acados	57.4	179	0.38	0.94

6.1.5 Discussion

The results presented on the simple 2D example of tripedal climbing support our claim that tripedal climbing is feasible, and that reasonable control of a climbing robot can be achieved with only two points in contact. It was not necessary to include any dynamic behaviours or models to facilitate climbing, though we expect such inclusions would benefit the climbing efficiency. Through exploration of different planners, we noted that simple heuristics can result in effective climbing behaviours. We also note the efficacy of solving an OCP in the trajectory planning, and expect that further exploration of planning methods that can consider the robot's pose as a conditioner for force production could have significant effect on forces experienced at the joints and energy used. With the goal of reducing robot mass, methods that can successfully utilise robot kinematics or dynamics to reduce necessary torque production during climbing could enable mass reduction. The preliminary demonstration of climbing with a simple 2D robot has several caveats. Firstly, there are no limitations placed on the magnitude of force producible at the contact points. Exceeding the capabilities of the contact is primarily how a reduction in the control space occurs, and so by having these unbounded, the robot is always assured to be overactuated. Secondly, since no kind of adhesion mechanism is defined, the robot control is not currently developed limitations on these contacts defined. It's likely for a real system that an optimal control method, that takes into account these limitations would be needed for a real system.

6.2 ParCli Robot Design

The design of the ParCli robot is based on the 3D robot kinematics defined in Section 5.3 and is completed in accordance with the lessons explored in Section 3.1; especially the reduction of limb inertia and associated centralisation of mass (Section 3.1.1). Whilst the 2D simulated robot allows fast development of algorithms under idealised conditions, our 3D robot will allow us to test algorithms with sufficient complexity for implementation on a real robot. The ParCli robot is designed specifically for climbing a 2D ladder under lab conditions, it will become a test bed for the exploration of control and planning strategies for tripedal climbing robots. In Section 6.1 we made the assumption that all limbs combined should make up approximately 10% of the total mass of the robot, which motivated the lumped mass control strategy in Section 5.5.1. In the design of ParCli we achieved approximately 30% of the total mass being located in the limbs and tail, with the body making up the remaining 70%. Some liberties are taken in this approximation; all of the large motors mounted near to the body are considered part of the body mass, for example. For a breakdown of mass with respect to the links defined in the dynamical model used in Section 6.3.2 for the control, see Table 6.4. The design of Parcli, which is the first physical realisation of the kinematic design described in section 5.3, is shown in figure 6.5. The physical systems allows us to validate design assumptions, challenge the conditions programmed in our simulation, so that is can be improved where large discrepancies are found. We are also able to validate that the kinematic design results in a feasible climbing robot.

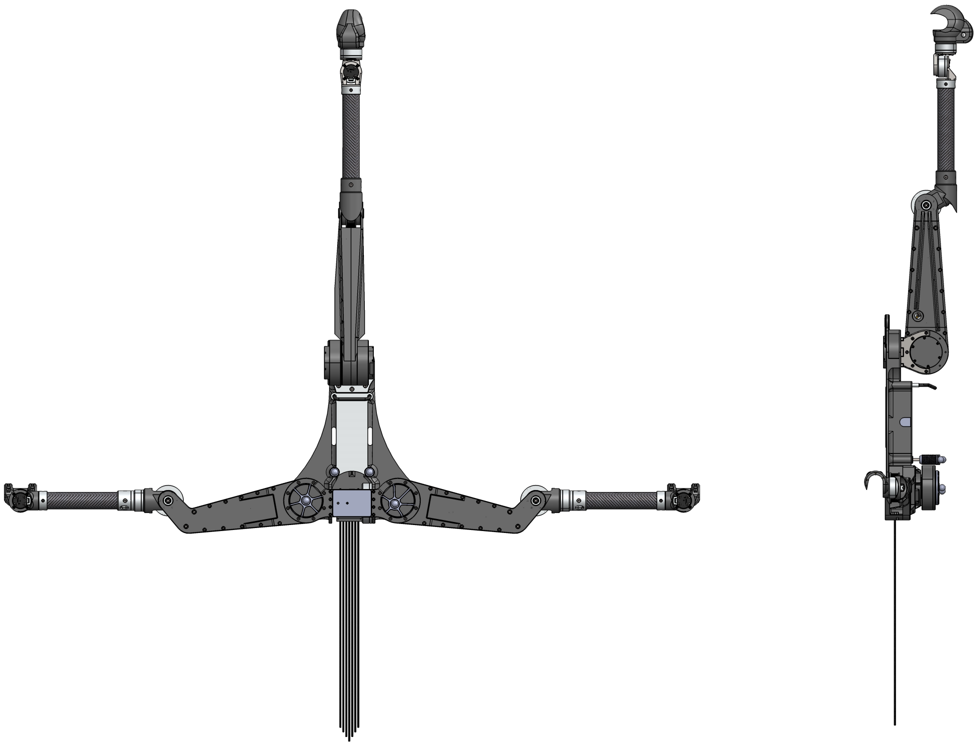

(A) FRONT View (B) SIDE View

Figure 6.5: Front and side views of the ParCli robot in its zero configuration.

6.2.1 Motor Configuration and Electronics

Across the 14 motors used in the robot, three models of actuator are used:

1. Ak80-9 dynamic robot servo from T-motor. This motor is a radial flux brushless DC motor with a 9:1 planetary gearbox built into its centre. A design inspired from work developing quadrupeds at MIT [143]. This motor is optimised to have a good power to weight ratio (in line with the lesson in Section 3.1.2), whilst maintaining reasonable backdrivability.
2. GL40 gimbal motors from T-motor are used for the wrist joints
3. A single GL80 gimbal motor from T-motor is used for the tail

Joint	Actuator Model	Peak Torque [N.m]	Continuous Torque [N.m]	Joint Limits	
				Upper	Lower
1	Ak80-9	18	9	-45°	+155°
2	Ak80-9	18	9	-85°	+90°
3	GL40 KV210	1	0.33	-180°	180°
4	GL40 KV210	1	0.33	*continuous*	
5	Ak80-9	18	9	-45°	+155°
6	Ak80-9	18	9	-85°	+90°
7	GL40 KV210	1	0.33	-180°	180°
8	GL40 KV210	1	0.33	*continuous*	
9	Ak80-9	18	9	-90°	+90°
10	Ak80-9	18	9	-12°	+140°
11	Ak80-9	18	9	-50°	+174°
12	GL40 KV210	1	0.33	-100°	+100°
13	GL40 KV210	1	0.33	*continuous*	
14	GL80 KV30	2.9	0.98	-80°	+60°

Table 6.3: Joints, their motor performance characteristics, and limits in the ParCli robot. Joints are enumerated with respect to 5.2.

Specifications for each motor can be found in Table 6.3. The Ak80-9 comes with a motor controller mounted to the back of the motor and is natively capable of CAN-BUS communications. The GL40s and GL80 are controlled using Odrive v3.6 motor controllers, which are mounted to the body and proximal leg links (Link 1 and 5). All motors are run in torque control mode. In order to facilitate good torque control, precise positioning of the rotor is required. To achieve this, a custom magnetic encoder board was designed around the AS5047U chip, which is a 14-bit on-axis magnetic rotary position sensor. The incremental pulse output of this sensor gives 4096 pulses per revolution, and was wired directly to the Odrives. The AS5047U sensor has the capacity for absolute position sensing, but unfortunately, at the time of writing the ODrive boards did not support the SPI communications protocol the chip needs to run in this mode.

The robot is equipped with an onboard 22.2V 6800mAh 6S Li-ion battery, which sits in the centre of the body. A 150A automotive relay is used to isolate the positive terminal of the battery during operation. They relay is powered from the ground and accompanies the CAN-BUS cables that are run up to robot.

6.2.2 Mechanical Design

ParCli is made from a combination of 3D-printed nylon and other plastics, machined aluminum, carbon fibre tube, and steel. In general, minimal analysis of forces and strengths was performed in favour of creating a prototype quickly. Sound engineering judgement was used in the selection of materials, and hand calculations that are not included here, were used when deciding relative thicknesses. Limb lengths were chosen based on rough analysis for what the motors can deliver and what is convenient for mechanical design. The selection of motors and validation that torque limits are appropriate are conducted in simulation in Section 6.4.1. In the remainder of this section we will present details of the mechanical and system design for the robot.

6.2.2.1 Centre Limb

The centre limb (also referred to as ‘beak’ limb) has six DoF, five active, and one passive about the free axis of the end effector. In line with the mass centralisation lesson discussed in Section 3.1.1, three Ak80-9 motors are connected in a serial configuration, and in close proximity (Figure 6.6a), with the first joint (joint 9) being embedded in the robot base. A steel bracket is fabricated to connect joints 9 and 10, which becomes the load path for the full force of the arm. Joint 11 is held by the structural components of the proximal link which is made up of two 3D printed halves. Joint 11 is driven via a synchronous belt that runs up to the elbow which puts the actuator for this joint in line with joint 10, centralising the mass distribution and reducing the inertia of the arm.

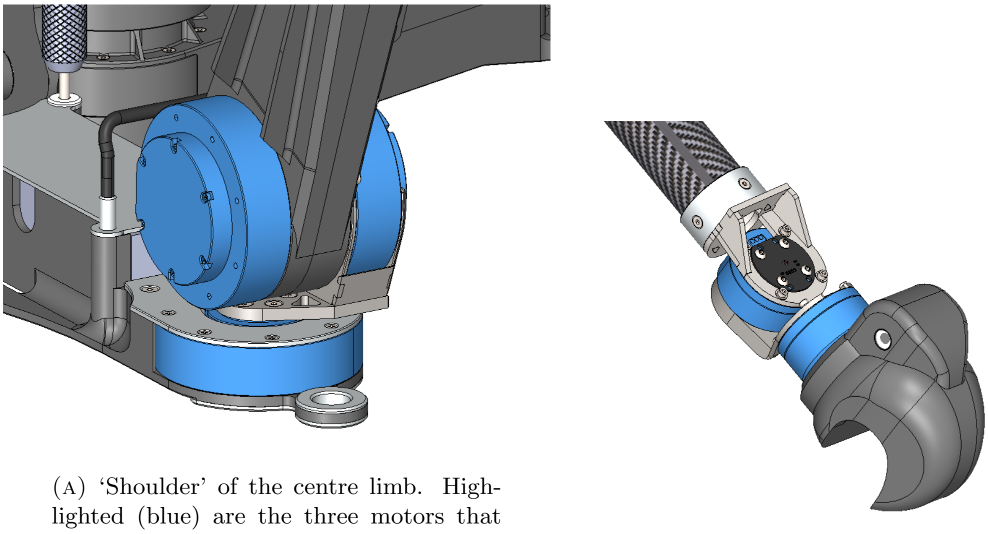

(A) 'Shoulder' of the centre limb. Highlighted (blue) are the three motors that drive joints 9 to 11. Joint 9 is embedded in the base, joint 10 connects directly to the steel bracket, and joint 11 hangs off the neck structure.

(B) Distal joints (12 and 13) of the centre limb. GL40 motors are highlighted in blue.

FIGURE 6.6: Detail view of the motor configuration of the centre limb.

The primary structure making up the distal link is made from a ⌀38mm×1mm thick carbon fibre tube. The hollow nature of the tube supports the internal routing of cable to ensure that they do not interact with and get tangled in the end effectors. The distal motors are held using fabricated steel brackets. An unintended effect of the design is that the power and encoder cables running to joint 12 are stiff enough to act like a mild spring, returning joint 11 to approximately its zero position when perturbed.

6.2.2.2 Leg Design

Each leg has five-DoFs, two active joints proximal to the body (Figure 6.7a), two active distal joints (Figure 6.7b), and one passive joint about the free axis of the end effector. When accounting for the passive free axis of the end effector, the three distal joint make a spherical joint for attachment to the ladder. The two proximal motors are mounted on top of one another (Figure 6.7a), and a synchronous belt is run along the proximal link to power the elbow joint. The skewed belt path (Figure 6.8) ensures asymmetric joint limits

(Table 6.3) from the zero position. Since an elbow down configuration is chosen when solving the IK, this asymmetry ensures the usual operating region of the limb is closer to the workspace centre, and allows for greater reachability when the end effector is near the body.

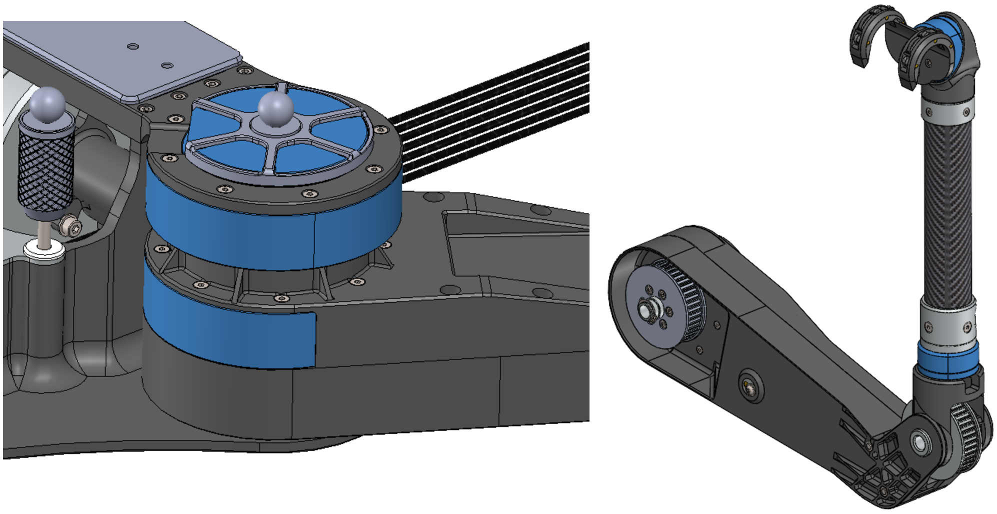

(A) The two proximal motors (blue) of the left leg (joints 1 and 2) shown stacked with coincident axes.

(B) The two distal motors (joints 3 and 4) that make up the active portion of the three-DoF wrist joint.

Figure 6.7: Motor configuration of the left leg

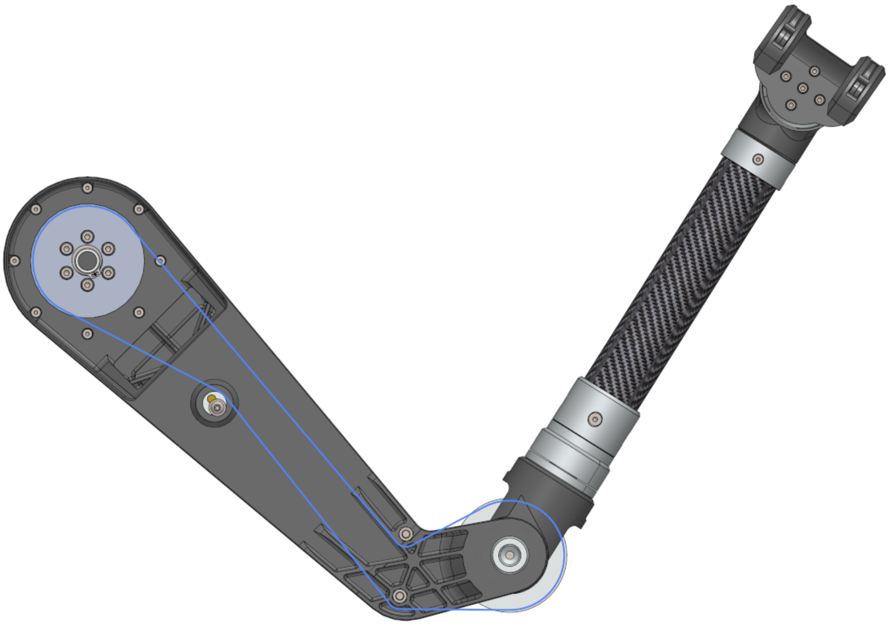

Figure 6.8: Belt path (blue) showing how power is delivered to the elbow joint (joint 2) of the left leg. The belt travels around an eccentric nut and bearing system which is used to tension the belt. The gearing between the driving and driven pulleys is 1:1

6.2.2.3 Tail Design

The tail is designed to be light weight and low inertia. It is composed of 7×⌀3mm carbon fibre rods and has a length of 520mm. The length of the tail is arbitrary and will be the subject to future investigation. The diameter and number of rods was chosen based what the authors consider to be *reasonable deformation*, which is based empirically on the tail deformation observed in the climbing cockatiels presented earlier (Figure 4.5). Based on the loads computed in early simulation models, a cantilever beam model is used to estimate deformation.

6.2.2.4 Body Design

The body (or ‘chassis’) houses the onboard battery and makes available two posts for connecting power (Figure 6.9). At the top of the body is a belay point for connecting a tether for preventing the robot from being damaged should it fall during climbing trials. Aluminium plates are used in key locations where the loads are high, to increase body stiffness and prevent failure of the 3D printed plastic (Figure 6.10). Adjacent to the battery is an aluminium heat-sink that does not provide any structural support to the body. At the leg joints are two aluminium bearing retainers for the bearing feeds loads into the chassis from the legs.

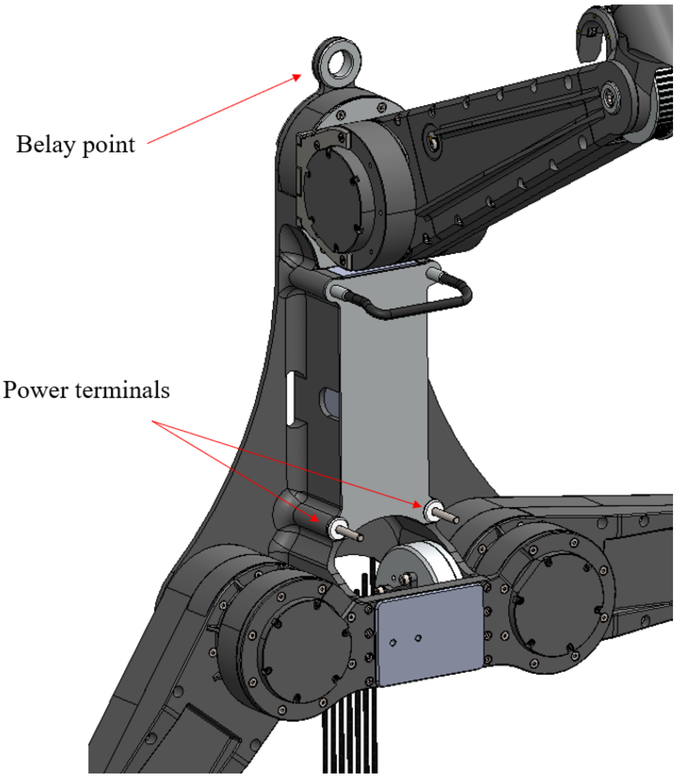

FIGURE 6.9: Close up of the ParCli main chassis. At the top is a belay point for roper support during climbing, near the bottom of the battery compartment are two power terminals for wiring.

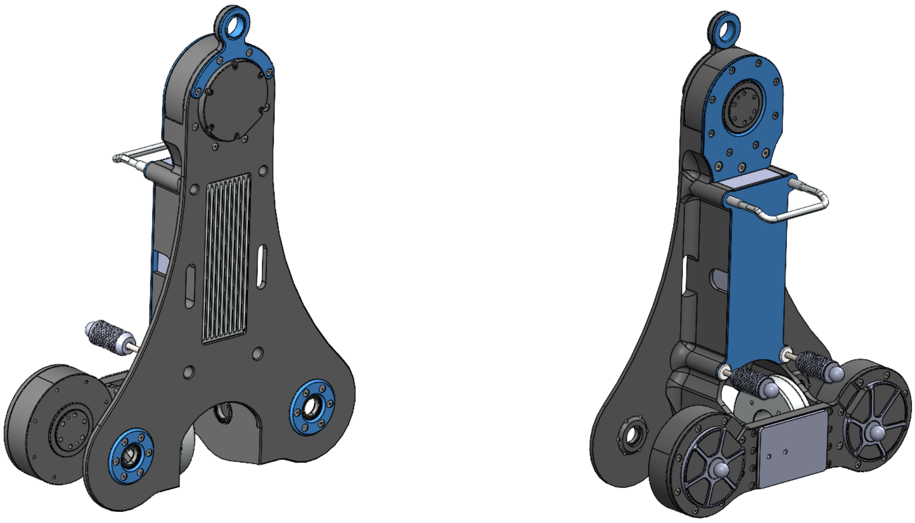
(A) (B)

Figure 6.10: Parcli body link. Highlighted in blue are machined aluminium components that add strength and stiffness to the 3D printed plastic. Four motion capture markers on the back of the joint 1 and 4 motors, and two are mounted on the power terminals.

6.2.2.5 Prehensile End effectors

The leg and beak grippers are design as simple hooks for simplicity. The leg grippers (often referred to as 'feet') have a wide hook-like design with a 10° opening to allow for misalignment when attempting to contact a rung (Figure 6.11). The feet have three sets of bearings around the circumference to allow for smooth rotation around the free-axis of the end effector.

The centre limb end effector (called the 'beak') is designed to be reminiscent of a parrot's head, but in reality has none of the complexity. Like the feet, it is modelled as a hook. Instead of bearings the contact surface is made small, and the structure above these contact is hollow, but has a geometry that facilitates stiffness. This contact point also has a 10° opening as shown in Figure 6.12.

6.2.3 System Design

The ParCli robot has no onboard computing for determination of joint torques or state estimation. The full system includes a computer on the ground and a VICON motion

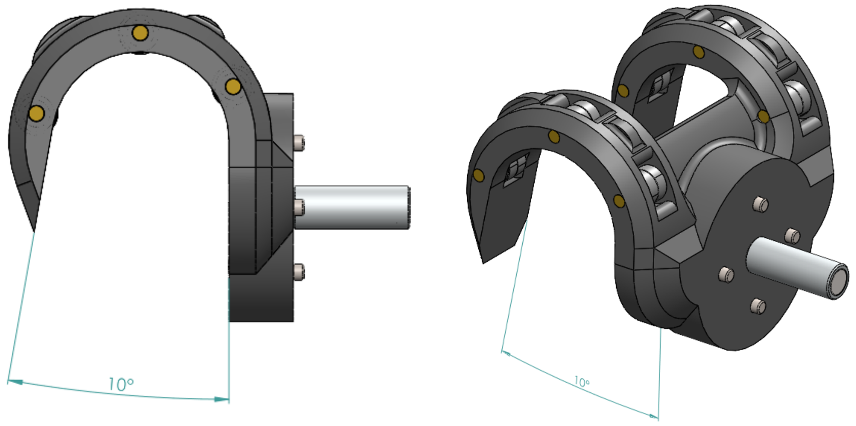

(A) SIDE View (B) ISOMETRIC View

Figure 6.11: Prehensile end-effector for the hindlimbs. Two sets of bearings allow rotation about the end-effector free-axis. The 10° opening assists in guiding the end-effector on to the cylindrical support.

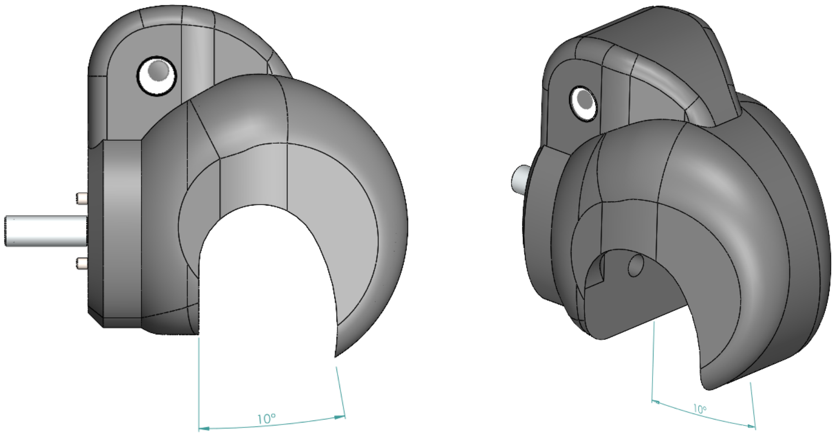

(A) SIDE View (B) ISOMETRIC View

Figure 6.12: Prehensile end-effector for the centre limb. The 10° opening assists in guiding the end-effector on to the cylindrical support.

capture system installed on the wall opposite the climbing structure. The system is controlled from the ground computer, and torque commands and motion feedback from the joints are communicated over CAN-BUS. The motion capture system tracks four markers installed on the robot body that make a unique and asymmetric pattern for detection. A diagram of the information flow between major system elements in shown in 6.13. The control loop on the ground computer is run in SIMULINK, with robotic operating system (ROS) acting as a middleware to handle data from the VICON system, and to pass data to and from the robot.

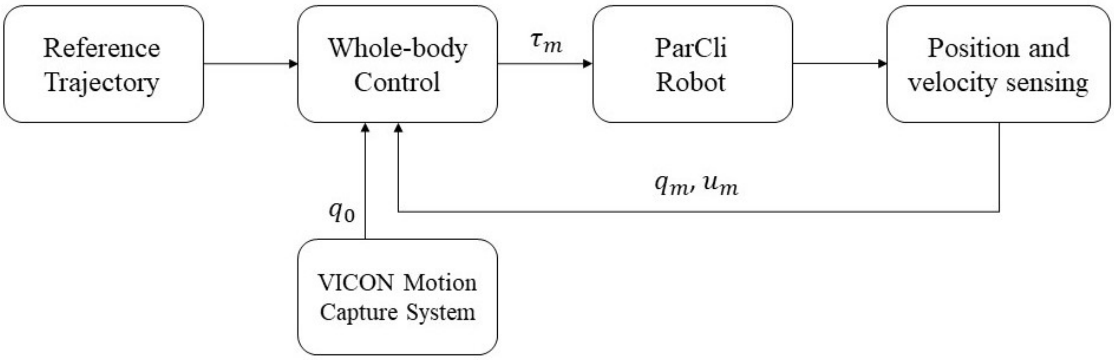

FIGURE 6.13: A diagram of the major elements of the control system loop.

6.2.4 Design Summary

Execution of the design work presented here, has allowed us to generate a physical model based on the kinematics presented in Section 5.3. By simulating a model that is physically realisable, rather than just a kinematic representation, we ensure we are pushing towards developing control approaches and planning approaches that are realisable on a physical machine. The feedback from the mechanical design process has allowed us to validate assumptions made about limb lengths, inertias and masses, and contact constraints, that we might not have otherwise considered. In the following two sections we will describe how this robot is constructed in simulation, and the results of the implementation of our control theory that will validate the kinematic design, as well as the motor selection for the physical design.

6.3 Simulation of the ParCli Robot

The ParCli robot is simulated in Simulink using Simscape Multibody, and the Simscape Multibody Contact Forces Library [140]. The robot is imported into simulink using the `smimport()` function in MATLAB, which reads from a manually generated URDF file which can be viewed in Appendix C. The files for the graphics are imported as STEP files that are generated from the mechanical design files using SolidWorks. Estimates of the dynamic properties of each of the links are performed using SolidWorks. These properties are reported in Table 6.4.

6.3.1 Contact Modelling

To facilitate contact at each of the three prehensile end effectors, two Sphere to Tube Force Enabled blocks are used, one either side of the grasping centre (Figure 6.14). When in contact, the two spheres inside the hollow tube allow us to approximate the function of the hook style grippers being used, as they allow free rotation only about tube's axis.

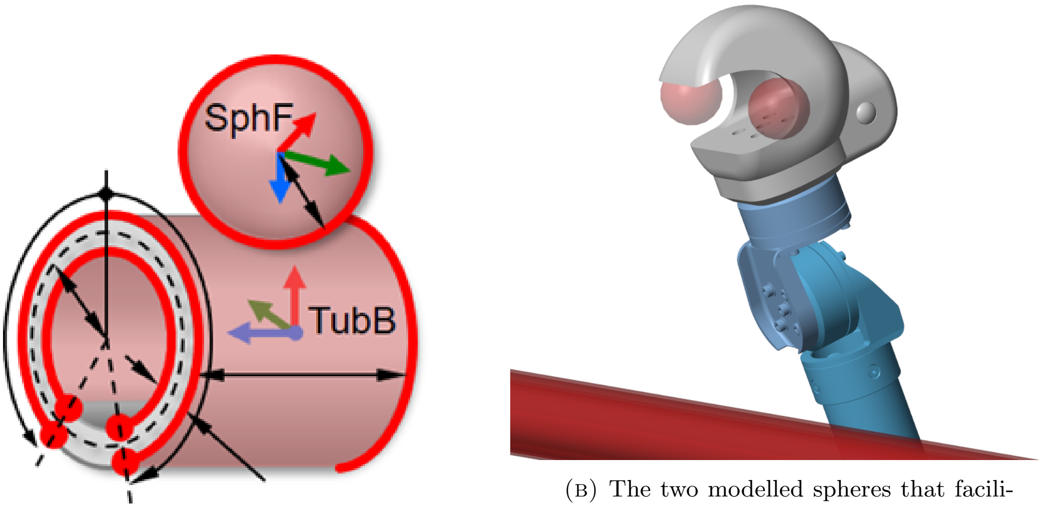

(A) Definition of the contact force block being used in simulation.

(B) The two modelled spheres that facilitate contact when inside the hollow tube, each are placed approximately 40mm from the centre of the contact point

FIGURE 6.14: 3D contact modelling for grasping end effectors

The tail uses a Sphere to Plane Force Enabled block such that contact against the ladder rungs can be roughly approximated. For this work, the contact point is fixed at 500mm below the tail joint axis; however, in reality we expect the centre of the contact patch to move as the tail makes contact with different rungs.

6.3.2 Dynamic Model

The dynamic model used for our control strategy does not include gearbox inertia or friction. We also did not split the mass of the motor from the driven and non-driven sides, as these details were not available. As the static side of the motor makes up a majority of the mass, we assume that the link connected to the static side has the full mass and inertia of the static motor. Figures 6.15 to 6.17 show the link by link breakdown of the robot, and Table 6.4 records the mass and inertia of each link. This information is also encoded in the URDF file in Appendix C.

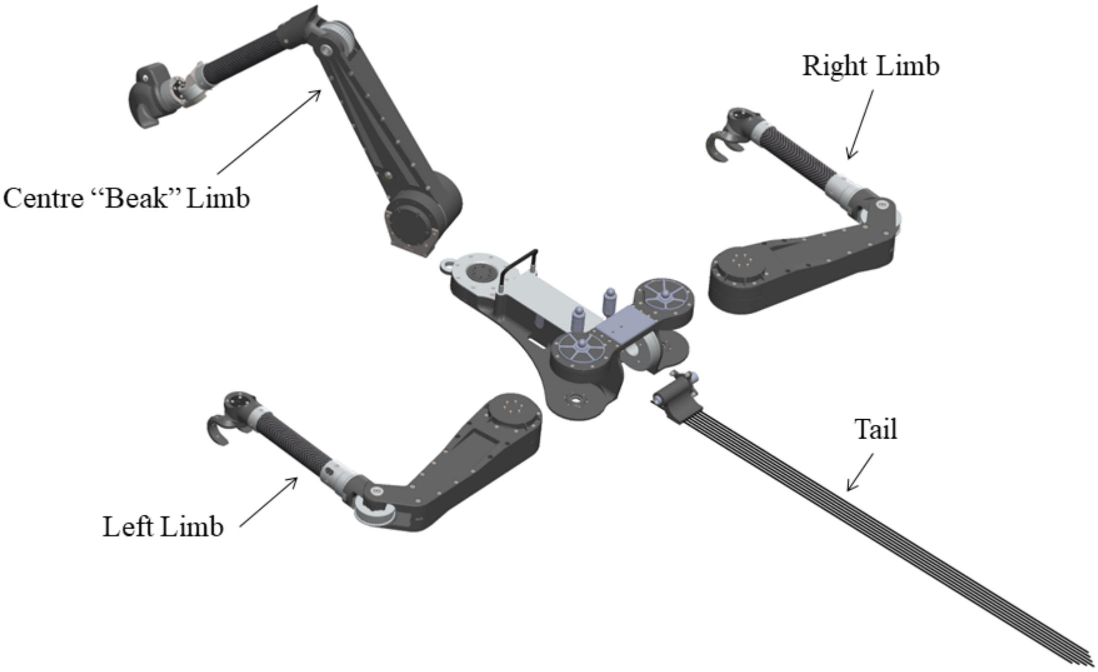

Figure 6.15: ParCli robot exploded assembly showing each limb

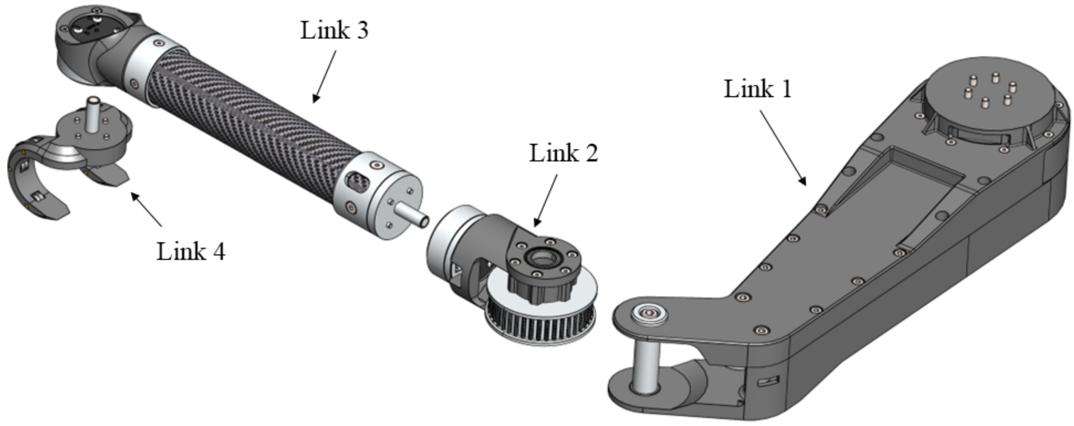

Figure 6.16: Exploded assembly view showing each link of the left leg. The right leg is similarly numbered, starting at link 5 on the proximal side and going to link 8 as we progress distally.

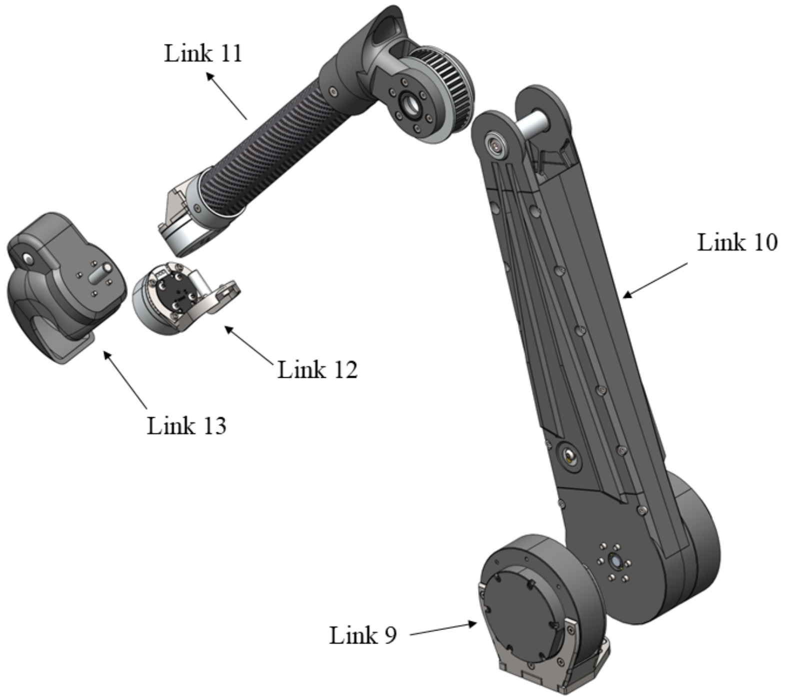

FIGURE 6.17: Exploded assembly view showing each link in the of centre limb

Limb	Link	Mass [kg]
Body	Link 0	3.166
Left,Right	Link 1,5	1.064
Left,Right	Link 2,6	0.341
Left,Right	Link 3,7	0.262
Left,Right	Link 4,8	0.057
Centre	Link 9	0.768
Centre	Link 10	1.022
Centre	Link 11	0.584
Centre	Link 12	0.166
Centre	Link 13	0.168
Tail	Link 14	0.178
	TOTAL	9.852

TABLE 6.4: Mass values for each link in the ParCli dynamic model. Left and right limbs are mirror copies of each other and have the same values. Inertia values can be found encoded in the URDF file presented in Appendix C.

6.3.3 Control Loop

The whole-body control loop (Figure 6.18) is implemented in Simulink. The control loop is set to run at 200Hz, solving the constrained quadratic program (5.47) at each time step. The control rate is chosen based on what is realisable in the preliminary tests conducted on our hardware. The main function which computes the constrained dynamics in the control loop is written using functions from the spacecraft robotics toolkit (SPART) [144], which uses a Newton-Euler approach [145] to computing the instantaneous robot dynamic model. We implement the convex optimisation with MATLAB's `quadprog` function. The main control function (Control Block in Figure 6.13) that computes the constrained dynamics and performs the optimisation, can run up to approximately 520Hz on a laptop PC with a 2.3GHz Intel Core i7 processor. The variable-step `daessc` solver in Simulink is used to solve the system dynamics, with a full 12s simulation (including control loop) taking approximately 558s to run on the same machine. The `daessc` solver provides algorithms specifically for solving differential algebraic equations (DAEs). Whilst this solver works very well for floating base systems, the solver slows down considerably when solving for the stiff contacts used in our modelling. As such, quick succession of contacts slows down simulation time drastically.

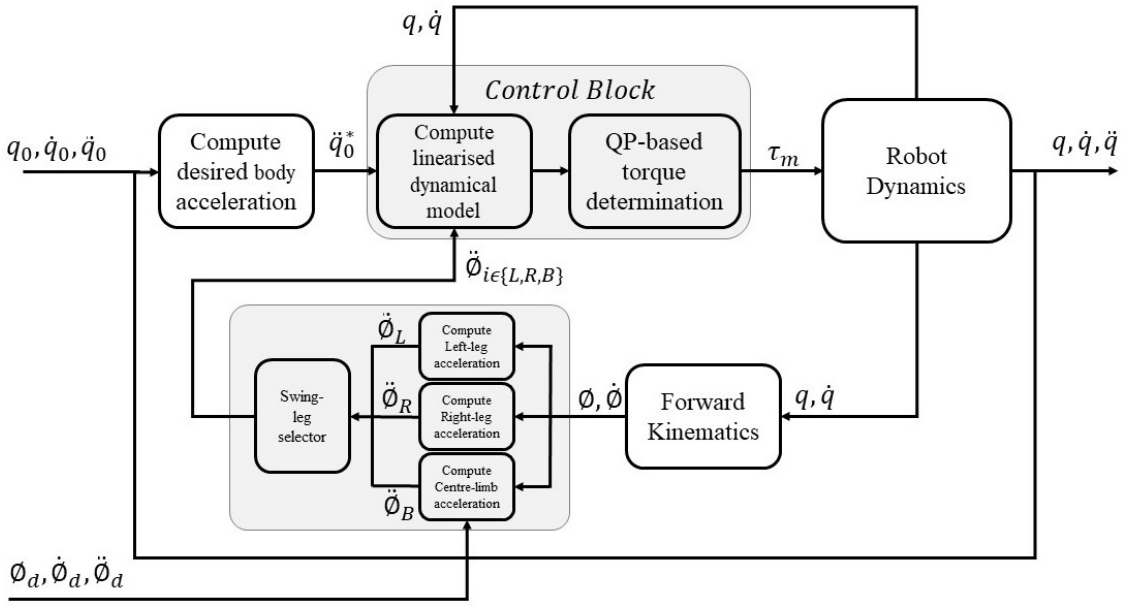

FIGURE 6.18: Structure of the control loop implemented in Simulink

6.3.4 Computing Accelerations

The desired body and swing leg end effector accelerations are the control objectives fed into the control block in Figure 6.18. Accelerations are computed in each of the preceding blocks using the control law defined in (5.48), which utilises proportional feedback on both position and velocity errors, integral control on the position error, and using the desired path acceleration as a feed-forward term. The gains are manually tuned for step responses and recorded in Table 6.5. Each gain is expressed as a diagonal matrix, $K \in \mathbb{R}^{6\times 6}$ for body control, and $K^{\phi} = diag([\phi \quad \theta \quad \psi \quad x \quad y \quad z])$ for swing legs. Different gains are used for the centre limb and the hindlimbs due to observed differences in performance during tuning, likely due to the different mechanical properties of the limbs.

Descriptor	Gain	*diag*(Value)
Body Proportional Gain (Position error)	$K_P^{\mathbf{q}_0}$	[50 80 80 400 400 600]
Body Proportional Gain (Velocity error)	$K_D^{\mathbf{q}_0}$	[40 30 30 150 150 200]
Body Integral Gain (Position error)	$K_I^{\mathbf{q}_0}$	[10 10 10 30 30 30]
Centre Limb Proportional Gain (Position error)	$K_P^{\phi_B}$	[250 0 250 100 100 100]
Centre Limb Proportional Gain (Velocity error)	$K_D^{\phi_B}$	[60 0 60 15 15 15]
Centre Limb Integral Gain (Position error)	$K_I^{\phi_B}$	[3 0 3 3 3 3]
Hindlimb Proportional Gain (Position error)	$K_P^{\phi_{L,R}}$	[250 0 250 100 100 120]
Hindlimb Proportional Gain (Velocity error)	$K_D^{\phi_{L,R}}$	[60 60 0 15 15 15]
Hindlimb Integral Gain (Position error)	$K_I^{\phi_{L,R}}$	[3 0 3 3 3 3]

TABLE 6.5: Set-point control gains used in the simulated ParCli climbing experiments

6.3.5 Optimiser Gain Tuning

The optimiser weighting matrices, $\boldsymbol{W}_{\ddot{\mathbf{q}}}$ and $\boldsymbol{W}_{\boldsymbol{\tau}}$, were tuned using the commonly known Bryson's rule [146], where

$$\boldsymbol{W}_{\ddot{\mathbf{q}},ii} = 1/\text{maximum acceptable value of } [(\mathbf{q}_0 - \mathbf{q})_i^2]$$

and,

$$\boldsymbol{W}_{\boldsymbol{\tau},ii} = 1/\text{maximum acceptable value of } [\tau_i^2].$$

For elements associated with the translational dimensions of $\boldsymbol{W}_{\ddot{\mathbf{q}}}$, the maximum acceptable error is chosen to be 10mm, and 1° for rotational error. The values chosen for $\boldsymbol{W}_{\boldsymbol{\tau}}$ correspond to the peak torque capacity for each of the motors as defined in Table 6.3.

6.4 Experiments with the Simulated ParCli Robot

Several experiments were conducted in simulation to validate the design of the ParCli Robot, and the whole-body control theory presented in section 5.5.2, these include: testing the torque limits of the selected motors are appropriate; validating the control theory and evaluating the PID gain tuning and optimiser weighting matrix values; and validating the kinematic design is capable of swing leg operations necessary for climbing.

6.4.1 Actuator Torque Validation

To validate that the actuator torque limits (Table 6.3) are sufficient for climbing, we simulate the robot performing five steps with a handcrafted, set-point trajectory. The handcrafted trajectory specifies times and locations that are fed into the simulation for the body and swing legs set-points. This trajectory is reflected in Table 6.6, which records each event in the trajectory. As discussed in Section 5.5.2.5, when tracking set-points, the feedforward term is set to zero, and the PID gains are used to compute the acceleration that the optimal controller then tries to produce. These gains are shown in Table 6.5. During set-point tracking, provisions for the end effectors to maintain the appropriate approach angle, which are necessary for the physical implementation, are ignored; instead the end effectors are allowed to pass through the structure to settle at the desired locations.

For the initial simulation, peak joint torques are set to those specified in Table 6.3. Unfortunately, with the torque limits at this level, poor pitch-back performance was observed, with the body often pitching undesirably in the positive Y-direction, away from the structure. Upon inspection, and as seen in Figure 6.19, the tail motor reaches its peak torque value and saturates for times when the centre limb is in its swing phase. During the swing phase of either of the hind limbs, good trajectory tracking and little body pitch-back was observed. To validate that a deficiency in tail motor torque is responsible for the undesirable behaviour, a second test was run where the tail motor torque limit was increased from 3 Nm to 10 Nm. The torques for the climbing sequence are shown in Figures 6.19 and 6.20, and snapshots showing the climbing sequences comparing the undesirable pitch-back events to the desirable case are shown in Figure 6.21. As shown, the increase in tail motor torque limit adequately resolves the pitch-back issue being seen in the original experiment.

Time [s]	Swing Leg	Swing Leg Set-point	Body Set-point
0.0	B	[0.9; 0]	[0.15; 0.0]
1.0	R	[0.6; 0.3]	[0.3; 0.0]
2.0	B	[1.2; -0.05]	[0.48; 0.05]
3.0	L	[0.9; -0.4]	[0.7; -0.05]
4.0	B	[1.5; 0]	[0.8; -0.05]

Table 6.6: Set-point trajectory for actuator validation experiments. Set-points are recorded as [X; Y] in meters from the origin of the climbing plane

In addition to poor pitch-back performance, when the tail motor had insufficient torque capacity, the CoT also suffered. For the climbing experiment where the tail had its nominal limit set, the robot had a CoT of 2.05 compared to 1.45 when the tail motor torque limit was increased to 10 Nm. The new value of 10Nm is used for the remainder of the experiments.

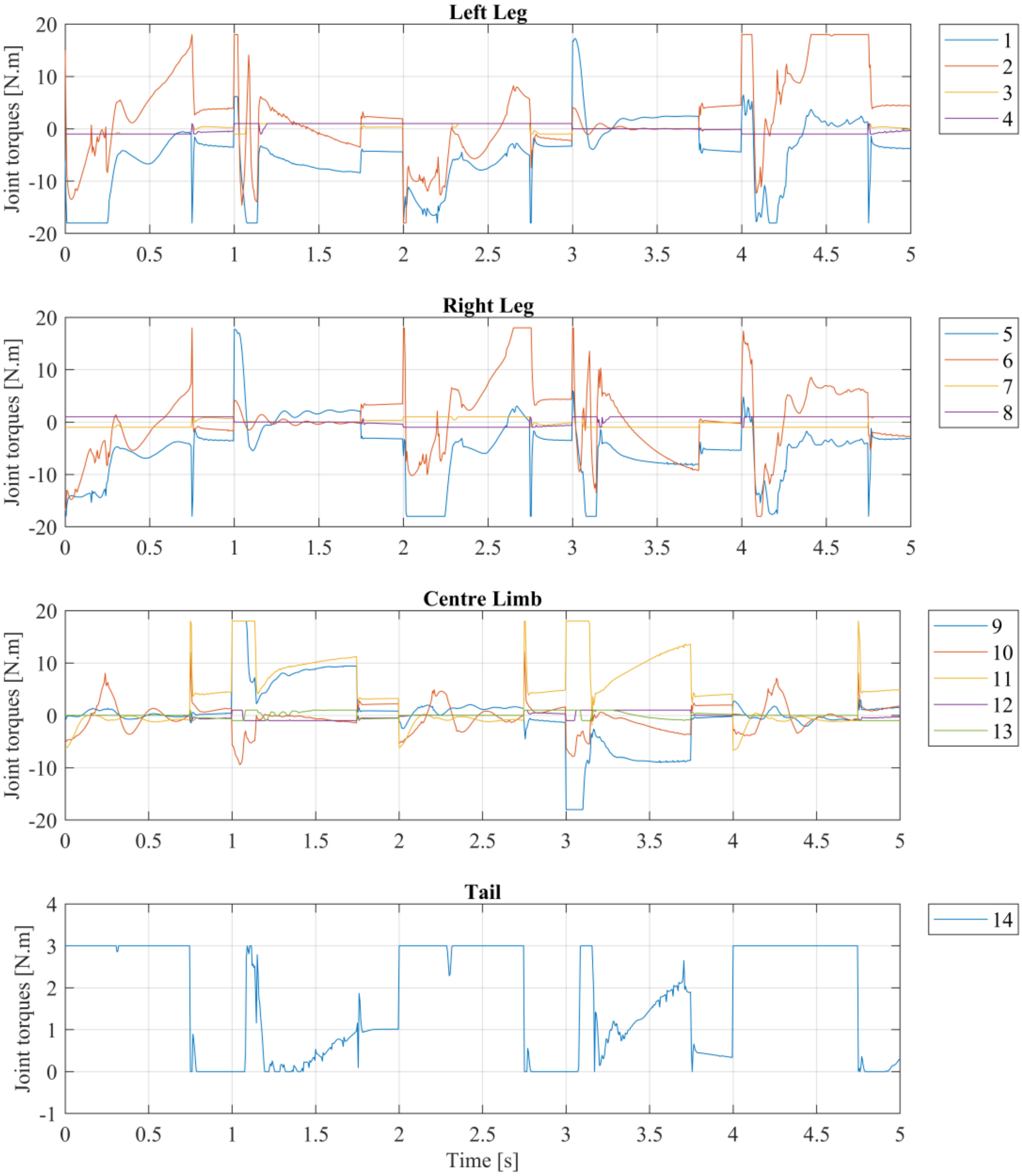

Figure 6.19: Joint torques from five-step climbing attempt with all motor torques set to their design limits as recorded in Table 6.3. Note that the tail motor is saturated in all instances where the centre limb enters its swing phase which is characterised by low torque values.

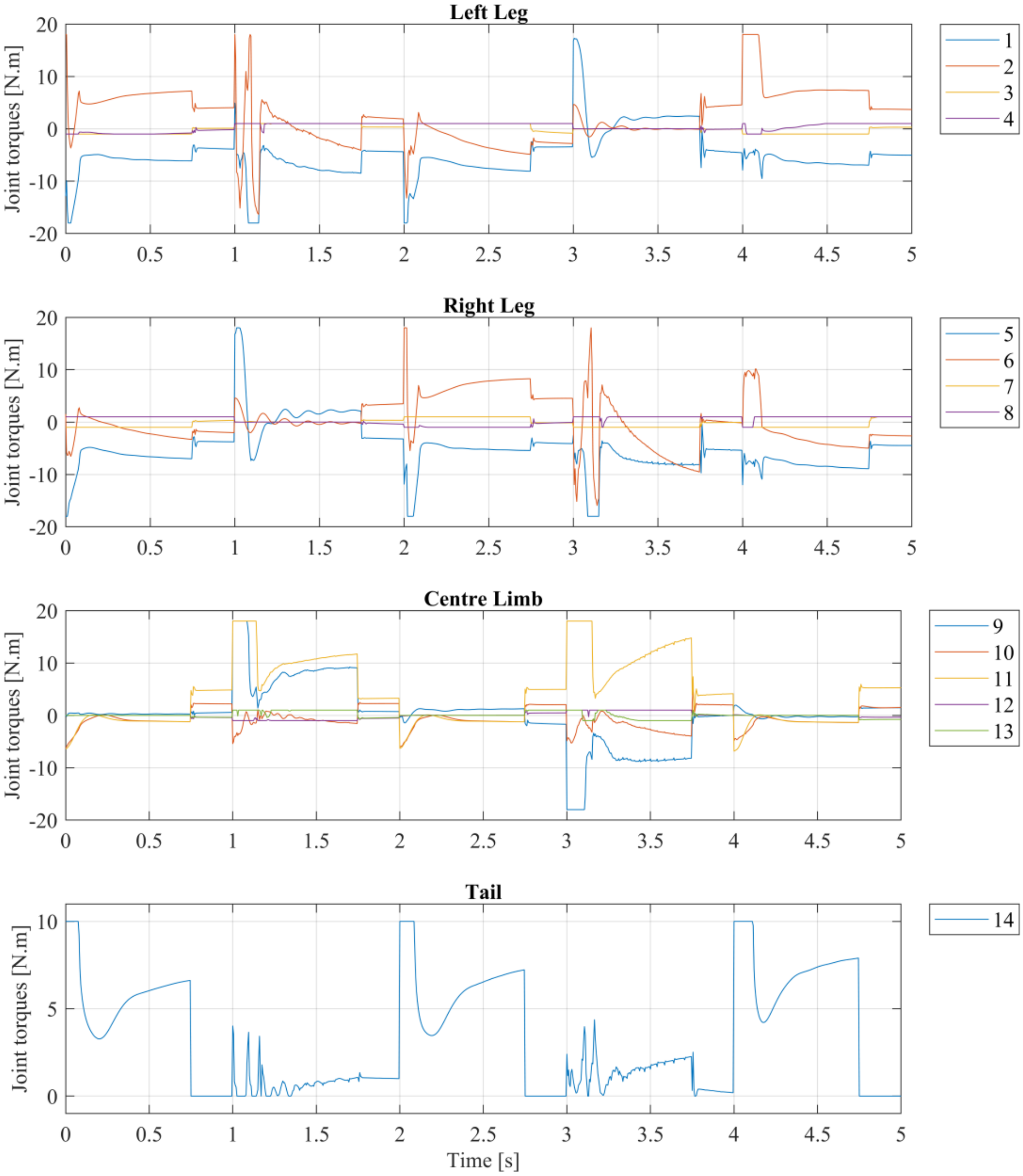

FIGURE 6.20: Joint torques from five-step climbing attempt with all motor torques set to their design limits as recorded in Table 6.3 except for the tail motor which has been increased to 10 Nm

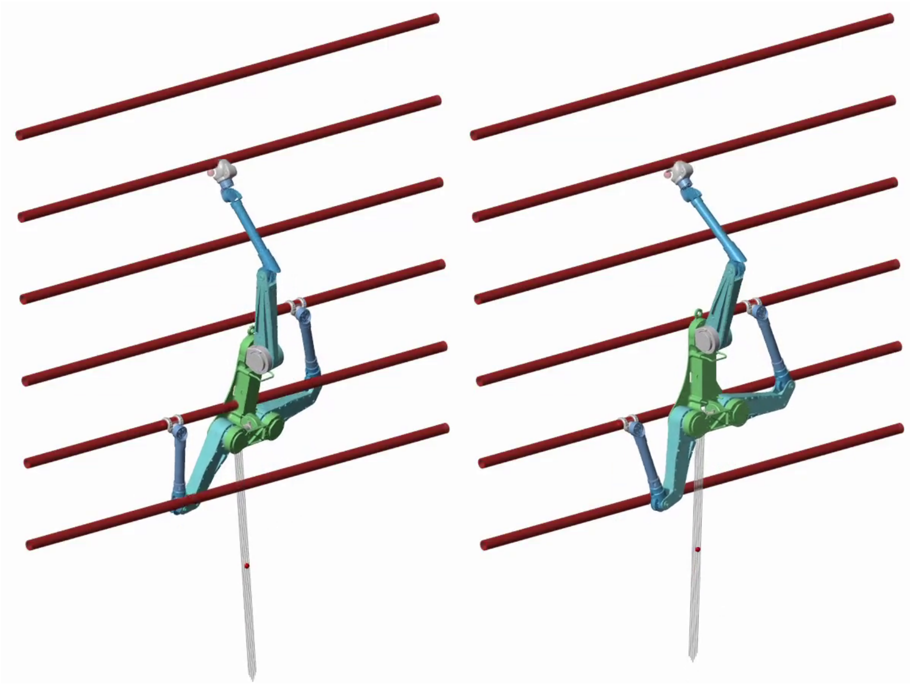

(A) Centre limb swing phase at 2.5s into the set-point climbing experiment. All torques set to design limits (LEFT) compared to climbing where the tail toque limit has been increased to 10 Nm (RIGHT). Note the significant body pitch that is causing the robot body to collide with the ladder structure

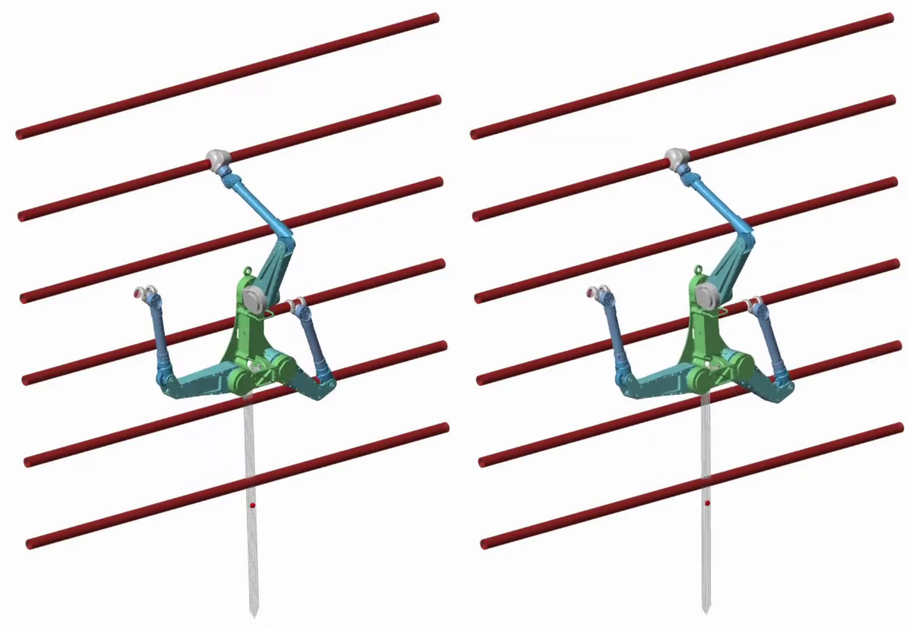

(B) Left limb swing phase at 3.5s into the set-point climbing experiment. All torques set to design limits (LEFT) compared to climbing where the tail toque limit has been increased to 10 Nm (RIGHT). No significant difference in performance is noted during the hindlimb swing phases

FIGURE 6.21: A comparison of climbing behaviours for over and under specified tail torque limits. On the left, the tail torque limit is in adequate to prevent the body from rotating into the ladder, on the right the limit has been increased substantially

6.4.2 Swing-Phase Testing

In order to climb, the robot must have reasonable control of its swing legs whilst maintaining control of the body with the stance limbs. To validate this, two experiments are conducted looking at simple trajectory tracking of the body and end effectors. First we test how the system performs when the beak is in its swing phase, and secondly the left leg. The same test is not performed for the right leg as the system is symmetrical, and the left and right legs have the same performance characteristics and tuning parameters.

6.4.2.1 Centre limb swing phase testing

The body trajectory generated for this experiment uses handcrafted points that have been fit with a cubic spline using the `CSpline` function from Woolfrey's RobotToolbox [147]. This ensures the trajectory has feasible acceleration profiles as needed for the feedforward term in our acceleration control.

For the swing leg trajectory, a simple sin function is used as it can be differentiated multiple times. The goal of this experiment is to test the simultaneous position tracking of the commanded end effector and body trajectories. The end effector trajectory extends in and out of the climbing plane as this capability is necessary for climbing.

Results of this experiment can be seen in Figure 6.22a and 6.22b. A torque plot for the duration of the experiment in shown in Figure 6.23. These results indicate that our control framework is performing as expected when the trajectories are within the feasible workspace of the robot. Early simulations where the trajectory of the body and the swing leg caused the goal points to fall out of the feasible workspace of the body resulted unstable performance, and so it is critical with the framework and tuning reported here that trajectories are feasible.

6.4.2.2 Hind limb swing phase testing

The hind limb swing test is used to determine if our control strategy is capable of performing a swing step with either of the hind limbs. An important characteristic of whole-body

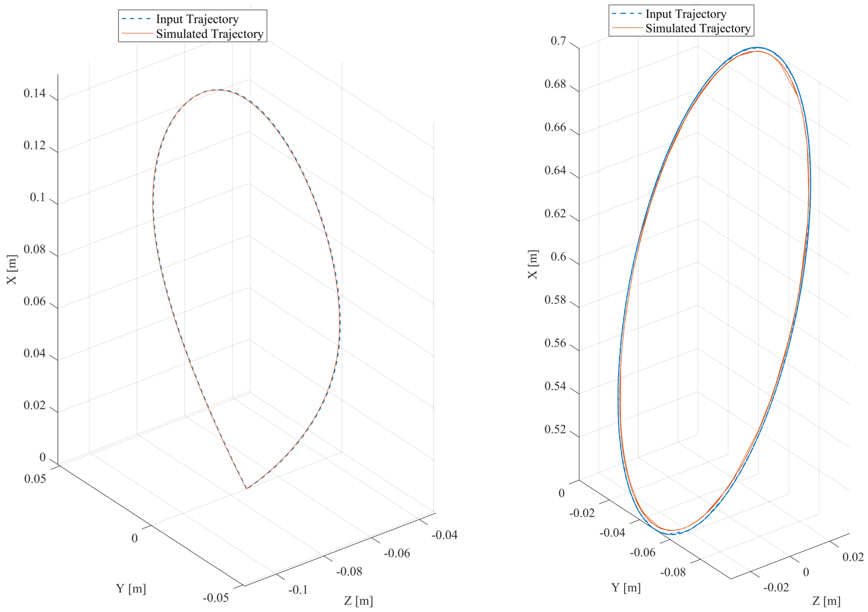

(A) Body trajectory tracking for centre limb swing phase

(B) Centre-limb trajectory tracking in swing phase

FIGURE 6.22: Input vs. achieved trajectories for the robot body and centre-limb end effector during swing phase.

the control is that accelerations of the hind limb end effectors in the Z-direction are not facilitated by the limb itself due to the kinematics of the limb. Instead, motion in the Z-direction is facilitated through body roll, the torque for which is produced by the stance limb, primarily the centre limb and tail.

The body trajectory for this experiment was created using a straight line minimum jerk strategy that allows us to easily modify the start and end location of the trajectory, the duration, thus ensuring that we have feasible acceleration targets for our feedforward control term. The swing leg trajectory was created using a sequence of points connected by a cubic spline and demonstrate a path necessary to perform a single step. The body trajectory results are recorded in Figure 6.24, the swing leg results in Figure 6.25, and torque plots for the experiment are available in Figure 6.26.

We can see from these figures that the robot was successful in executing a swing phase with its left leg. The difference between the body trajectory and that achieved in simulation can be attributed to the lack of feasible body solutions chosen for the swing leg path, that is, only a planar trajectory for the body was generated that did not account for the deviations in the Z-dimension or the body roll required by the swing leg. This behaviour

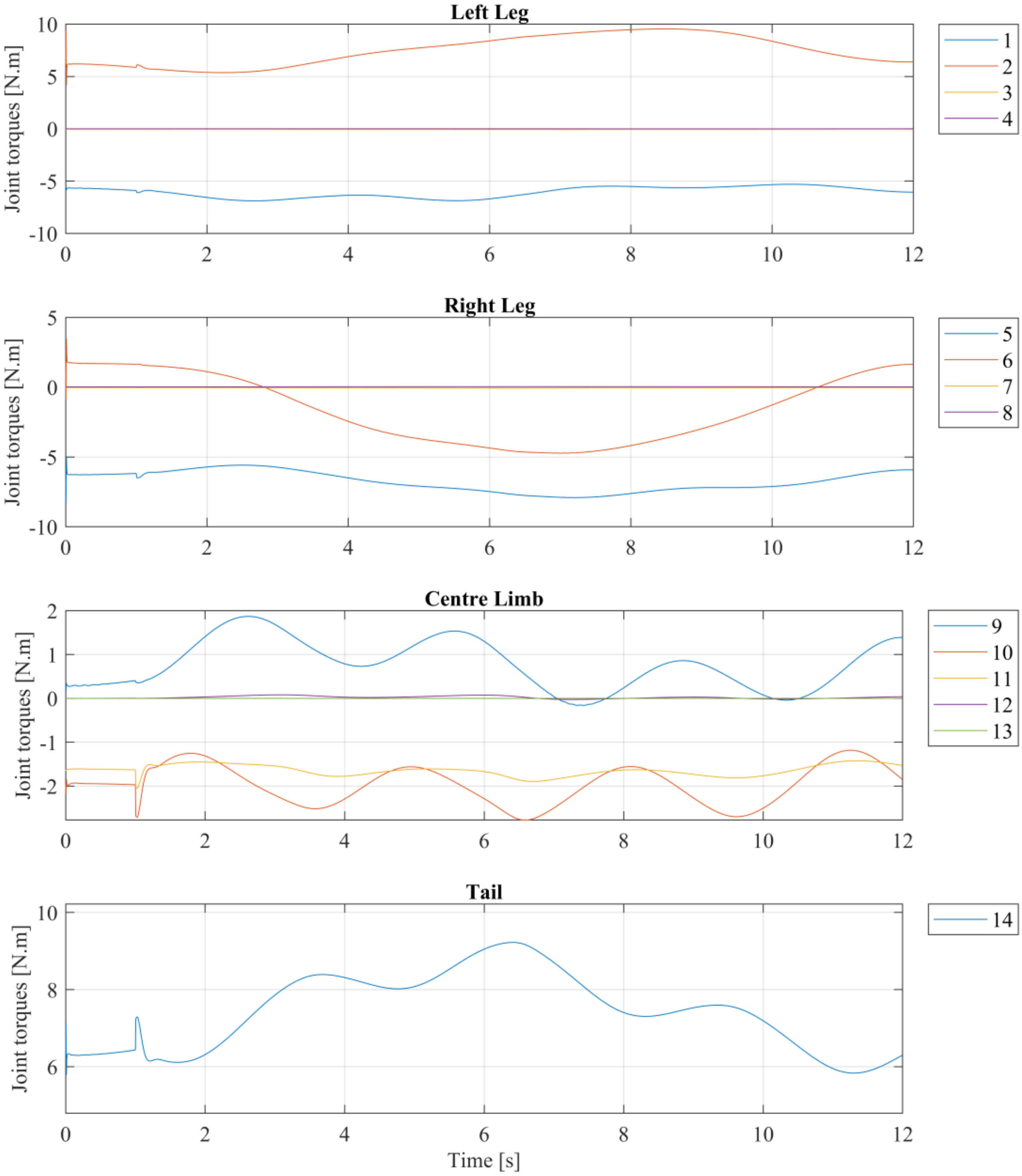

Figure 6.23: Torque plot for centre limb swing phase test

is the result of the different ways in which the end effector and body accelerations are commanded. As the end effector acceleration is accounted for in an equality constraint, and the body acceleration error from that commanded is minimised in the quadratic program, the acceleration of the end effector takes priority. The accelerations demanded by the body controller to correct roll and Z-axis deviations were not in the dynamically feasible space defined by Equation 5.38.

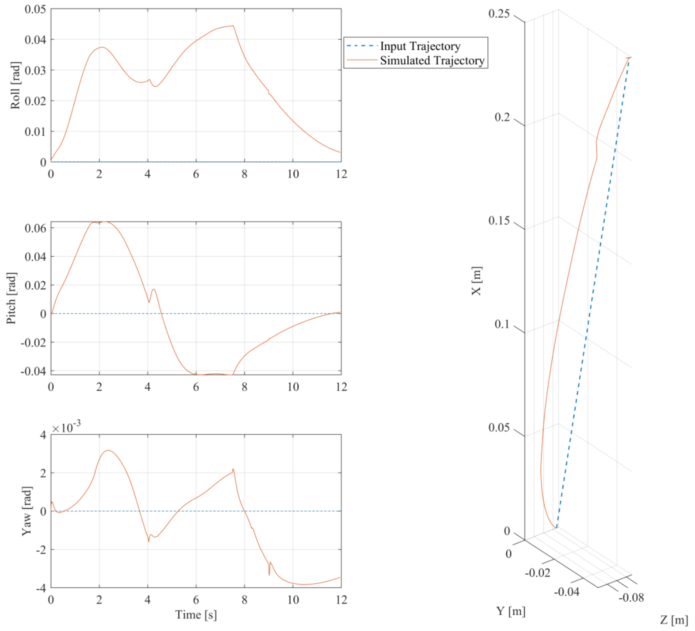

FIGURE 6.24: Body trajectory vs. body path during left leg swing testing.

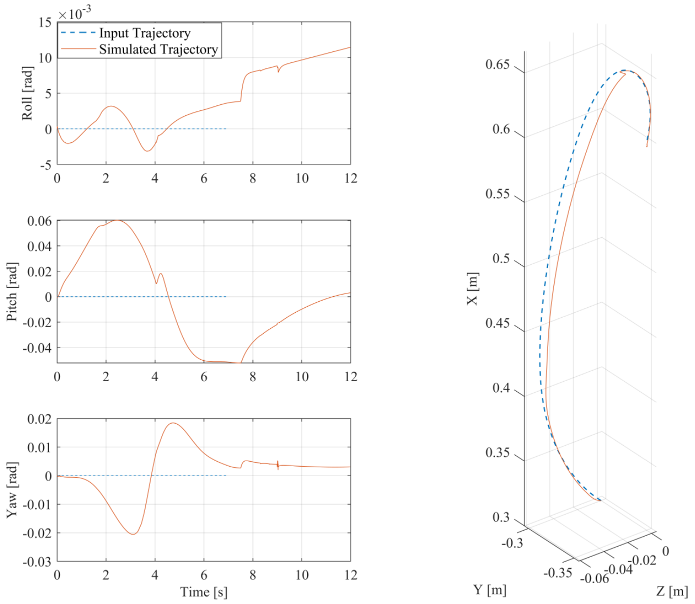

FIGURE 6.25: Swing leg input trajectory compared the simulated trajectory for the left leg swing test.

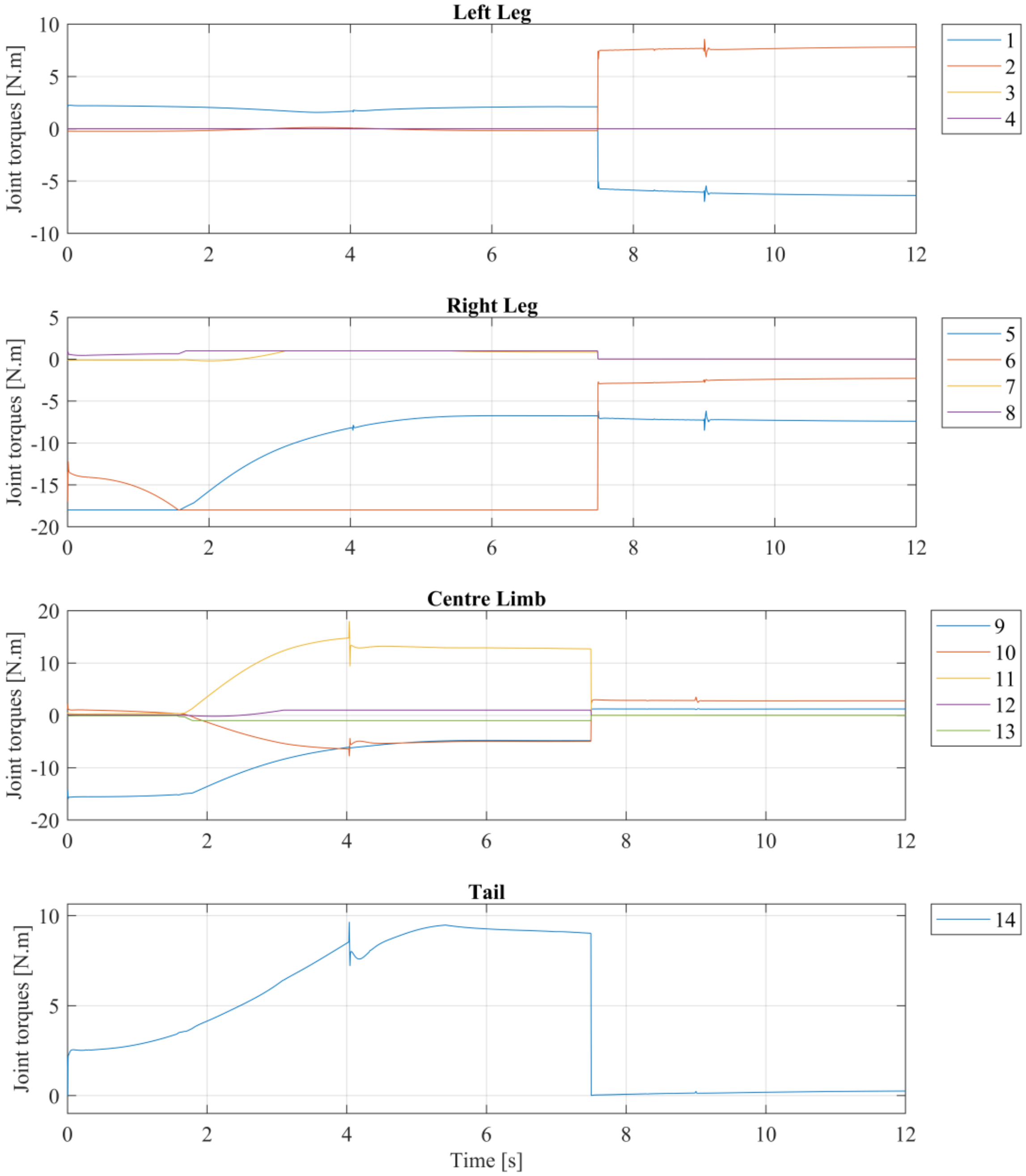

FIGURE 6.26: Joint torques during the left leg swing phase test.

6.4.3 Discussion

The experiments conducted demonstrate that the modelling and control framework presented in this work are a valid approach to the whole-body control of the ParCli robot. The additional equality constraint that drives contact torques about the free axis to zero is a successful strategy. Similarly, our approach to relaxing the Pfaffian constraint to enable velocities about the free axis is also successful. Completion of the swing phase testing shows that the kinematic design is viable for climbing a simple 2D ladder. The actuator torque verification experiment shows us that all but the tail motor have appropriately selected maximum torque values. The new maximum torque value for the tail of 10Nm seems to be appropriate, enabling the swing phase control in the subsequent experiments.

From the left leg swing phase test we saw the right limb approaching undesirable loading conditions which will be discussed further below. Tail utility is an important feature of our design and also merits further discussion.

6.4.3.1 Design Limitations

Several features of the mechanical and kinematic design demonstrate unintended limitations; two primary aspects are of note. Firstly, when either of the proximal limb joints (joints 3 and 7) are aligned, but not coincident with the free axis of the their respective contact, the loading conditions easily exceed the capacity of the joint. This can be seen in the torque plot of the right limb of Figure 6.26, and a visual depiction of the configuration can be seen in Figure 6.27. In this condition, the motor torques are saturated, and since the torque limit is expressed as the peak torque rating of the motor, holding this condition in a real system may cause motor performance issues, or burnout of the motor. Unfortunately, the duration limits for the motor applying its peak torque are not stated in the OEM's data sheet, though, usually these limitations are bounded by the motor operating temperature which is effected by several ambient factors such as temperature and airflow. Whilst we cannot say this condition would damage the motor over this duration, it is undesirable.

The second major design limitation is in the elbow joint of the centre limb (joint 11). The torques that the joint must produce are much higher than originally anticipated. This is due to the kinematics and primarily the large distance the joint must sit from the climbing plane in a large majority of poses. This configuration is not particularly efficient for producing climbing forces. It may, in the future, be superseded by the 'S' shaped morphology of the avian craniocervical column [148, 94], which at the cost of adding

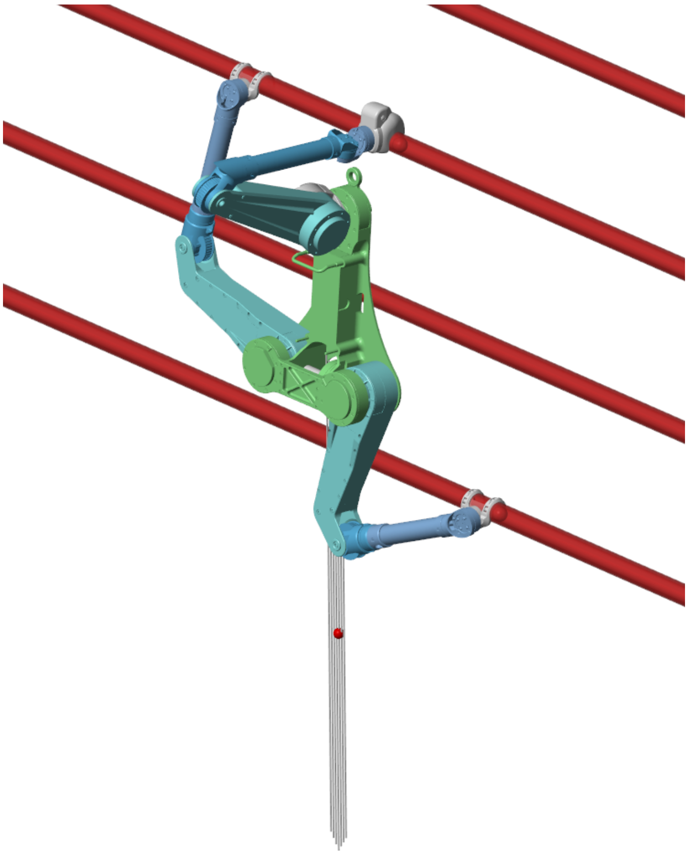

Figure 6.27: Undesirable loading condition of the right leg as joint 7 approaches being aligned with the end effector free axis.

joints could keep them much closer to the climbing plane, reducing the perpendicular distance from the joint axis to the force vector, thereby reducing torque.

6.4.3.2 Tail utilisation

Tail utilisation is an important feature of the ParCli design. Whilst tail utilisation is noted in both animals and robots [45, 24], it is of particular importance in our work. The legs do not have the capacity to modify forces in and out of the climbing plane, and therefore have no capacity to produce torques to prevent the body pitching away from the structure. In our design this is a deliberate and successful attempt to reduce the number of DoF of the design; however, it does mean the tail has to work harder than originally anticipated, instead of acting like a redundant safety feature to prevent falling as it does in climbing lizards [45].

It is important to note that the tail is not considered a limb in the scope of this, or other work [5]. A limb should provide propulsive force for locomotion or significant manipulation capabilities. In this work, due to the friction between the tail and structure, the tail actually works against the propulsive force moving the body, which is another cost of providing pitch-back stability with this strategy.

6.4.3.3 Modeling and Control Limitations

Several limitations exist in the modeling that will be different from the hardware implementation. The first significant difference is the lack of motor inertia and gearbox modelling, which will introduce inertial forces and large frictional damping forces in the joints. This will require additional torque to overcome and likely be compensated for in the tuning of the feedback gains for the real system. The second major factor is the modelling of the tail contact, which has two major discrepancies. Firstly, in our work the tail contact is modelled as a sphere to plane contact, such that the tail is always in contact with the structure at the same location relative to the robot, and the forces produced are always normal to the plane. Secondly, the distance the tail force acts on is fixed, both in our control and in our modelling. In reality this will change depending on the number of rungs the tail contacts, and the angle at which rungs are contact. Further investigation into this modelling and estimation of the tail contact parameters will be the focus of future work.

Another consideration is the lack of modelling of friction at the prehensile end effectors. Whilst the hind-limbs of ParCli have bearings in order to reduce friction, that centre limb does not, and relies on a very low contact area and low friction materials to ensure it can slide in line with our control assumptions. This assumption is yet to be validated or characterised in hardware. It might also be possible to include a friction model in modelling of the ParCli robot; however, this will also be left for future work.

6.5 Summary

In summary, our experiments in simulation show that the ParCli robot is a viable first pass design of a tripedal ladder climbing robot. Both kinematic designs and several control laws presented in Chapter 5 are validated and are shown to be successful strategies to facilitate tripedal climbing in a reticular structure in simulation. The importance of adequately specifying the tail torque capacity and its importance to the kinematic design of our 3D robot are accentuated by the robots poor performance in the initial experiments. The mechanical design will therefore need updating to provide this additional torque before the full robot can be tested. Another near term inclusion is characterisation of the friction limits of the physical contacts, and the development and application of a friction model in the whole-body controller. We also take note of the neck design in *aves*, and suggest that in future work, the S-shaped kinematic structure may be beneficial for reducing joint torques in the centre limb, as if may reduce the maximum distance any joint is from the transnational components of the end effector wrench.

Chapter 7

Conclusions and Future Work

Climbing tall, sparse, and complex structures is a challenge at the forefront of legged robotic development. The challenges presented by reticular structures are multifaceted and require innovative, out of the box solutions. Whilst it is still a long way away, a capable robotics solution to the inspection and maintenance of reticular structures will have significant implications for a diverse range of sectors, including in energy, telecommunications, and space. In this thesis we have developed the case for three limbs in the design of RSRs, and presented and validated the design of the world's first robot based on this concept.

The published observations of this thesis' author in [1], have spurred new discussion amongst biologists on what the definition of a 'limb' is and provided a new model for locomotion previously unconsidered in biology [6, 5]. This was confirmed via email to the author (M. Granatosky, private communication, May. 23, 2022):

> "*...it was your chapter published in 2017 that got me initially interested in parrots as a model species.*"

By leveraging this novel model, and especially focusing on the limb-like qualities of the craniocervical system, a fresh concept for the development of RSRs was proposed.

In this concluding chapter, a summary of the thesis is provided in Section 7.1 and a summary of the main contributions in Section 7.2. In Section 7.3, areas of future work are discussed and preliminary experiments with the physical ParCli robot are presented. Finally, Section 7.4 concludes this thesis with remarks on the outlook for the future development of this robotic concept.

7.1 Thesis Summary

7.1.1 Design Principles for Reticular Structure Robots (Chapter 3)

This thesis first presented our design principles, which are based on two significant insights. Firstly, we review a board spectrum of biological literature and distill several lessons that are applicable to the development of RSRs, principles that we then include in the design of our ParCli robot. Next, we look at the application environment, present a set of constituent elements of reticular structures, and define motion primitives about these structures. This is important in the consideration of a RSR, as to master its environment a robot should be at least capable of this set.

It is our observation that roboticists often neglect aspects of these two insights during the design process. It should be acknowledged, that the nature inspired design lessons presented in this thesis are not exhaustive, and it is very likely that nature has many more lessons to offer us. The motion primitive framework is also not as yet validated. The breakdown of elements represents a method for categorising different behaviours of a robotic agent but may not be complete. Further work is required to validate that this approach will result in a fully capable climbing in a RSR.

7.1.2 Bioinspired Tripedal Climbing (Chapter 4)

In this chapter, we devised a method to learn firsthand from parrots to garner insight as to how and when they started demonstrating tripedal behaviours and if these behaviours truly are tripedalism as we suspected. Through the evidence we present, we discover that tripedalism is a quantitatively different behaviour in parrots, as the model we impose on their biomechanics shifts in response to both beak usage and the inclination of the structure. The data presented in this study goes on to inform two bioinspired planning algorithms that are implement in the simulated version of our simple robot.

There is still much more we can learn by closely studying parrot biomechanics and behaviours. The study we presented here shows only a single type amongst a wide variety of arboreal behaviours that parrots exhibit [6]. We have nevertheless begun this journey and sparked new interest in the biological community for studying parrots as a model for locomotion.

7.1.3 Kinematic Design and Control (Chapter 5)

In this Chapter we presented two kinematic designs for ladder climbing robots. The first, a simple experiment that allowed us to test our approach and explore suitable planning and control algorithms in simulation. The second, a somewhat more complex kinematic structure intended to be physically realisable. In this more complex version, we saw the need to utilise and develop whole-body control to achieve full and precise control of the robot. The footfall planning and trajectory planning approaches were simple first steps necessary to get a simple robot climbing; however, most of the work in this field is still ahead of us.

7.1.4 Experiments (Chapter 6)

We then presented our experimental results validating our kinematic design, control, and planning algorithms in a simulated environment. We also presented the mechatronics design of the ParCli robot based on the 3D robot kinematics described in Section 5.3. The hardware design then informed our simulation model, which aimed to validate the hardware design. For the most part, the current hardware design is viable; however, several nonviable elements were discovered, mainly that the tail torque was incorrectly specified and will need updating before physical climbing in the lab can be achieved. Ideally a smaller than 1:1 gear ratio that would increase the torque output in joint 11 might also be desirable; however, the robot is not currently limited by this, the motor simply needs to apply higher torques than it might be capable of for a long duration.

7.2 Summary of Contributions

7.2.1 Tripedal Climbing Robots

Prior to this work, tripedalism in a climbing robot for reticular structures had never been considered. By making the observation that parrots employ this strategy successfully and finding a physical basis for this to be a reasonable approach, we contribute a new morphology for roboticists to explore. We explore this morphology, in *in vivo* experiments with cockatiels and in our own designs, before validating that three limbs is a sounds approach as long as reasonable assumptions about the degrees of control at the contact point can be made.

7.2.2 Design Principles

Learning from nature is not a new concept; however, the concise list of mechanical design principles with supporting evidence and context is the first we know of to surmise multiple principles to make them available for design engineers. Furthermore, attempting the consideration of a complete set of motion scenarios will hopefully allow roboticists to create machines that have demonstrated capabilities beyond the limited few that are often considered.

7.2.3 Tripedal Climbing Parrots

Before this work, the craniocervical system of the parrot as being a 'limb' was an unproven and unsupported claim. Contributed by publications supporting this thesis [1], and in supporting [5] and tangential [94] work, biologists are around to the idea that the craniocervical system could have the function necessary to support this categorisation. Furthermore, the definition of climbing is not truly settled either. Contributions of the data and discussions presented in Chapter 4 are working towards answering that question [7], which is important both in biology, and robotics. Knowing whether a robot needs to climb up a hill or simply walk up it is a nuanced question; one of importance to people considering the design of such machines.

We have also contributed a new method for the analysis of animal kinematics, with the implementation of a multivariate mixed-effect regression model, that allows us insight into the effect of confounding factors influencing kinematic change.

7.3 Future Work

In this section, we explore future work for the development and implementation of the ParCli robot, and for our proposed tripedal climbing concept in general. We begin by presenting the preliminary hardware experiments being conducted on the ParCli robot, before discussing upgrades to the control and planning we intend to accomplish in the near future. Finally, we the next steps for the development of the new iterations of tripedal, parrot-inspired, climbing robots.

7.3.1 Preliminary Hardware Experiments

An image of the physical hardware is available in Figure 7.1. Some initial control and calibration tests have been conducted on the ParCli robot. These include calibration of gimbal motor with respect to encoders, calibration of motor zero positions and calibration of the body transform in the motion capture system's world frame, and finally trajectory tracking test with the centre limb. At the time of writing, issues with motor drivers have prevented a full body control test, with several instances of network communication of the CAN-BUS network.

7.3.1.1 Calibration of gimbal motors

The GL40 and GL80 motors that are being controlled by the ODrive v3.6 controllers, require a full rotation calibration sequence. One issue we have encountered is that several of the joints, especially joint 13, are unable to perform a full rotation once assembled in the robot. This issue might, in future, be resolved by having absolute encoders that

Figure 7.1: The ParCli robot passively perching on a vertical ladder

can communicate with the driver board. The work around solution has been a semi-disassembly of the joint to perform motor calibration, before reassembling without moving the encoder board with respect to the encoder magnet mounted in the centre of the motor.

Fortunately, this only needs to be done once, as long as saving the motor configuration to the driver board is successful, something that we found would intermittently fail, potentially due to user error.

7.3.1.2 Calibration of the joint zero position

In order for the state feedback to be accurate, the motors need to be zeroed according to the zero state shown in Figure 6.5. At this stage, zeroing has been facilitated by roughly holding each limb at its zero configuration and running a script to manually mark the current encoder value as the zero state; however, in future this will be accomplished with custom designed jigs to hold the joint more precisely at their modelled zero position.

7.3.1.3 World frame calibration

Four reflective markers are used to track the body frame of the robot. In order to track the body frame of our robot that is modelled, we need to calibrate these markers with respect to that frame. Calibration involves finding the transformation between the automatically created object frame and the body frame that we wish to track. This process is done manually and is valid unless the markers on the robot are moved. Our current process for calibration is as follows:

1. Measure the install height of the power terminal markers and update in the CAD model.
2. Create an ‘object’ using VICON’s Tracker Software from the desired markers which should be in the cameras field of view (FOV). This object is a collection of markers that is automatically assigned a frame at the centroid of the object markers and aligned with the world frame at the moment the object was created.
3. Record the location of each marker and the object frame’s transform from the VICON Tracker software
4. Using SolidWorks, input this information into an assembly such that the assembly world frame is the same as the world frame of the motion capture system. In this frame, align the body with markers as best as can me managed those measured from the motion capture software.
5. Define points in the body frame of the robot in CAD, and record the locations of these points in the the model of the world frame aligned body.
6. Input this into (7.1) and compute.[1]

---

[1] As SolidWorks has no inbuilt capacity to output a rotation matrix, we solve a simple linear system to compute the full transform.

7. Manually enter this transformation back into the VICON Tracker software which will update the location of the object frame to the position in the body we desire tracking.

The following determinate system is used to compute the calibration transform.

$$T_B = p_m p^{-1} \tag{7.1}$$

Where, $T_B \in \mathbb{R}^{4\times 4}$ is the transformation matrix between the original VICON object frame, and the frame we wish to track, p_m are the arbitrarily defined body points measured in the world frame aligned CAD model, and p are the arbitrarily defined points in the body frame of the robot.

In the future intend to update this process to fit measured point to the model, as significant variance exists between the marker locations as measured by the VICON system, and how they are modelled. This variance is injected by imperfect manufacturing and positioning of the markers.

7.3.1.4 Trajectory Tracking Tests

A preliminary trajectory tracking experiment has been performed with the ParCli's 5-DoF centre limb. In this experiment, we attempt to track a simple circular trajectory in 3D space. Determination of the end effector location is done through forward kinematics and is effected by the imprecise zeroing of the arm. At this stage, the zeroing has been performed only roughly, which may have significant impact on the tracking performance. The effect of poor zeroing of the end effector is twofold. Firstly, as poor zeroing can mean some discrepancy between the measured output and what has occurred in reality; and secondly, because the dynamic model, especially the gravity term, is a function of joint states. For this experiment, the circular trajectory is defined with respect to position and velocity only, and the feed-forward term was left as zero. This means that the performance is based only on the reactive PID control.

The results shown in Figure 7.2 show reasonable tracking for the imprecisely calibrated system, with the circular trajectory commanded being roughly adhered to. A plot of the

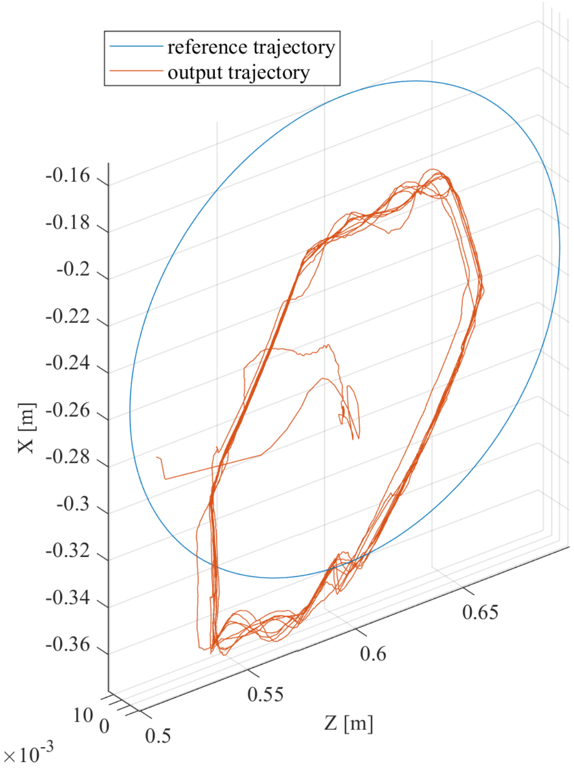

Figure 7.2: Tracking performance of the ParCli centre limb.

motor torques for the arm is shown in Figure 7.3 which can be seen to have roughly the same magnitude of torques as in the centre-limb swing-phase experiments performed in simulation (Figure 6.23). These results confirm that we have approximate control of the system and that our software pipeline for communication and control of the robot are working as intended. In future stages, we will be refining control gains and calibration methods to achieve more precise results.

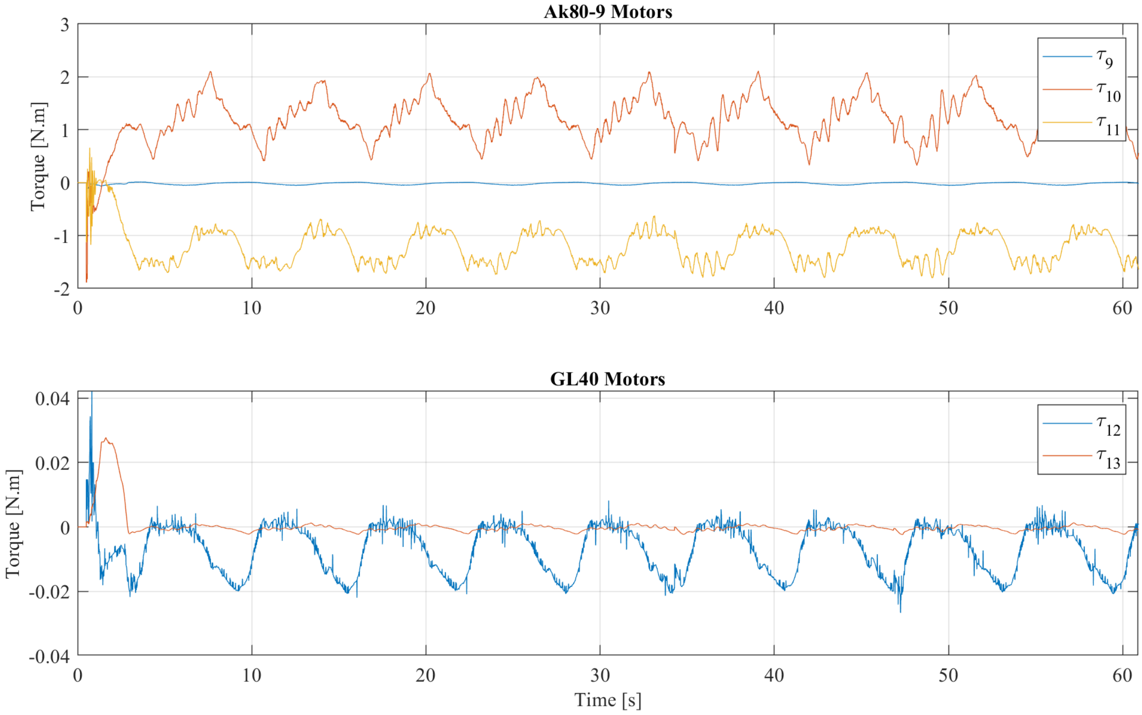

Figure 7.3: Joint torques for the trajectory tracking experiment with ParCli's centre limb. Plots are divided into motor type for readability.

7.3.2 Future Development with ParCli

There are several goals on the immediate horizon for the ParCli robot:

1. Update the design of the tail (joint 14) such that it has a peak torque capacity of at least 10 Nm.
2. Develop 3D trajectory planning algorithm to automatically compute feasible climbing trajectories.
3. Perform a whole-body control test where the body frame position is controlled.
4. Achieve successful single step test similar to the simulated experiments in Section 6.4.2.
5. Execute a climbing trajectory up a simple ladder in the lab.

Longer term, ParCli will likely become a test bed for the implementation of different footfall and trajectory planning algorithms, as well as testing popular control algorithms, like model predictive control (MPC). Estimation of the tail contact location and condition will be useful such that modelling can be more precise. A state observer that detects contact with the climbing substrate (similar to [149]) or detects if a slip has occurred is likely to be useful. Precise pose estimation based on internal sensing (for example [150]) will allow us to move away from an external motion capture system, which is likely to be beneficial when we want to move away from lab experiments. We would also like to produce trajectories based on more dynamic climbing behaviours based on the FG model for dynamic climbing, or some other suitable dynamic model that is more suited to the tripedal form.

7.3.3 The Future for Tripedal Climbing Robots

Moving forward, we intend to tackle the remaining motion primitives defined in Section 3.2 with new kinematic designs that improve the robot's capabilities. By fusing biology and engineering, we hope to uncover more about how parrots achieve these feats whilst learning useful approaches for our own development. Solutions to a plethora of problems will need to be devised to see a successful RSR deployed in an application environment, a short list of these include:

1. Designing versatile and strong prehensile gasping end effectors that can adhere to structures in our application environment.
2. Designing end effectors that are capable for both climbing and maintenance activities.
3. Designing lightweight, high-strength limbs with likely more DoF than our current designs.
4. Looking at methods for optimally resolving redundancy for both climbing and maintenance tasks.
5. Designing optimal foot placement methods that take into consideration task space control objectives.
6. Developing footfall planning and trajectory planning algorithms for climbing in application environment that are cognizant of a robot's capabilities.

7.4 Outlook

In this thesis, we have taken the first steps to creating capable tripedal RSRs, a concept that may have the potential to completely change the way we approach the inspection and maintenance of tall, sparse infrastructure. These structures are crucial to the operation of modern society, and reducing the burden of inspection and maintenance with robotic agents has the potential to make a resounding difference. By lowering the barrier to entry, we can make maintenance more common place, shifting it from reactive to proactive activity. The use of robotics in these structures has great potential to derisk the work, ensuring the safety and comfort of the human operators. Furthermore, when it comes to space applications, there is a ripe opportunity to replace the need for astronauts to do extra-vehicular activities (EVA), again derisking the activity, and enabling maintenance and life extension activities of space structures that are currently unmanned.

Whilst the work presented here is preliminary, we are inspired by a functioning model of the concept in nature that displays analogous behaviour to those we wish to develop. This inspiration gives us confidence that we are on the right track and that as our understanding develops, so to will the capabilities of our robots.

Bibliography

[1] Clyde Webster, Ardian Jusufi, and Dikai Liu. "A comparative survey of climbing robots and arboreal animals in scaling complex environments". In: *IFToMM International Symposium on Robotics and Mechatronics*. Springer. 2017, pp. 31–45.

[2] Clyde Webster, Felix Kong, and Robert Fitch. "Bio-inspired 2D Vertical Climbing with a Novel Tripedal Robot". In: *2022 IEEE/RSJ International Conference on Intelligent Robots and Systems (IROS)*. IEEE. 2022.

[3] Melody W Young et al. "What does climbing mean exactly? Assessing spatiotemporal gait characteristics of inclined locomotion in parrots". In: *Journal of Comparative Physiology A* (2023), pp. 1–15.

[4] Clyde Webster and William Reid. "A Comparative Rover Mobility Evaluation for Traversing Permanently Shadowed Regions on the Moon". In: *2022 IEEE Aerospace Conference (AERO)*. IEEE. 2022, pp. 1–15.

[5] Melody W Young et al. "Overcoming a 'forbidden phenotype': the parrot's head supports, propels and powers tripedal locomotion". In: *Proceedings of the Royal Society B* 289.1975 (2022), p. 20220245.

[6] Michael C. Granatosky et al. "Positional Behavior of Introduced Monk Parakeets (Myiopsitta monachus) in an Urban Landscape". In: *Animals* 12.18 (2022), p. 2372.

[7] Michael C. Granatosky et al. "What does climbing mean exactly? Assessing spatiotemporal gait characteristics of inclined locomotion in parrots". In: *Integrative and Comparative Biology*. Unpublished. 2023.

[8] Christine Böhmer et al. "Correlated evolution of neck length and leg length in birds". In: *Royal Society open science* 6.5 (2019), p. 181588.

[9] Gyula K. Gajdon, Natasha Fijn, and Ludwig Huber. “Testing social learning in a wild mountain parrot, the kea (Nestor notabilis)”. In: *Animal Learning & Behavior* 32.1 (2004), pp. 62–71.

[10] GHD. *Infrastructure maintenance–A report for Infrastructure Australia.* `https://www.infrastructureaustralia.gov.au/sites/default/files/2019-07/GHD-Infrastructure-Maintenance.pdf`. 2015.

[11] *Transmission Tower Maintenance.* Jan. 2019. URL: `https://www.srgglobal.co.nz/what-we-do/asset-maintenance/transmission-tower-maintenance/`.

[12] Alec J Cavaciuti, Joseph H Heying, and Joshua Davis. “IN-SPACE SERVICING, ASSEMBLY, AND MANUFACTURING FOR THE NEW SPACE ECONOMY”. In: (). URL: `https://csps.aerospace.org/sites/default/files/2022-07/Cavaciuti-Davis-Heying_ISAM_20220715.pdf`.

[13] David L Akin and Mary L Bowden. “EVA, robotic, and cooperative assembly of large space structures”. In: *Proceedings, IEEE Aerospace Conference.* Vol. 7. IEEE. 2002, pp. 7–7.

[14] Daniel Schmidt and Karsten Berns. “Climbing robots for maintenance and inspections of vertical structures—A survey of design aspects and technologies”. In: *Robotics and Autonomous Systems* 61.12 (2013), pp. 1288–1305.

[15] Manuel F Silva and JA Tenreiro Machado. “A survey of technologies and applications for climbing robots locomotion and adhesion”. In: *Climbing and walking robots* (2010), pp. 1–22.

[16] Wing Kwong Chung. “Truss Climbing Robot for Space Station: Design, Analysis, and Motion Control”. PhD thesis. The Chinese University of Hong Kong, 2012.

[17] Tirthankar Bandyopadhyay et al. “Magneto: A versatile multi-limbed inspection robot”. In: *2018 IEEE/RSJ International Conference on Intelligent Robots and Systems (IROS).* IEEE. 2018, pp. 2253–2260.

[18] *Transmission Tower Maintenance.* Jan. 2021. URL: `https://www.utilityproducts.com/home/article/16003357/transmission-tower-maintenance`.

[19] Caiwu Ding et al. “Design, Sensing, and Control of a Novel UAV Platform for Aerial Drilling and Screwing”. In: *IEEE Robotics and Automation Letters* 6.2 (2021), pp. 3176–3183. DOI: `10.1109/LRA.2021.3062305`.

[20] Dongbin Kim and Paul Y. Oh. “Human-Drone Interaction for Aerially Manipulated Drilling using Haptic Feedback”. In: *2020 IEEE/RSJ International Conference on Intelligent Robots and Systems (IROS)*. 2020, pp. 9774–9780. DOI: `10.1109/IROS45743.2020.9340726`.

[21] Carlos Balaguer et al. “A climbing autonomous robot for inspection applications in 3d complex environments”. In: *Robotica* 18.3 (2000), pp. 287–297.

[22] Yisheng Guan et al. “Climbot: A modular bio-inspired biped climbing robot”. In: *2011 IEEE/RSJ International Conference on Intelligent Robots and Systems*. IEEE. 2011, pp. 1473–1478.

[23] Yeoreum Yoon and Daniela Rus. “Shady3D: A Robot that Climbs 3D Trusses”. In: *Proceedings 2007 IEEE International Conference on Robotics and Automation*. Institute of Electrical & Electronics Engineers (IEEE), Apr. 2007. DOI: `10.1109/robot.2007.364104`. URL: `http://dx.doi.org/10.1109/ROBOT.2007.364104`.

[24] MJ Spenko et al. “Biologically inspired climbing with a hexapedal robot”. In: *Journal of Field Robotics* 25.4-5 (2008), pp. 223–242.

[25] G Clark Haynes et al. “Rapid pole climbing with a quadrupedal robot”. In: *Robotics and Automation, 2009. ICRA’09. IEEE International Conference on*. IEEE. 2009, pp. 2767–2772.

[26] Kenji Hashimoto et al. “WAREC-1—A four-limbed robot having high locomotion ability with versatility in locomotion styles”. In: *2017 IEEE International Symposium on Safety, Security and Rescue Robotics (SSRR)*. IEEE. 2017, pp. 172–178.

[27] Yusuke Tanaka et al. “Scaler: A tough versatile quadruped free-climber robot”. In: *arXiv preprint arXiv:2207.01180* (2022).

[28] David Pagano, Dikai Liu, and Kenneth Waldron. “A method for optimal design of an inchworm climbing robot”. In: *Robotics and Biomimetics (ROBIO), 2012 IEEE International Conference on*. IEEE. 2012, pp. 1293–1298.

[29] Seungwoo Hong et al. “Agile and versatile climbing on ferromagnetic surfaces with a quadrupedal robot”. In: *Science Robotics* 7.73 (2022), eadd1017.

[30] BL Luk, AA Collie, and J Billingsley. “Robug II: An intelligent wall climbing robot”. In: *Robotics and Automation, 1991. Proceedings., 1991 IEEE International Conference on.* IEEE. 1991, pp. 2342–2347.

[31] BL Luk et al. “Robug iii: a tele-operated climbing and walking robot”. In: *Control’96, UKACC International Conference on (Conf. Publ. No. 427).* Vol. 1. IET. 1996, pp. 347–352.

[32] Zhou Qing et al. “Research of climbing tower robot based on under actuated gripper”. In: *2016 International Conference on Integrated Circuits and Microsystems (ICICM).* IEEE. 2016, pp. 359–362.

[33] Andrés Faina et al. “Development of a climbing robot for grit blasting operations in shipyards”. In: *Robotics and Automation, 2009. ICRA’09. IEEE International Conference on.* IEEE. 2009, pp. 200–205.

[34] DI Jones et al. “Development of a robot for inspecting electricity transmission support towers”. In: *Proc 3rd IFAC Symposium on Mechatronic Systems, Manly Beach, Australia.* 2004, pp. 739–744.

[35] Jeremy Heaston et al. “STriDER: Self-excited tripedal dynamic experimental robot”. In: *Proceedings 2007 IEEE International Conference on Robotics and Automation.* IEEE. 2007, pp. 2776–2777.

[36] Akihiro Torii, Akiteru Ueda, and Kae Doki. “Control of a tripedal robot walking with a shuffle”. In: *IEEJ Transactions on Electronics, Information and Systems* 129.3 (2009), pp. 467–474.

[37] Mark Hermes et al. “Locomotion and Control of a Friction-Driven Tripedal Robot”. In: *2021 IEEE International Conference on Robotics and Automation (ICRA).* IEEE. 2021, pp. 2170–2176.

[38] David Pagano, Dikai Liu, and Kenneth Waldron. “A method for optimal design of an inchworm climbing robot”. In: *2012 IEEE International Conference on Robotics and Biomimetics (ROBIO).* IEEE. 2012, pp. 1293–1298.

[39] Johanna T Schultz et al. “Using a biologically mimicking climbing robot to explore the performance landscape of climbing in lizards”. In: *Proceedings of the Royal Society B* 288.1947 (2021), p. 20202576.

[40] Bing L Luk et al. “Intelligent legged climbing service robot for remote maintenance applications in hazardous environments”. In: *Robotics and Autonomous Systems* 53.2 (2005), pp. 142–152.

[41] Xiao Sun et al. “Planning and control of stable ladder climbing motion for the four-limbed Robot “WAREC-1””. In: *2017 IEEE/RSJ International Conference on Intelligent Robots and Systems (IROS)*. IEEE. 2017, pp. 6547–6554.

[42] Tim Bretl et al. “Free-climbing with a multi-use robot”. In: *Experimental Robotics IX*. Springer, 2006, pp. 449–458.

[43] Avishai Sintov, Tomer Avramovich, and Amir Shapiro. “Design and motion planning of an autonomous climbing robot with claws”. In: *Robotics and Autonomous Systems* 59.11 (2011), pp. 1008–1019.

[44] Avishai Sintov, Tomer Avramovich, and Amir Shapiro. “Design and motion planning of an autonomous climbing robot with claws”. In: *Robotics and Autonomous Systems* 59.11 (2011), pp. 1008–1019.

[45] Ardian Jusufi et al. “Active tails enhance arboreal acrobatics in geckos”. In: *Proceedings of the National Academy of Sciences* 105.11 (2008), pp. 4215–4219.

[46] Sangbae Kim et al. “Whole body adhesion: hierarchical, directional and distributed control of adhesive forces for a climbing robot”. In: *Proceedings 2007 IEEE International Conference on Robotics and Automation*. IEEE. 2007, pp. 1268–1273.

[47] A Jusufi et al. “Righting and turning in mid-air using appendage inertia: reptile tails, analytical models and bio-inspired robots”. In: *Bioinspiration & biomimetics* 5.4 (2010), p. 045001.

[48] R Soler and J Guillet. “Robotic Maintenance of the EDF transmission (63 to 400 kV) network: feasibility Study and effects on tower design”. In: *Transmission and Distribution Construction and Live Line Maintenance, 1993. Proceedings from ESMO-93., Sixth International Conference on*. IEEE. 1993, pp. 459–468.

[49] *Home*. URL: `https://www.tepco.co.jp/en/hd/challenges/open-innovation/index-e.html`.

[50] John J. Craig. *Introduction to Robotics Mechanics and Control*. 3rd ed. Prentice Hall, 2005.

[51] Wesley Au, Tomoki Sakaue, and Dikai Liu. “A Model for Optimising the Size of Climbing Robots for Navigating Truss Structures”. In: *2020 IEEE/RSJ International Conference on Intelligent Robots and Systems (IROS)*. IEEE. 2020, pp. 3754–3760.

[52] William R Provancher, Samuel I Jensen-Segal, and Mark A Fehlberg. “ROCR: An energy-efficient dynamic wall-climbing robot”. In: *IEEE/ASME Transactions on Mechatronics* 16.5 (2011), pp. 897–906.

[53] Jonathan E Clark et al. “Design of a bio-inspired dynamical vertical climbing robot”. In: *Robotics:Science and Systems III* (2007).

[54] Daniel I Goldman et al. “Dynamics of rapid vertical climbing in cockroaches reveals a template”. In: *Journal of Experimental Biology* 209.15 (2006), pp. 2990–3000.

[55] Jonathan E Clark et al. “Toward a dynamic vertical climbing robot”. In: *Departmental Papers (ESE)* (2006), p. 504.

[56] Goran A Lynch et al. “A bioinspired dynamical vertical climbing robot”. In: *The International Journal of Robotics Research* 31.8 (2012), pp. 974–996.

[57] Jared Di Carlo et al. “Dynamic locomotion in the mit cheetah 3 through convex model-predictive control”. In: *2018 IEEE/RSJ international conference on intelligent robots and systems (IROS)*. IEEE. 2018, pp. 1–9.

[58] Marco Hutter et al. “Anymal-a highly mobile and dynamic quadrupedal robot”. In: *2016 IEEE/RSJ International Conference on Intelligent Robots and Systems (IROS)*. IEEE. 2016, pp. 38–44.

[59] LK Takahashi. “Morphological basis of arm-swinging: multivariate analyses of the forelimbs of Hylobates and Ateles”. In: *Folia Primatologica* 54.1-2 (1990), pp. 70–85.

[60] Uwe Hollihn. "Bimanual suspensory behavior: morphology, selective advantages and phylogeny". In: *The lesser apes: Evolutionary and behavioral biology* (1984), pp. 85–95.

[61] C Laschi and B Mazzolai. "Lessons from Animals and Plants: The Symbiosis of Morphological Computation and Soft Robotics". In: *IEEE Robotics & Automation Magazine* 23.3 (2016), pp. 107–114.

[62] GAFI. *Great Apes.* http://www.gafi4apes.org/gafi-species/. 2016. URL: `http://www.gafi4apes.org/gafi-species/`.

[63] Fana Michilsens et al. "Functional anatomy of the gibbon forelimb: adaptations to a brachiating lifestyle". In: *Journal of Anatomy* 215.3 (2009), pp. 335–354.

[64] Animals Club. *Gibbon.* http://elelur.com/mammals/gibbon.html. 2016. URL: `http://elelur.com/mammals/gibbon.html`.

[65] Kim Ann Zimmermann. *Muscular System: Facts, Functions & Diseases.* http://www.livescience muscular-system-facts-functions-diseases.html. 2011. URL: `http://www.livescience.com/26854-muscular-system-facts-functions-diseases.html`.

[66] Daichi Maita and Gentiane Venture. "Influence of the model's degree of freedom on human body dynamics identification". In: *Engineering in Medicine and Biology Society (EMBC), 2013 35th Annual International Conference of the IEEE.* IEEE. 2013, pp. 4609–4612.

[67] Adrienne L Zihlman and Robin K McFarland. "Body mass in lowland gorillas: a quantitative analysis". In: *American Journal of Physical Anthropology* 113.1 (2000), pp. 61–78.

[68] Karin Isler. "3D-kinematics of vertical climbing in hominoids". In: *American Journal of Physical Anthropology* 126.1 (2005), pp. 66–81.

[69] Kenneth J Waldron and Christopher Hubert. "Scaling of robotic mechanisms". In: *Robotics and Automation, 2000. Proceedings. ICRA'00. IEEE International Conference on.* Vol. 1. IEEE. 2000, pp. 40–45.

[70] JE Bertram et al. "A point-mass model of gibbon locomotion". In: *Journal of Experimental Biology* 202.19 (1999), pp. 2609–2617.

[71] Toshio Fukuda, H Hosokai, and Yuji Kondo. “Brachiation type of mobile robot”. In: *Advanced Robotics, 1991.'Robots in Unstructured Environments', 91 ICAR., Fifth International Conference on.* IEEE. 1991, pp. 915–920.

[72] Fuminori Saito, Toshio Fukuda, and Fumihito Arai. “Swing and locomotion control for a two-link brachiation robot”. In: *IEEE Control Systems* 14.1 (1994), pp. 5–12.

[73] Toshio Fukuda and Fuminori Saito. “Motion control of a brachiation robot”. In: *Robotics and autonomous systems* 18.1-2 (1996), pp. 83–93.

[74] Jun Nakanishi, Toshio Fukuda, and Daniel E Koditschek. “A brachiating robot controller”. In: *IEEE Transactions on Robotics and Automation* 16.2 (2000), pp. 109–123.

[75] Gibbon Research Lab. *Locomotion.* http://www.gibbons.de. 2016. URL: `http://www.gibbons.de/main/introduction/chapter_english05.html`.

[76] William Reid. “System Design, Motion Modelling and Planning for a Recon figurable Wheeled Mobile Robot”. PhD thesis. 2017.

[77] H Preuschoft. “Gravity in primates and its relation to body shape and locomotion”. In: *Human evolution* 5.6 (1990), pp. 559–578.

[78] Phil Vinter. *Baby balancing act! Mother gibbon takes her offspring for a tightrope walk on the wild side.* http://www.dailymail.co.uk/news/article-2203603/Baby-balancing-act-Mother-gibbon-takes-offspring-tightrope-walk-wild-side.html. 2012. URL: `http://www.dailymail.co.uk/news/article-2203603/Baby-balancing-act-Mother-gibbon-takes-offspring-tightrope-walk-wild-side.html`.

[79] Siddhant Gangapurwala et al. “Rloc: Terrain-aware legged locomotion using reinforcement learning and optimal control”. In: *IEEE Transactions on Robotics* 38.5 (2022), pp. 2908–2927.

[80] Karin Isler. “Characteristics of vertical climbing in gibbons”. In: *Evolutionary Anthropology: Issues, News, and Reviews* 11.S1 (2002), pp. 49–52.

[81] Daniel L Gebo. “Climbing, brachiation, and terrestrial quadrupedalism: historical precursors of hominid bipedalism”. In: *American Journal of Physical Anthropology* 101.1 (1996), pp. 55–92.

[82] Susan G Larson and Jack T Stern. “Maintenance of above-branch balance during primate arboreal quadrupedalism: Coordinated use of forearm rotators and tail motion”. In: *American journal of physical anthropology* 129.1 (2006), pp. 71–81.

[83] Donald C Dunbar. “Aerial maneuvers of leaping lemurs: The physics of whole-body rotations while airborne”. In: *American Journal of Primatology* 16.4 (1988), pp. 291–303.

[84] A Peters and H Preuschoft. “External biomechanics of leaping in Tarsius and its morphological and kinematic consequences”. In: *Biology of tarsiers* (1984), pp. 227–255.

[85] Graham C Hickman. “The mammalian tail: a review of functions”. In: *Mammal review* 9.4 (1979), pp. 143–157.

[86] Randall Briggs et al. “Tails in biomimetic design: Analysis, simulation, and experiment”. In: *Intelligent Robots and Systems (IROS), 2012 IEEE/RSJ International Conference on.* IEEE. 2012, pp. 1473–1480.

[87] Amir Patel and M Braae. “Rapid acceleration and braking: Inspirations from the cheetah’s tail”. In: *2014 IEEE International Conference on Robotics and Automation (ICRA).* IEEE. 2014, pp. 793–799.

[88] Anna L Brill et al. “Tail-assisted rigid and compliant legged leaping”. In: *Intelligent Robots and Systems (IROS), 2015 IEEE/RSJ International Conference on.* IEEE. 2015, pp. 6304–6311.

[89] Avik De and Daniel E Koditschek. “Parallel composition of templates for tail-energized planar hopping”. In: *2015 IEEE International Conference on Robotics and Automation (ICRA).* IEEE. 2015, pp. 4562–4569.

[90] Amir Patel and Edward Boje. “On the conical motion of a two-degree-of-freedom tail inspired by the Cheetah”. In: *IEEE Transactions on Robotics* 31.6 (2015), pp. 1555–1560.

[91] Amir Patel et al. “Quasi-steady state aerodynamics of the cheetah tail”. In: *Biology Open* 5.8 (2016), pp. 1072–1076.

[92] Thomas Libby et al. “Tail-assisted pitch control in lizards, robots and dinosaurs”. In: *Nature* 481.7380 (2012), pp. 181–184.

[93] R Åke Norberg. "Treecreeper climbing; mechanics, energetics, and structural adaptations". In: *Ornis Scandinavica* (1986), pp. 191–209.

[94] Ryan D Marek et al. "Evolutionary versatility of the avian neck". In: *Proceedings of the Royal Society B* 288.1946 (2021), p. 20203150.

[95] Boston Dynamics. *RISE*. Youtube. 2009. URL: `https://youtu.be/MZGGL20g99A?t=38`.

[96] SK Mahmood, Sadeq H Bakhy, and MA Tawfik. "Novel wall-climbing robot capable of transitioning and perching". In: *IOP Conference Series: Materials Science and Engineering*. Vol. 881. 1. IOP Publishing. 2020, p. 012049.

[97] Karl Iagnemma, Frank Genot, and Steven Dubowsky. "Rapid physics-based rough-terrain rover planning with sensor and control uncertainty". In: *Proceedings 1999 IEEE International Conference on Robotics and Automation (Cat. No. 99CH36288C)*. Vol. 3. IEEE. 1999, pp. 2286–2291.

[98] Joseph C Spagna et al. "Distributed mechanical feedback in arthropods and robots simplifies control of rapid running on challenging terrain". In: *Bioinspiration & biomimetics* 2.1 (2007), p. 9.

[99] Hironari Yoneda et al. "Vertical ladder climbing motion with posture control for multi-locomotion robot". In: *2008 IEEE/RSJ International Conference on Intelligent Robots and Systems*. IEEE. 2008, pp. 3579–3584.

[100] Joris Vaillant et al. "Vertical ladder climbing by the hrp-2 humanoid robot". In: *2014 IEEE-RAS International Conference on Humanoid Robots*. IEEE. 2014, pp. 671–676.

[101] Kevin D Hunt et al. "Standardized descriptions of primate locomotor and postural modes". In: *Primates* 37.4 (1996), pp. 363–387.

[102] Evie E Vereecke, Kristiaan D'Août, and Peter Aerts. "Locomotor versatility in the white-handed gibbon (Hylobates lar): A spatiotemporal analysis of the bipedal, tripedal, and quadrupedal gaits". In: *Journal of Human Evolution* 50.5 (2006), pp. 552–567.

[103] William C Dilger. "The comparative ethology of the African parrot genus Agapornis." In: *Zeitschrift für Tierpsychologie* (1960).

[104] Frank Alexander Hartman. “Locomotor mechanisms of birds”. In: *Smithsonian miscellaneous collections* (1961).

[105] Eldar Insafutdinov et al. “Deepercut: A deeper, stronger, and faster multi-person pose estimation model”. In: *European conference on computer vision*. Springer. 2016, pp. 34–50.

[106] Alexander Mathis et al. “DeepLabCut: markerless pose estimation of user-defined body parts with deep learning”. In: *Nature neuroscience* 21.9 (2018), pp. 1281–1289.

[107] Robert J Full and Daniel E Koditschek. “Templates and anchors: neuromechanical hypotheses of legged locomotion on land”. In: *Journal of experimental biology* 202.23 (1999), pp. 3325–3332.

[108] Anick Abourachid and Elizabeth Höfling. “The legs: a key to bird evolutionary success”. In: *Journal of Ornithology* 153.1 (2012), pp. 193–198.

[109] Gerrit A Folkertsma, Sangbae Kim, and Stefano Stramigioli. “Parallel stiffness in a bounding quadruped with flexible spine”. In: *2012 IEEE/RSJ International Conference on Intelligent Robots and Systems*. IEEE. 2012, pp. 2210–2215.

[110] Mahdi Khoramshahi et al. “Benefits of an active spine supported bounding locomotion with a small compliant quadruped robot”. In: *2013 IEEE international conference on robotics and automation*. IEEE. 2013, pp. 3329–3334.

[111] Mohammad Hasan H Kani et al. “Effect of flexible spine on stability of a passive quadruped robot: Experimental results”. In: *2011 IEEE International Conference on Robotics and Biomimetics*. IEEE. 2011, pp. 2793–2798.

[112] Peter Eckert et al. “Comparing the effect of different spine and leg designs for a small bounding quadruped robot”. In: *2015 IEEE International Conference on Robotics and Automation (ICRA)*. IEEE. 2015, pp. 3128–3133.

[113] Marc H Raibert. “Running with symmetry”. In: *Autonomous Robot Vehicles*. Springer, 1986, pp. 45–61.

[114] Marc H Raibert. “Symmetry in running”. In: *Science* 231.4743 (1986), pp. 1292–1294.

[115] John Schmitt and Philip Holmes. “Mechanical models for insect locomotion: dynamics and stability in the horizontal plane I. Theory”. In: *Biological cybernetics* 83.6 (2000), pp. 501–515.

[116] John Schmitt and Philip Holmes. “Mechanical models for insect locomotion: dynamics and stability in the horizontal plane–II. Application”. In: *Biological cybernetics* 83.6 (2000), pp. 517–527.

[117] Philip Holmes et al. “The dynamics of legged locomotion: Models, analyses, and challenges”. In: *SIAM review* 48.2 (2006), pp. 207–304.

[118] Benjamin Fasquelle et al. “Modelling, design and control of a bird neck using tensegrity mechanisms”. In: *ICRA'2019 Worskhop on Tensegrity.* 2019.

[119] Masaki Fujita, Kazuto Kawakami, and Hiroyoshi Higuchi. “Hopping and climbing gait of Japanese Pygmy Woodpeckers (Picoides kizuki)”. In: *Comparative Biochemistry and Physiology Part A: Molecular & Integrative Physiology* 148.4 (2007), pp. 802–810.

[120] Lowell W Spring. “Climbing and pecking adaptations in some North American woodpeckers”. In: *The Condor* 67.6 (1965), pp. 457–488.

[121] Charles G Sibley. “Notes on the birds of New Georgia, central Solomon Islands”. In: *The condor* 53.2 (1951), pp. 81–92.

[122] Anick Abourachid. “A new way of analysing symmetrical and asymmetrical gaits in quadrupeds”. In: *Comptes rendus biologies* 326.7 (2003), pp. 625–630.

[123] Harvey Goldstein. *Multilevel statistical models.* John Wiley & Sons, 2011.

[124] Herbert Friedmann and Malcolm Davis. "“Left-handedness” in parrots”. In: *The Auk* 55.3 (1938), pp. 478–480.

[125] Raymond McNeil, José R Rodriguez, and Damelys M Figuera. “HANDEDNESS IN THE BROWN-THROATED PARAKEET ARATINGA PERTINAX EST RELATION WITH SKELETAL ASYMMETRY”. In: *Ibis* 113.4 (1971), pp. 494–499.

[126] Culum Brown and Maria Magat. “The evolution of lateralized foot use in parrots: a phylogenetic approach”. In: *Behavioral Ecology* 22.6 (2011), pp. 1201–1208.

[127] Lauren J Harris. “Footedness in parrots: three centuries of research, theory, and mere surmise.” In: *Canadian Journal of Psychology/Revue canadienne de psychologie* 43.3 (1989), p. 369.

[128] Peter J Snyder and Lauren Julius Harris. “Lexicon size and its relation to foot preference in the African grey parrot (Psittacus erithacus)”. In: *Neuropsychologia* 35.6 (1997), pp. 919–926.

[129] Lesley J Rogers. “Development and function of lateralization in the avian brain”. In: *Brain research bulletin* 76.3 (2008), pp. 235–244.

[130] Digby Elliott and Eric A Roy. *Manual asymmetries in motor performance.* CRC Press, 1996.

[131] L Workman and RJ Andrew. “Asymmetries of eye use in birds.” In: *Animal Behaviour* (1986).

[132] Robert D Gregg et al. “The basic mechanics of bipedal walking lead to asymmetric behavior”. In: *2011 IEEE International Conference on Rehabilitation Robotics.* IEEE. 2011, pp. 1–6.

[133] Guillaume Sartoretti et al. “Central pattern generator with inertial feedback for stable locomotion and climbing in unstructured terrain”. In: *2018 IEEE International Conference on Robotics and Automation (ICRA).* IEEE. 2018, pp. 5769–5775.

[134] Kellar Autumn et al. “Robotics in scansorial environments”. In: *Unmanned ground vehicle technology VII.* Vol. 5804. International Society for Optics and Photonics. 2005, pp. 291–302.

[135] Kenneth V Kardong. *Vertebrates: comparative anatomy, function, evolution.* McGraw-Hill Education, 2018.

[136] Kevin M Lynch and Frank C Park. *Modern robotics.* Cambridge University Press, 2017.

[137] Gerardo Bledt et al. “MIT Cheetah 3: Design and control of a robust, dynamic quadruped robot”. In: *2018 IEEE/RSJ International Conference on Intelligent Robots and Systems (IROS).* IEEE. 2018, pp. 2245–2252.

[138] Nathan Kau et al. *Stanford Doggo: An Open-Source, Quasi-Direct-Drive Quadruped.* 2019. arXiv: `1905.04254 [cs.RO]`.

[139] Nathan Ratliff. *Robot Dynamics Lecture Notes.* 2017. URL: `https://ethz.ch/content/dam/ethz/special-interest/mavt/robotics-n-intelligent-systems/rsl-dam/documents/RobotDynamics2017/RD_HS2017script.pdf`.

[140] Steve Miller. *Simscape Multibody Contact Forces Library.* 2022. URL: `https://github.com/mathworks/Simscape-Multibody-Contact-Forces-Library/releases/tag/21.2.5.0` (visited on 02/23/2022).

[141] Robin Verschueren et al. “acados—a modular open-source framework for fast embedded optimal control”. In: *Mathematical Programming Computation* (2021), pp. 1–37.

[142] William R Provancher, Samuel I Jensen-Segal, and Mark A Fehlberg. “ROCR: An energy-efficient dynamic wall-climbing robot”. In: *IEEE/ASME Transactions on Mechatronics* 16.5 (2010), pp. 897–906.

[143] Benjamin G Katz. “A low cost modular actuator for dynamic robots”. PhD thesis. Massachusetts Institute of Technology, 2018.

[144] Josep Virgili-Llop et al. *SPART: an open-source modeling and control toolkit for mobile-base robotic multibody systems with kinematic tree topologies.* `https://github.com/NPS-SRL/SPART`.

[145] Josep Virgili-Llop et al. “Spacecraft robotics toolkit: an open-source simulator for spacecraft robotic arm dynamic modeling and control”. In: *6th International Conference on Astrodynamics Tools and Techniques.* 2016.

[146] Gene F Franklin et al. *Feedback control of dynamic systems.* Vol. 4. Prentice hall Upper Saddle River, 2002.

[147] Woolfrey Jonathan. *Robotics Toolbox.* `https://github.com/Woolfrey/RobotToolbox.git`. 2029.

[148] RG Bout. “Postures of the avian craniocervical column”. In: *Journal of Morphology* 231.3 (1997), pp. 287–295.

[149] Gerardo Bledt et al. “Contact model fusion for event-based locomotion in unstructured terrains”. In: *2018 IEEE International Conference on Robotics and Automation (ICRA).* IEEE. 2018, pp. 4399–4406.

[150] Michael Bloesch et al. “State estimation for legged robots-consistent fusion of leg kinematics and IMU”. In: *Robotics* 17 (2013), pp. 17–24.

Appendices

A Multivariate Mixed-Effect Regression Model

$$\begin{aligned}
l =& \beta^{(l)}_{jkl} + \beta^{(l)}_1 t + \beta^{(l)}_2 t^2 + \beta^{(l)}_3 t^3 + \beta^{(l)}_4 t^4 + \beta^{(l)}_5 x_t + \beta^{(l)}_6 x_t t + \beta^{(l)}_7 x_t t^2 + \beta^{(l)}_8 x_t t^3 \\
&+ \beta^{(l)}_9 x_t t^4 + \beta^{(l)}_{10} x_s + \beta^{(l)}_{11} x_s t + \beta^{(l)}_{12} x_s t^2 + \beta^{(l)}_{13} x_s t^3 + \beta^{(l)}_{14} x_s t^4 + \beta^{(l)}_{15} x_t x_s \\
&+ \beta^{(l)}_{16} x_t x_s t + \beta^{(l)}_{17} x_t x_s t^2 + \beta^{(l)}_{18} x_t x_s t^3 + \beta^{(l)}_{19} x_t x_s t^4
\end{aligned}$$

$$\beta^{(l)}_{jkl} = \beta^{(l)} + f^{(l)}_l + v^{(l)}_{kl} + u^{(l)}_{jkl}$$

$$\theta = \beta^{(\theta)}_{jkl} + \beta^{(\theta)}_1 t + \beta^{(\theta)}_2 t^2 + \beta^{(\theta)}_3 t^3 + \beta^{(\theta)}_4 t^4 + \beta^{(\theta)}_5 x_t + \beta^{(\theta)}_6 x_t t + \beta^{(\theta)}_7 x_t t^2 + \beta^{(\theta)}_8 x_t t^3$$
$$+ \beta^{(\theta)}_9 x_t t^4 + \beta^{(\theta)}_{10} x_s + \beta^{(\theta)}_{11} x_s t + \beta^{(\theta)}_{12} x_s t^2 + \beta^{(\theta)}_{13} x_s t^3 + \beta^{(\theta)}_{14} x_s t^4 + \beta^{(\theta)}_{15} x_t x_s$$
$$+ \beta^{(\theta)}_{16} x_t x_s t + \beta^{(\theta)}_{17} x_t x_s t^2 + \beta^{(\theta)}_{18} x_t x_s t^3 + \beta^{(\theta)}_{19} x_t x_s t^4$$

$$\beta^{(\theta)}_{jkl} = \beta^{(\theta)} + f^{(\theta)}_l + v^{(\theta)}_{kl} + u^{(\theta)}_{jkl}$$

$$\begin{bmatrix} f_l^{(l)} \\ f_l^{(\theta)} \end{bmatrix} \tilde{N}(0,\Omega_f) : \Omega_f = \begin{bmatrix} \sigma_{fl}^2 & \\ \sigma_{fl\theta} & \sigma_{f\theta}^2 \end{bmatrix}$$

$$\begin{bmatrix} v_{kl}^{(l)} \\ v_{kl}^{(\theta)} \end{bmatrix} \tilde{N}(0,\Omega_v) : \Omega_v = \begin{bmatrix} \sigma_{vl}^2 & \\ \sigma_{vl\theta} & \sigma_{v\theta}^2 \end{bmatrix}$$

$$\begin{bmatrix} u_{jkl}^{(l)} \\ u_{jkl}^{(\theta)} \end{bmatrix} \tilde{N}(0,\Omega_u) : \Omega_u = \begin{bmatrix} \sigma_{ul}^2 & \\ \sigma_{ul\theta} & \sigma_{u\theta}^2 \end{bmatrix}$$

Where f, v, and u, dictate the variance with respect to each bird, cycle and response respectively. The mixed effect was only placed on the intercept variable to give us an idea of how each quartic shifted and is not computed with respect to the general shape of the quartic. For this model, time is normalised between 0 and 100% of the cycle duration due to the large variation in cycle durations present.

B Regression Coefficients

Length	Left Bipedal	$[+x_s]$ Right Bipedal	Left Tripedal	$[+x_s]$ Right Tripedal
	26.00 (1.48)	1.496 (2.086)	31.24 (0.962)	-7.611 (1.358)
t	-12.01 (4.228)	0.037 (5.844)	-58.17 (3.652)	91.38 (5.102)
t^2	405.36 (17.36)	-65.16 (24.01)	30.99 (15.044)	-372.45 (21.01)
t^3	-506.85 (26.24)	141.2 (36.28)	303.49 (22.78)	573.72 (31.80)
t^4	100.84 (13.05)	-76.15 (18.04)	-284.26 (11.35)	-287.95 (15.84)
Angle				
	1.864 (0.034)	0.026 (0.048)	1.037 (0.062)	0.397 (0.087)
t	7.689 (0.104)	-1.529 (0.144)	2.933 (0.152)	1.022 (0.212)
t^2	-21.25 (0.427)	5.196 (0.591)	1.899 (0.625)	-12.29 (0.873)
t^3	27.93 (0.646)	-6.487 (0.893)	-1.709 (0.947)	21.96 (1.322)
t^4	-14.60 (0.321)	2.825 (0.444)	-2.877 (0.472)	-10.72 (0.658)

TABLE 1: Model 1 polynomial coefficients. Coloured cells represent coefficients with a low confidence ($p > 0.05$) and whose mean does not vary significantly from zero. The standard error (SE) of each coefficient is in parenthesis after each result.

55°				
Length	Left Bipedal	[+x_s] Right Bipedal	Left Tripedal	[+x_s] Right Tripedal
	26.51 (0.853)	-2.312 (1.202)	-3.706 (1.387)	4.133 (1.914)
t	-47.01 (3.2)	25.34 (4.317)	47.78 (10.21)	-13.18 (14.24)
t^2	458.4 (13.07)	-153.6 (17.54)	-228.8 (41.61)	-83.24 (58.04)
t^3	-531.2 (19.74)	276.9 (26.43)	299.4 (62.74)	252.2 (87.4)
t^4	108.7 (9.835)	-148.2 (13.15)	-112.1 (31.2)	-159.4 (43.36)
Angle				
	1.75 (0.037)	-0.059 (0.053)	0.095 (0.029)	0.099 (0.039)
t	7.034 (0.071)	-0.273 (0.064)	-1.296 (0.119)	-0.767 (0.09)
t^2	-16.99 (0.267)	0.706 (0.149)	3.051 (0.261)	0.946 (0.087)
t^3	21.23 (0.39)	-0.419 (0.098)	-2.087 (0.169)	
t^4	-11.35 (0.192)			
65°				
Length	Left Bipedal	[+x_s] Right Bipedal	Left Tripedal	[+x_s] Right Tripedal
	27.54 (1.027)	-4.355 (1.446)	-3.164 (0.823)	7.487 (1.141)
t	-56.82 (3.727)	27.62 (4.468)	34.37 (4.369)	-11.91 (3.961)
t^2	342.3 (14.85)	-125.6 (16.65)	-268 (16.67)	-21.85 (9.288)
t^3	-231.9 (22.18)	213.9 (24.1)	453.9 (24.4)	31.28 (6.134)
t^4	-65.26 (11.02)	-113.1 (11.87)	-216.2 (12.06)	
Angle				
	1.399 (0.059)	0.035 (0.083)	0.062 (0.028)	0.077 (0.04)
t	6.773 (0.161)	0.58 (0.226)	-1.121 (0.21)	-1.894 (0.294)
t^2	-13.45 (0.663)	-3.65 (0.929)	2.783 (0.863)	6.853 (1.205)
t^3	16.88 (1.004)	5.03 (1.405)	-2.733 (1.306)	-7.334 (1.821)
t^4	-10.01 (0.5)	-1.997 (0.7)	0.907 (0.65)	2.398 (0.906)
75°				
Length	Left Bipedal	[+x_s] Right Bipedal	Left Tripedal	[+x_s] Right Tripedal
	30.35 (1.58)	-11.55 (2.29)	-2.278 (1.444)	8.419 (2.1)
t	-85.3 (9.455)	141.9 (14)	39.95 (9.969)	-78.58 (14.68)
t^2	282 (38.93)	-521.2 (57.74)	-234.6 (41.04)	227.4 (60.54)
t^3	-54.33 (58.95)	743.2 (87.62)	353.9 (62.14)	-278.9 (91.84)
t^4	-156.2 (29.39)	-355.2 (43.75)	-153.6 (30.97)	124.9 (45.84)
Angle				
	1.03 (0.074)	0.28 (0.106)	0.152 (0.061)	-0.045 (0.089)
t	6.76 (0.418)	1.549 (0.618)	-2.488 (0.44)	-1.164 (0.648)
t^2	-8.824 (1.719)	-12.86 (2.55)	5.248 (1.813)	7.236 (2.674)
t^3	9.205 (2.604)	20.29 (3.87)	-4.505 (2.745)	-9.792 (4.057)
t^4	-6.641 (1.298)	-9.232 (1.932)	1.483 (1.368)	3.977 (2.025)

TABLE 2: Model 2 polynomial coefficients. Coloured cells represent coefficients with a low confidence ($p > 0.05$) and whose mean does not vary significantly from zero. The standard error (SE) of each coefficient is in parenthesis after each result.

C ParCli URDF

```
<?xml version="1.0" ?>

<robot name="parody-mark1">

  <!-- Colors -->
  <material name="Red">
    <color rgba="1 0 0 1.0"/>
  </material>
  <material name="Light Green">
    <color rgba="0.6 1.0 0.6 1.0"/>
  </material>
  <material name="Light Blue">
    <color rgba="0.6 1.0 1.0 1.0"/>
  </material>
  <material name="Middle Blue">
    <color rgba="0.4 0.8 1.0 1.0"/>
  </material>
  <material name="Distal Blue">
    <color rgba="0.6 0.8 1.0 1.0"/>
  </material>
  <material name="White">
    <color rgba="1.0 1.0 1.0 1.0"/>
  </material>

  <!-- Body -->

  <link name="body">
    <inertial>
      <origin rpy="0 0 0" xyz="0 0 0"/>
      <mass value="3.16587"/>
      <inertia ixx="0.0182112" ixy="-0.0009653" ixz="0.0094585" iyy="0.0518129" iyz="0.0000029" izz="0.0609009"/>
    </inertial>
    <visual>
      <origin rpy="0 0 0" xyz="0 0 0"/>
      <geometry>
        <mesh filename="Body.STEP"/>
      </geometry>
      <material name="Light Green"/>
    </visual>
  </link>

  <!-- Left Leg -->

  <joint name="joint1" type="continuous">
    <parent link="body"/>
    <child link="left_proximal"/>
    <origin rpy="0 0 -1.570796326794897" xyz="-0.1 -0.1 0"/>
    <axis xyz="0 0 1"/>
  </joint>
  <link name="left_proximal">
    <inertial>
      <origin rpy="0 0 0" xyz="0.0544406 -0.0078896 0.0100639"/>
      <mass value="1.0637477"/>
```

```
      <inertia ixx="0.0013191" ixy="-0.0016013" ixz="0.0012142" iyy="0.0132247" iyz="-0.0001724" izz="0.0135818"/>
    </inertial>
    <visual>
      <origin rpy="0 0 0" xyz="0 0 0"/>
      <geometry>
        <mesh filename="LinkL1.STEP"/>
      </geometry>
      <material name="Light Blue"/>
    </visual>
  </link>

  <joint name="joint2" type="continuous">
    <parent link="left_proximal"/>
    <child link="left_medial"/>
    <origin rpy="0 0 0" xyz="0.3 0 0.02397"/>
    <axis xyz="0 0 1"/>
  </joint>
  <link name="left_medial">
    <inertial>
      <origin rpy="0 0 0" xyz="0.0235637 0 0.0032756"/>
      <mass value="0.3413668"/>
      <inertia ixx="0.0001202" ixy="0" ixz="0" iyy="0.0005919" iyz="0" izz="0.0006052"/>
    </inertial>
    <visual>
      <origin rpy="0 0 0" xyz="0 0 0"/>
      <geometry>
        <mesh filename="LinkL2.STEP"/>
      </geometry>
      <material name="Middle Blue"/>
    </visual>
  </link>

  <joint name="joint3" type="continuous">
    <parent link="left_medial"/>
    <child link="left_distal"/>
    <origin rpy="0 0 0" xyz="0.07 0 0"/>
    <axis xyz="1 0 0"/>
  </joint>
  <link name="left_distal">
    <inertial>
      <origin rpy="0 0 0" xyz="0.157 0 0.004"/>
      <mass value="0.2615387"/>
      <inertia ixx="0.0000762" ixy="0" ixz="0.0002701" iyy="0.0093326" iyz="0" izz="0.0093351"/>
    </inertial>
    <visual>
      <origin rpy="0 0 0" xyz="0 0 0"/>
      <geometry>
        <mesh filename="LinkL3.STEP"/>
      </geometry>
      <material name="Distal Blue"/>
    </visual>
  </link>

  <joint name="joint4" type="continuous">
    <parent link="left_distal"/>
```

```
    <child link="left_gripper"/>
    <origin rpy="0 0 1.570796326794897" xyz="0.24675 0 0.02075"/>
    <axis xyz="0 0 1"/>
  </joint>
  <link name="left_gripper">
    <inertial>
      <origin rpy="0 0 0" xyz="0.01309 0 0.01808"/>
      <mass value="0.0565791"/>
      <inertia ixx="0.0000451" ixy="0" ixz="0.0000073" iyy="0.0000295" iyz="0" izz="0.0000386"/>
    </inertial>
    <visual>
      <origin rpy="0 0 0" xyz="0.0125 0 0.0285"/>
      <geometry>
        <mesh filename="Link4.STEP"/>
      </geometry>
      <material name="White"/>
    </visual>
  </link>

<!-- Right Leg -->

  <joint name="joint5" type="continuous">
    <parent link="body"/>
    <child link="right_proximal"/>
    <origin rpy="0 0 1.570796326794897" xyz="-0.1 0.1 0"/>
    <axis xyz="0 0 -1"/>
  </joint>
  <link name="right_proximal">
    <inertial>
      <origin rpy="0 0 0" xyz="0.0545837 0.0078708 0.0079537"/>
      <mass value="1.0637266"/>
      <inertia ixx="0.0012778" ixy="0.0016043" ixz="0.0010925" iyy="0.0132004" iyz="0.0001550" izz="0.0135970"/>
    </inertial>
    <visual>
      <origin rpy="0 0 0" xyz="0 0 0"/>
      <geometry>
        <mesh filename="LinkR1.STEP"/>
      </geometry>
      <material name="Light Blue"/>
    </visual>
  </link>

  <joint name="joint6" type="continuous">
    <parent link="right_proximal"/>
    <child link="right_medial"/>
    <origin rpy="0 0 0" xyz="0.3 0 0.02397"/>
    <axis xyz="0 0 -1"/>
  </joint>
  <link name="right_medial">
    <inertial>
      <origin rpy="0 0 0" xyz="0.0235637 0 0.0033434"/>
      <mass value="0.3413668"/>
      <inertia ixx="0.0001205" ixy="0" ixz="0" iyy="0.0005922" iyz="0" izz="0.0006052"/>
    </inertial>
    <visual>
```

```
      <origin rpy="0 0 0" xyz="0 0 0"/>
      <geometry>
        <mesh filename="LinkR2.STEP"/>
      </geometry>
      <material name="Middle Blue"/>
    </visual>
  </link>

  <joint name="joint7" type="continuous">
    <parent link="right_medial"/>
    <child link="right_distal"/>
    <origin rpy="0 0 0" xyz="0.07 0 0"/>
    <axis xyz="1 0 0"/>
  </joint>
  <link name="right_distal">
    <inertial>
      <origin rpy="0 0 0" xyz="0.157 0 0.004"/>
      <mass value="0.2615387"/>
      <inertia ixx="0.0000762" ixy="0" ixz="0.0002701" iyy="0.0093326" iyz
    ="0" izz="0.0093351"/>
    </inertial>
    <visual>
      <origin rpy="0 0 0" xyz="0 0 0"/>
      <geometry>
        <mesh filename="LinkR3.STEP"/>
      </geometry>
      <material name="Distal Blue"/>
    </visual>
  </link>

  <joint name="joint8" type="continuous">
    <parent link="right_distal"/>
    <child link="right_gripper"/>
    <origin rpy="0 0 -1.570796326794897" xyz="0.24675 0 0.02075"/>
    <axis xyz="0 0 -1"/>
  </joint>
  <link name="right_gripper">
    <inertial>
      <origin rpy="0 0 0" xyz="0.01309 0 0.01808"/>
      <mass value="0.0565791"/>
      <inertia ixx="0.0000451" ixy="0" ixz="0.0000073" iyy="0.0000295" iyz
    ="0" izz="0.0000386"/>
    </inertial>
    <visual>
      <origin rpy="0 0 0" xyz="0.0125 0 0.0285"/>
      <geometry>
        <mesh filename="Link4.STEP"/>
      </geometry>
      <material name="White"/>
    </visual>
  </link>

<!-- Neck -->

  <joint name="joint9" type="continuous">
    <parent link="body"/>
    <child link="neck_rotation"/>
    <origin rpy="0 0 0" xyz="0.2 0 0"/>
```

```
    <axis xyz="0 0 1"/>
  </joint>
  <link name="neck_rotation">
    <inertial>
      <origin rpy="0 0 0" xyz="0.000 -0.035 -0.025"/>
      <mass value="0.7683982"/>
      <inertia ixx="0.0022174" ixy="-0.0000030" ixz="-0.0000014" iyy="0.0015748" iyz="0.0007947" izz="0.0015312"/>
    </inertial>
    <visual>
      <origin rpy="0 0 0" xyz="0 0 0"/>
      <geometry>
        <mesh filename="LinkB1.STEP"/>
      </geometry>
      <material name="White"/>
    </visual>
  </link>

  <joint name="joint10" type="continuous">
    <parent link="neck_rotation"/>
    <child link="neck_proximal"/>
    <origin rpy="0 0 0" xyz="0 -0.002 -0.0385"/>
    <axis xyz="0 1 0"/>
  </joint>
  <link name="neck_proximal">
    <inertial>
      <origin rpy="0 0 0" xyz="0.175 0 0"/>
      <mass value="1.0222199"/>
      <inertia ixx="0.0010737" ixy="-0.0000721" ixz="0.0000137" iyy="0.0138997" iyz="0.0000022" izz="0.0139322"/>
    </inertial>
    <visual>
      <origin rpy="0 0 0" xyz="0 0 0"/>
      <geometry>
        <mesh filename="LinkB2.STEP"/>
      </geometry>
      <material name="Light Blue"/>
    </visual>
  </link>

  <joint name="joint11" type="continuous">
    <parent link="neck_proximal"/>
    <child link="neck_medial"/>
    <origin rpy="0 0 0" xyz=".325 0 0"/>
    <axis xyz="0 -1 0"/>
  </joint>
  <link name="neck_medial">
    <inertial>
      <origin rpy="0 0 0" xyz="0.122 0 -0.026"/>
      <mass value="0.5840906"/>
      <inertia ixx="0.0008194" ixy="0" ixz="-0.0029173" iyy="0.0198718" iyz="0" izz="0.0192133"/>
    </inertial>
    <visual>
      <origin rpy="0 0 0" xyz="0 0 0"/>
      <geometry>
        <mesh filename="LinkB3.STEP"/>
      </geometry>
```

```
      <material name="Middle Blue"/>
    </visual>
  </link>

  <joint name="joint12" type="continuous">
    <parent link="neck_medial"/>
    <child link="neck_distal"/>
    <origin rpy="0 0 0" xyz=".307 0 -0.0433"/>
    <axis xyz="0 0 1"/>
  </joint>
  <link name="neck_distal">
    <inertial>
      <origin rpy="0 0 0" xyz="0.031 0 0.005"/>
      <mass value="0.1659947"/>
      <inertia ixx="0.0000603" ixy="0" ixz="0.0000047" iyy="0.0002441" iyz="0" izz="0.0002350"/>
    </inertial>
    <visual>
      <origin rpy="0 0 0" xyz="0 0 0"/>
      <geometry>
        <mesh filename="LinkB4.STEP"/>
      </geometry>
      <material name="Distal Blue"/>
    </visual>
  </link>

  <joint name="joint13" type="continuous">
    <parent link="neck_distal"/>
    <child link="neck_gripper"/>
    <origin rpy="0 0 0" xyz="0.052 0 0"/>
    <axis xyz="1 0 0"/>
  </joint>
  <link name="neck_gripper">
    <inertial>
      <origin rpy="0 0 0" xyz="0.02324066 0 -0.01504931"/>
      <mass value="0.1679844"/>
      <inertia ixx="0.00016428" ixy="0" ixz="-0.00006062" iyy="0.00028473" iyz="0" izz="0.00019284"/>
    </inertial>
    <visual>
      <origin rpy="0 0 0" xyz="0 0 0"/>
      <geometry>
        <mesh filename="LinkB5.STEP"/>
      </geometry>
      <material name="White"/>
    </visual>
  </link>

<!-- Tail -->

  <joint name="joint14" type="continuous">
    <parent link="body"/>
    <child link="tail"/>
    <origin rpy="0 0 0" xyz="-0.1055 0 0"/>
    <axis xyz="0 1 0"/>
  </joint>
  <link name="tail">
    <inertial>
```

```
      <origin rpy="0 0 0" xyz="-0.20511 0 0.01811"/>
      <mass value="0.1775"/>
      <inertia ixx="0.0001044" ixy="0.0000639" ixz="-0.0004584" iyy="0.0142036" iyz="-0.0000058" izz="0.0142267"/>
    </inertial>
    <visual>
      <origin rpy="0 0 0" xyz="0 0 0"/>
      <geometry>
        <mesh filename="LinkT1.STEP"/>
      </geometry>
      <material name="White"/>
    </visual>
  </link>

<!-- End-effectors -->

  <joint name="LeftJoint_EE" type="fixed">
    <parent link="left_gripper"/>
    <child link="Left_EE"/>
    <origin rpy="0 0 0" xyz="0.0125 0 0.0285"/>
    <axis xyz="1 0 0"/>
  </joint>
    <!-- Left End-Effector -->
  <link name="Left_EE">
    <inertial>
      <origin rpy="0 0 0" xyz="0 0 0"/>
      <mass value="0"/>
      <inertia ixx="0" ixy="0" ixz="0" iyy="0" iyz="0" izz="0"/>
    </inertial>
    <visual>
      <origin rpy="0 0 0" xyz="0 0 0"/>
      <geometry>
        <sphere radius="0.01"/>
      </geometry>
      <material name="Red"/>
    </visual>
  </link>

  <joint name="RightJoint_EE" type="fixed">
    <parent link="right_gripper"/>
    <child link="Right_EE"/>
    <origin rpy="0 0 0" xyz="0.0125 0 0.0285"/>
    <axis xyz="1 0 0"/>
  </joint>
    <!-- Right End-Effector -->
  <link name="Right_EE">
    <inertial>
      <origin rpy="0 0 0" xyz="0 0 0"/>
      <mass value="0"/>
      <inertia ixx="0" ixy="0" ixz="0" iyy="0" iyz="0" izz="0"/>
    </inertial>
    <visual>
      <origin rpy="0 0 0" xyz="0 0 0"/>
      <geometry>
        <sphere radius="0.01"/>
      </geometry>
      <material name="Red"/>
    </visual>
```

```
  </link>

  <joint name="BeakJoint_EE" type="fixed">
    <parent link="neck_gripper"/>
    <child link="Beak_EE"/>
    <origin rpy="0 0 0" xyz="0.045 0 0.00904"/>
    <axis xyz="1 0 0"/>
  </joint>
    <!-- End-Effector -->
  <link name="Beak_EE">
    <inertial>
      <origin rpy="0 0 0" xyz="0 0 0"/>
      <mass value="0"/>
      <inertia ixx="0" ixy="0" ixz="0" iyy="0" iyz="0" izz="0"/>
    </inertial>
    <visual>
      <origin rpy="0 0 0" xyz="0 0 0"/>
      <geometry>
        <sphere radius="0.01"/>
      </geometry>
      <material name="Red"/>
    </visual>
  </link>

  <joint name="TailJoint_EE" type="fixed">
    <parent link="tail"/>
    <child link="Tail_EE"/>
    <origin rpy="0 0 0" xyz="-0.5 0 0.03076"/>
    <axis xyz="1 0 0"/>
  </joint>
    <!-- End-Effector -->
  <link name="Tail_EE">
    <inertial>
      <origin rpy="0 0 0" xyz="0 0 0"/>
      <mass value="0"/>
      <inertia ixx="0" ixy="0" ixz="0" iyy="0" iyz="0" izz="0"/>
    </inertial>
    <visual>
      <origin rpy="0 0 0" xyz="0 0 0"/>
      <geometry>
        <sphere radius="0.01"/>
      </geometry>
      <material name="Red"/>
    </visual>
  </link>

</robot>
```